Distribution Agreement

In presenting this thesis or dissertation as a partial fulfillment of the requirements for an advanced degree from Emory University, I hereby grant to Emory University and its agents the non-exclusive license to archive, make accessible, and display my thesis or dissertation in whole or in part in all forms of media, now or hereafter known, including display on the world wide web. I understand that I may select some access restrictions as part of the online submission of this thesis or dissertation. I retain all ownership rights to the copyright of the thesis or dissertation. I also retain the right to use in future works (such as articles or books) all or part of this thesis or dissertation.

Signature: DocuSigned by: Ellen Grace Krall 8B29B9812CFE43B...

Ellen Grace Krall
Name

7/3/2024 | 11:54 AM EDT
Date

Title Investigating SWR1 Recruitment in the Maintenance of the epigenomic H2A.Z landscape

Author Ellen Grace Krall

Degree Doctor of Philosophy

Program Biological and Biomedical Sciences
Genetics and Molecular Biology

Approved by the Committee

DocuSigned by:
Roger Deal
E48B09A892AD4A7...

Roger Deal
Advisor

DocuSigned by:
William Kelly
72474D887F3E4C6...

William Kelly
Committee Member

DocuSigned by:
Anita Corbett
0DEDD157A18D495...

Anita Corbett
Committee Member

DocuSigned by:
Leila Rieder
432D17DDA0EE4B1...

Leila Rieder
Committee Member

DocuSigned by:
Jie Jiang
AEE7F604AE794B5...

Jie Jiang
Committee Member

Committee Member

Accepted by the Laney Graduate School:

_____
Kimberly Jacob Arriola, Ph.D, MPH
Dean, James T. Laney Graduate School

_____
Date

Investigating SWR1 Recruitment in the Maintenance of the epigenomic H2A.Z landscape

by

Ellen Grace Krall

B.S., University of Georgia, 2018

Advisor: Roger Deal, Ph.D.

An abstract of

A dissertation submitted to the Faculty of the

James T. Laney School of Graduate Studies of Emory University

in partial fulfillment of the requirements for the degree of

Doctor of Philosophy

in the Graduate Division of Biological and Biomedical Sciences

Genetics and Molecular Biology

2024

Abstract

Investigating SWR1 Recruitment in the Maintenance of

the epigenomic H2A.Z landscape

By Ellen Grace Krall

H2A.Z is a histone variant which is essential for embryonic development and environmental response across eukaryotes. H2A.Z has a dual role in transcriptional regulation of genes; transcription start site (TSS)-proximal H2A.Z is positively associated with transcription, while gene body H2A.Z is negatively associated with transcription. In plants, H2A.Z is found at actively transcribed genes in euchromatin, at facultatively repressed responsive genes, while H2A.Z is absent from gene poor constitutive heterochromatin. How these distinct profiles of H2A.Z are maintained in relation to deposition machinery the SWI2/SNF2-Related1 (SWR1) complex and the interactor, Methyl-CpG-Binding Domain-containing protein 9 (MBD9) is unclear. Using RNA-Seq and ChIP-Seq in *Arabidopsis thaliana*, we examined the localization of H2A.Z, the SWR1 catalytic component PIE1, and MBD9 under steady-state conditions, simulated stress, and after ectopic localization of SWR1 to constitutive heterochromatin. In Chapter 2, we demonstrate that normally, facultatively repressed genes have the most H2A.Z yet have the least occupancy of SWR1 and the interacting protein MBD9. Upon transcriptional activation, SWR1 moves to deposit and maintain H2A.Z at these responsive genes. MBD9 also moves to these genes, but it is not necessary for SWR1 recruitment or a proper transcriptional response to stimulus. In Chapter 3, we show that in SWR1 mutants there is ectopic accumulation of H2A.Z at constitutively repressed regions. Ectopic localization of SWR1 to these regions utilizing a transgenic methyl-CpG binding MBD9 mutant results in a partial rescue of normal H2A.Z levels, showing that MBD9 is sufficient to target SWR1 to these regions. Collectively, this work expands our understanding of the influence of H2A.Z and its regulatory network on transcriptional regulation in eukaryotes.

Investigating SWR1 Recruitment in the Maintenance of the epigenomic H2A.Z landscape

by

Ellen Grace Krall

B.S., University of Georgia, 2018

Advisor: Roger Deal, Ph.D.

A dissertation submitted to the Faculty of the

James T. Laney School of Graduate Studies of Emory University

in partial fulfillment of the requirements for the degree of

Doctor of Philosophy

in the Graduate Division of Biological and Biomedical Sciences

Genetics and Molecular Biology

2024

Acknowledgements

I have so many people to thank for professionally and personally helping me along my graduate school journey. Firstly, to Roger, thank you for being my primary guide through this endeavor. I feel very lucky to have a mentor that teaches from a place of kindness, respect, and with a true desire to see his mentees succeed. You allowed me to carve my own path while still being ready and willing to jump in whenever I needed more support. The inevitable mistakes and pitfalls inherent to science were always treated as learning experiences, which has only made me a more confident and resilient scientist. Thank you also to my undergraduate mentors David Garfinkel and Lisa Donovan for introducing me to research and starting me on this path.

Secondly, to my lab members, Paja, Maryam, Dylan H, Courtney and Bri, I imagine that I'll never have a work environment that I'll enjoy more. Paja, thank you for tolerating my neverending sarcasm, and thank you more for teaching me almost all the techniques I learned in the lab in *great* detail. Maryam, thank you for your kindness and compassion, and for always making sure we take lab photos and are well-fed with amazing Persian food. Dylan H, thank you for commiserating with me as we both muddled through writing our papers and theses, and thanks for being a great desk buddy and general goofball. Bless you. Courtney, you may not believe me, but thank you for being one of my best friends in and outside of the lab. You and the illustrious Al have taught me to embrace my inner nerd and also some very bad jokes. Bri, thank you for being a premium travel buddy and friend. You are such a light of positivity and I know you'll go on to do great things.

To my committee members, Leila, Anita, Bill and Jie, thank you for your guidance, encouragement, and suggestions over the years. My project took on many forms and permutations, and even when I couldn't see the end in sight you all encouraged me that I was still on a solid path. I always left committee meetings feeling encouraged, supported, and ready to take on the challenges at hand. To all the other members of GMB and Emory, thank you for everything. I have never had a community like I do at Emory. I knew at any moment I could

reach out to any student or faculty member in my sphere to ask for help knowing I would be met with open arms.

To my other close friends in and outside of Atlanta, I couldn't have endured these past 6 years without you. To Jesse, Jenn and Maria, our weekly brunches were the only thing keeping me together during the pandemic era, thank you for being with me through that difficult time. To specifically Jesse, I don't think I've ever made such a fast friend. We trudged through the early years of grad school together and are probably trauma bonded as a result. To Jessie, my forever best friend, your and Lowell's friendship means the world to me. You held my hand through all the lives I lived in grad school. Thank you for being there for me, even during the tough moments. To those in the 'Tony's Place' poker group, the Atlanta Community Symphony Orchestra, and my sloop-based DND group, thank you for being much needed distractions from science that kept me sane.

To Dylan R, my partner-in-and-outside-of-crime, I am so thankful and happy to have you in my life. You entered my life rather unexpectedly at a difficult transitional period and have shown me what true love and partnership looks like. Thank you for being with me through these last few crazy years of grad school and I'm excited to start our life together in the years to come. I love you!

To my family, Mom, Dad, Alex and Lily, thank you for encouraging and supporting me over the years. Mom and Dad, I never questioned that I could get my PhD because you taught me growing up that the sky's the limit and that hard work gets you far in life. Look at me now! To Lily and Alex, I'm happy that we remain close as we move through our own lives. Thank you for your endless support and love.

Table of Contents

Figures and Tables

Chapter 1

Introduction

Chapter 1: Introduction

In multicellular organisms, various cell types with disparate morphologies and characteristics arise from a single, common genome. For example, within a single animal, muscle cells and neurons arise from the same genome, while in plants, a root hair cell has the same genome as a stomatal guard cell (**Fig. 1**). Starting from a single cell, organisms develop specialized cell types in a temporally and spatially specific manner, forming tissues and structures that enable them to thrive as a highly organized cell ecosystem [1,2]. Beyond development, some cell types must also remain sensitive to their environment to help organisms adapt to their surroundings [3,4]. As these seemingly disparate cells share the exact same sequence of heritable information—DNA— how are these specialized cell types formed and maintained?

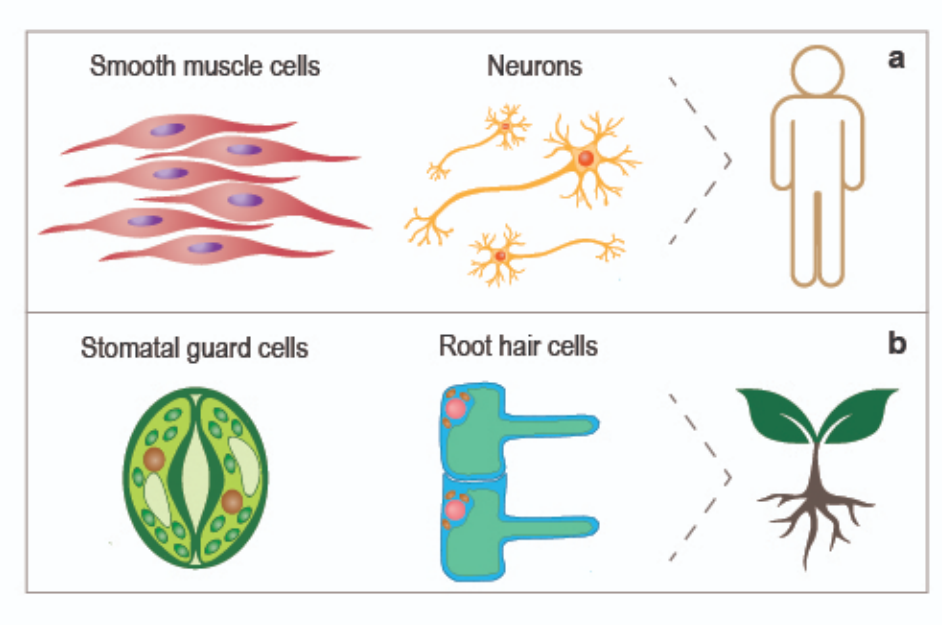

Fig.1 shows different cell types in humans and plants. **(a)** depicts smooth muscle cells (left) and neurons (right), which have disparate morphologies but the same genetic makeup. **(b)** shows stomatal guard cells (left), which function to open and close plant stomata (pores on the undersides of leaves) for gas exchange, while root hair cells (right) function to detect and absorb soil nutrients. Despite their different appearances, these cells also share the same sequence of DNA.

Ultimately, differential gene expression underlies a large portion of cell diversity. Gene expression involves transcription of a gene sequence into a short-lived messenger RNA (mRNA) molecule, which is then translated by molecular machinery into a protein. Proteins then

perform distinct functions within a cell. However, a cell must only express genes specific to its cell type; a muscle cell must only express muscle genes while a neuron must only express neuronal genes. If a single cell forgoes the confines of its own cell type-specific gene expression patterns to individually grow, this unregulated transcription can lead to cancer [5]. In sessile plants, if cells fail to respond appropriately to environmental cues, the plant cannot withstand environmental insults and may die [6]. But how does a cell 'know' which genes to express and when?

In short, access to inappropriate genes is physically restricted. DNA does not exist as a universally accessible molecule in the cell but as a complex mixture of DNA and proteins called chromatin. The most basic unit of chromatin is the nucleosome, composed of approximately 150 base pairs of DNA wrapped around a protein complex composed of 2 copies of each core histone protein H2A, H2B, H3, and H4 (**Fig. 2**). The positively charged histone proteins bind to the negatively charged DNA, creating a physical barrier that prevents transcription factors and other transcription machinery from accessing underlying DNA sequences [7]. Some regions of the genome are more accessible than others due to differences in nucleosome dynamics [8] . Regions where nucleosomes are more mobile and transcription is more prevalent are called euchromatin[9]. Regions where nucleosomes are more constrained and transcription is less prevalent are called heterochromatin [10]. Heterochromatin is further divided into constitutive and facultative

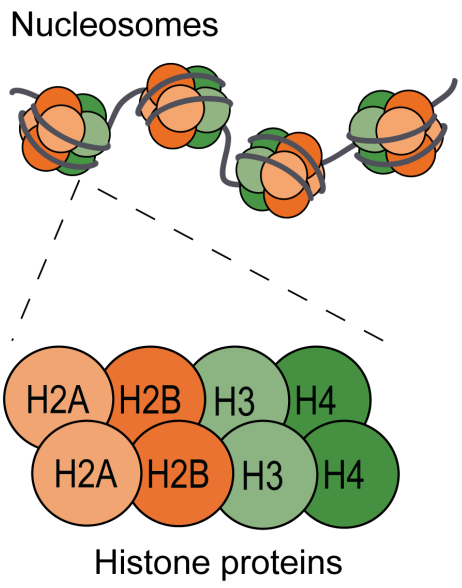

Fig. 2 depicts several nucleosomes compacting a region of DNA. If we zoom in on a single nucleosome, we can see that the octamer core is composed of two molecules of each histone protein H2A, H2B, H3 and H4.

heterochromatin. Constitutive heterochromatin is the least accessible and most transcriptionally repressed whereas facultative heterochromatin comprises regions that are inaccessible and inactive but can become more accessible and transcribed when the appropriate signal arises [11].

Modulation of histone-DNA interactions within these different chromatin environments therefore ensures that only genes specific to the developmental, environmental, and temporal status of a cell are accessible to transcription machinery. One mechanism of modulation is the modification of histone proteins and DNA through the covalent attachment of small molecules. Common post-translational modifications (PTMs) to histones include acetylation, phosphorylation, ubiquitylation and methylation [12,13]. Addition of acetyl groups to histones reduces their positive charge, thereby reducing their affinity for DNA and allowing their occupied areas to become more accessible to transcription machinery. On the other hand, methylation of histone proteins and cytosines in DNA often serve as binding platforms to recruit other protein complexes that can directly change chromatin structure.

One group of protein complexes called chromatin remodelers use ATP hydrolysis to directly eject and position nucleosomes as well as change the composition of nucleosomes through exchange of canonical histones for histone variants [14]. While all chromatin remodelers share a conserved ATPase domain, the addition of other unique domains separate the chromatin remodelers into four distinct classes. These classes are SWI/SNF (switch/sucrose-non-fermenting), ISWI (imitation switch), CHD (chromodomain-helicase-DNA binding) and INO80 (inositol requiring 80) [14]. SWI/SNF type chromatin remodelers are characterized by a C-terminal acetyl-binding Bromodomain along with a N-terminal HSA domain that mediates interactions with actin and actin-related proteins[14]. SWI/SNF-type remodelers affect nucleosomes in many ways including sliding and ejecting nucleosomes from chromatin [15]. ISWI-type remodelers contain tandem SANT and SLIDE domains that function cooperatively to bind to unmodified histone tails to optimize spacing and assembly of nucleosomes [15]. CHD-type

chromatin remodelers are characterized by their tandemly arranged, N-terminal Chromodomains, which mediate interactions with methylated histone residues[14]. Many CHD-type chromatin remodelers promote transcription through sliding and ejecting nucleosomes, whereas other remodelers in this category contribute to gene repression through histone deacetylation [15]. The final category of remodelers, INO80-type chromatin remodelers, are characterized by a large insertion within their ATPase domain and have a variety of diverse functions including DNA repair and transcriptional activation functions [15]. One member of the INO80 chromatin remodeling family, the SWI2/SNF2-Related1 (SWR1) complex, can also mediate exchanges of canonical histone H2A for the histone variant H2A.Z [16,17], while the INO80 complex is capable of performing the reverse reaction[18].

Histone variants are specialized versions of histones that are deposited outside of S phase and confer unique properties to their occupied nucleosomes [19,20]. Canonical histone deposition is driven by the doubling of DNA during replication, where newly synthesized histones are incorporated indiscriminately into nucleosome gaps in replicated DNA. Variants, on the other hand, are deposited throughout the cell cycle on a nucleosome-by-nucleosome basis by their respective chromatin remodelers. Histone variants are essential to the establishment and maintenance of chromatin states characteristic of eukaryotic chromatin [21–23].

The H2A variant H2A.Z is one of the most conserved histone variants across eukaryotes, with a sequence conservation of ~90% across organisms as opposed to only a ~60% identity with canonical histone H2A [24]. H2A.Z diverges from H2A at several regions including the histone fold domain and the docking domain, which mediates interactions with histone H3 within the nucleosome [24]. Differences within the histone fold domain in H2A.Z may affect how H2A.Z interacts with another H2A.Z molecule within the same nucleosome[24]. On the other hand, docking domain changes result in destabilization of H2A.Z/H3 interactions within the nucleosome, and contribute to an extended acidic patch, which affects interactions with adjacent

nucleosomes [24]. H2A.Z loss is lethal in many organisms including *Tetrahymena*, *Caenorhabditis elegans*, *Drosophila melanogaster*, *Mus musculus* and humans [24]. H2A.Z is also often overexpressed in cancers [25]. Loss of H2A.Z in plants such as *Arabidopsis thaliana* is not lethal, but results in phenotypes including early flowering, abnormal leaf growth, reduced fertility, and misregulation of environmental response genes [19,26]. This makes plants ideal model organisms to study H2A.Z.

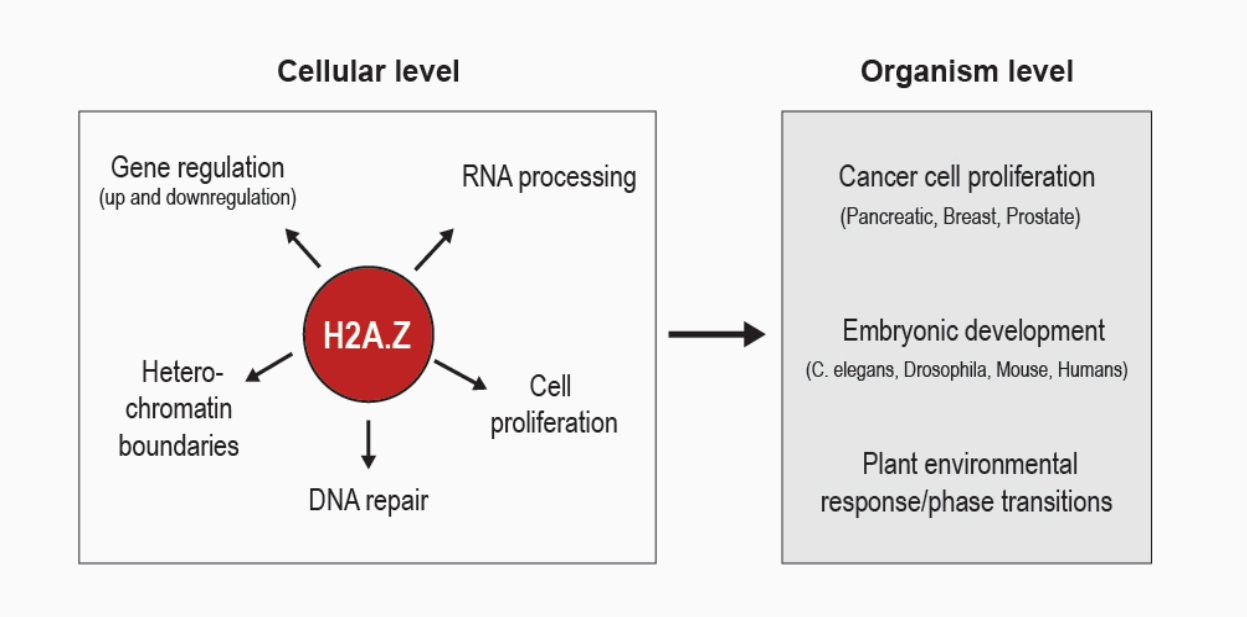

Fig. 3 summarizes the various processes H2A.Z has been implicated in at the cellular and organismal scales. At the cellular level (left) H2A.Z has been related to various processes from both up and downregulating nearby genes, to DNA repair, to maintaining heterochromatin boundaries, to cell proliferation. At the organismal level (right), H2A.Z contributes to embryonic development and plant environmental response/phase transitions, and can also contribute to cancer cell proliferation when misregulated.

At the molecular level, H2A.Z is linked to a wide variety of processes from maintaining heterochromatin boundaries to DNA repair to both positively and negatively regulating the transcription of nearby genes [24,27,28] (**Fig. 3**). The function of H2A.Z may change depending on the surrounding chromatin context, i.e., the presence of other histone variants, histone PTMs and position in reference to nearby genes and regulatory elements. Interestingly, while other well-known histone variants including CenH3, H2A.X and H3.3 are associated exclusively with

either euchromatin or heterochromatin, H2A.Z is found at both euchromatin and facultative heterochromatin across *Eukarya* [19,29].

H2A.Z is enriched at the nucleosomes flanking the transcription start site (TSS) in euchromatin, but this enrichment skews to cover whole gene bodies in facultative heterochromatin [26,30]. In euchromatin, H2A.Z promotes transcription in part by making nucleosomes around the TSS more unstable, which creates conditions more favorable for transcription by RNA polymerase [31,32]. However, there is also evidence that H2A.Z distributions around the TSS could be indicative of the direction of RNA polymerase elongation, rather than a proponent of the elongation itself [33]. In facultative heterochromatin, H2A.Z is enriched across the entirety of the gene body, where it plays a repressive role [19,30,34,35]. Post-translational modifications of H2A.Z may also be involved in distinguishing the effect of H2A.Z on transcriptional regulation. Acetylation of H2A.Z at N-terminal lysines K4, K7 and K11 contributes to gene activation in many contexts across eukaryotes and during tumorigenesis [36–39], while monoubiquitination of H2A.Z at its C-terminal end at multiple lysines contributes to gene repression [29,40–42]. Additionally, gene body H2A.Z is generally associated with the PRC2 mark, H3K27me3, where this PTM appears to be dependent on the presence of H2A.Z [43,44]. Furthermore, previous work established an anticorrelation between DNA methylation and H2A.Z across eukaryotes, which could explain why H2A.Z exclusively appears in genic facultative heterochromatin and euchromatin [45–47]. In Arabidopsis, it was shown that reduction of DNA methylation through mutation of the DNA methyltransferase *MET1* resulted in gains of H2A.Z in demethylated DNA regions, indicating that these marks are dynamically anticorrelated and perhaps antagonistic to one another [45].

Ultimately, deposition of H2A.Z into different chromatin environments depends on chromatin remodeling complexes responsible for exchanging H2A for H2A.Z, the SWI2/SNF2-Related1 (SWR1) complex. This multi-subunit INO80-type chromatin remodeler

was first identified in *S. cerevisiae*, and many of the 13 core subunits are conserved across eukaryotes [28]. The ATP-hydrolyzing catalytic subunit is known as Domino in Drosophila, SRCAP/TIP60 in vertebrates, and PHOTOPERIOD-INDEPENDENT EARLY FLOWERING 1 (PIE1) in plants [48]. Other broadly conserved subunits include Arp4, Arp6, Rvb1, Rvb2, Yaf9 and Act1. These core components lack DNA binding domains, so other accessory factors of SWR1 help target SWR1 to specific locations. For example, the yeast BromoDomain Factor 1 (BDF1) may bind to hyperacetylated histones around the TSS of active genes to recruit SWR1 [49]. The Arabidopsis SANT-domain containing protein SWC4 binds to DNA and recruits SWR1 through interaction with core SWR1 components [50]. Despite some understanding of factors that target SWR1, a full understanding of the rules governing SWR1 recruitment remain elusive.

Less is known about the components of the plant INO80 complex, which is responsible for performing the reverse reaction of SWR1; the exchange of H2A.Z for H2A [51]. The plant INO80 complex has not been successfully isolated or characterized, but sequence homology with yeast INO80 components suggest that many of the components are present in plants [18]. There are also four components of the INO80 complex that are shared with SWR1 (Rvb1, Rvb2, Arp4 and Act1) [18]. Although the INO80 and SWR1 complexes both belong to the INO80-type chromatin remodeling family and contain an insertion in their ATPase domains, there is only ~15% conservation in this ATPase insertion between the complexes [52]. These differences result in different modes-of-action between the complexes in terms of how they translocate DNA to perform histone exchange [52]. In plants, it was also shown that H2A.Z removal by INO80 is necessary for induction of environmental response genes including those responsive to temperature, far-red light, and ethylene [53–56].

In Arabidopsis, the plant-specific METHYL-CPG-BINDING DOMAIN-CONTAINING PROTEIN 9 (MBD9) protein was discovered as an interactor to the SWR1 complex [57–59]. Specifically it was proposed to bind to histone acetylation marks to recruit SWR1 for H2A.Z

deposition and mediate interactions with demethylation complexes and ISWI chromatin remodelers [59,60]. Our group as well as others demonstrated that MBD9 is necessary for proper H2A.Z enrichment in Arabidopsis [57–59]. This work demonstrated that MBD9 is necessary for H2A.Z enrichment at thousands of sites, and those MBD9-dependent H2A.Z sites were primarily localized to euchromatin. However, exactly when and how MBD9 is involved in SWR1 recruitment and subsequent H2A.Z deposition or maintenance throughout the genome remains unclear. Here we describe experiments aimed at defining the relationship between MBD9 and SWR1, with the goal of ultimately understanding the rules governing SWR1 recruitment and subsequent H2A.Z patterning across the *Arabidopsis thaliana* genome.

In Chapter 2, we analyze the binding patterns of MBD9, SWR1 and H2A.Z at steady-state and during a widespread transcriptional activation event to understand how their localization changes as genes become active within facultative heterochromatin. As mentioned previously, H2A.Z is commonly found both at euchromatin and facultative heterochromatin, but less is known about the distribution of SWR1 in relation to H2A.Z in these different chromatin compartments. To address this point, we developed antibodies against the plant catalytic subunit of the SWR1 complex, PIE1, and interactor MBD9, and utilized these antibodies for Chromatin Immunoprecipitation followed by high-throughput sequencing (ChIP-Seq). We found that at steady state, PIE1 and MBD9 are more enriched at actively transcribed genes than at facultatively repressed genes. This result is surprising considering there is more H2A.Z at facultatively repressed genes, where it occupies the entire gene body. Based on this observation, we hypothesized that SWR1 and MBD9 are only required at genes that are undergoing nucleosome loss due to transcription; when facultative heterochromatin genes are activated, PIE1 and/or MBD9 will move to these newly activated genes to replace H2A.Z. To test this hypothesis, we activated a subset of facultatively repressed genes through the exogenous application of the plant hormone Abscisic Acid (ABA). We saw that transcriptional induction at ABA-responsive genes resulted in a subtle loss of H2A.Z and a gain of MBD9 and PIE1. We

also saw that changes in H2A.Z enrichment did not result in a conversion of gene body H2A.Z to TSS-proximal H2A.Z, which suggests that H2A.Z distribution does not simply reflect the current transcriptional state of genes. We posited that the Bromodomain of MBD9 may be involved in the recruitment of MBD9, and perhaps SWR1, to these newly activated genes, but demonstrated that mutation of this domain does not cause wide-spread differences in MBD9 localization at steady-state or during an ABA response. We also performed similar experiments in plants lacking MBD9 to understand the necessity of MBD9 to this SWR1 recruitment and gene activation. Surprisingly, we saw that MBD9 null plants are able to recruit SWR1 properly and to respond efficiently to ABA at the transcriptional level, despite having a general reduction of H2A.Z at these response genes.

In Chapter 3, we investigate the ability of MBD9 to target SWR1 to constitutive heterochromatin, and the effects of such recruitment on H2A.Z enrichment. Although H2A.Z and DNA methylation are classically anticorrelated, we noticed when aligning H2A.Z ChIP-seq data to a newly released complete Arabidopsis genome assembly that several null mutants for SWR1 components (including the SWR1 interactor MBD9) resulted in gains of H2A.Z at transposable element genes in constitutive heterochromatin. Based on these observations, we hypothesized that SWR1 may be directly involved in preventing H2A.Z accumulation at these constitutively repressed regions, which would also explain the anticorrelation between H2A.Z and DNA methylation. To test this hypothesis, we designed a mutant version of MBD9 that now binds regions with DNA methylation to test targeting of SWR1 to these regions. Through ChIP-seq against MBD9, SWR1(PIE1) and H2A.Z, we found that supplementation of *mbd9-1* plants with this mutant MBD9 results in recruitment of MBD9 and PIE1 to constitutively repressed regions, highlighting that MBD9 is sufficient for SWR1 recruitment to these regions. We also provide evidence that new recruitment of SWR1 to these regions results in a partial rescue of H2A.Z back to WT levels. This rescue provides support to the notion that SWR1 may itself be responsible for the anticorrelation between H2A.Z and DNA methylation normally

observed across *Eukarya*, perhaps by directly removing H2A.Z that is aberrantly incorporated into nucleosomes in methylated DNA regions.

References

1. Hsieh, T.-F. & Fischer, R. L. Biology of chromatin dynamics. *Annu. Rev. Plant Biol.* **56**, 327–351 (2005).
2. Gopinathan, G. & Diekwisch, T. G. H. Epigenetics and Early Development. *J Dev Biol* **10**, (2022).
3. Baulcombe, D. C. & Dean, C. Epigenetic regulation in plant responses to the environment. *Cold Spring Harb. Perspect. Biol.* **6**, a019471 (2014).
4. Aguilera, O., Fernández, A. F., Muñoz, A. & Fraga, M. F. Epigenetics and environment: a complex relationship. *J. Appl. Physiol.* **109**, 243–251 (2010).
5. Dos Santos, G. A., Chatsirisupachai, K., Avelar, R. A. & de Magalhães, J. P. Transcriptomic analysis reveals a tissue-specific loss of identity during ageing and cancer. *BMC Genomics* **24**, 644 (2023).
6. Chang, Y.-N. *et al.* Epigenetic regulation in plant abiotic stress responses. *J. Integr. Plant Biol.* **62**, 563–580 (2020).
7. Li, B., Carey, M. & Workman, J. L. The Role of Chromatin during Transcription. *Cell* **128**, 707–719 (2007).
8. Morrison, O. & Thakur, J. Molecular complexes at euchromatin, heterochromatin and centromeric chromatin. *Int. J. Mol. Sci.* **22**, 6922 (2021).
9. Maeshima, K., Iida, S., Shimazoe, M. A., Tamura, S. & Ide, S. Is euchromatin really open in the cell? *Trends Cell Biol.* **34**, 7–17 (2024).
10. Grewal, S. I. S. & Jia, S. Heterochromatin revisited. *Nat. Rev. Genet.* **8**, 35–46 (2007).
11. Liu, J., Ali, M. & Zhou, Q. Establishment and evolution of heterochromatin. *Ann. N. Y. Acad.*

Sci. **1476**, 59–77 (2020).

12. Millán-Zambrano, G., Burton, A., Bannister, A. J. & Schneider, R. Histone post-translational modifications — cause and consequence of genome function. *Nat. Rev. Genet.* **23**, 563–580 (2022).
13. Bannister, A. J. & Kouzarides, T. Regulation of chromatin by histone modifications. *Cell Res.* **21**, 381–395 (2011).
14. Tyagi, M., Imam, N., Verma, K. & Patel, A. K. Chromatin remodelers: We are the drivers!! *Nucleus* **7**, 388–404 (2016).
15. Clapier, C. R. & Cairns, B. R. The biology of chromatin remodeling complexes. *Annu. Rev. Biochem.* **78**, 273–304 (2009).
16. Luk, E. *et al.* Stepwise histone replacement by SWR1 requires dual activation with histone H2A.Z and canonical nucleosome. *Cell* **143**, 725–736 (2010).
17. Fan, J., Moreno, A. T., Baier, A. S., Loparo, J. J. & Peterson, C. L. H2A.Z deposition by SWR1C involves multiple ATP-dependent steps. *Nat. Commun.* **13**, 1–15 (2022).
18. Wang, J., Gao, S., Peng, X., Wu, K. & Yang, S. Roles of the INO80 and SWR1 Chromatin Remodeling Complexes in Plants. *Int. J. Mol. Sci.* **20**, (2019).
19. Foroozani, M., Holder, D. H. & Deal, R. B. Histone Variants in the Specialization of Plant Chromatin. *Annu. Rev. Plant Biol.* **73**, 149–172 (2022).
20. Talbert, P. B. & Henikoff, S. Histone variants at a glance. *J. Cell Sci.* **134**, (2021).
21. Henikoff, S. & Smith, M. M. Histone variants and epigenetics. *Cold Spring Harb. Perspect. Biol.* **7**, a019364 (2015).
22. Jamge, B. *et al.* Histone variants shape chromatin states in Arabidopsis. *Elife* **12**, (2023).
23. Borg, M., Jiang, D. & Berger, F. Histone variants take center stage in shaping the epigenome. *Curr. Opin. Plant Biol.* **61**, 101991 (2021).
24. Zlatanova, J. & Thakar, A. H2A.Z: view from the top. *Structure* **16**, 166–179 (2008).
25. Ghiraldini, F. G., Filipescu, D. & Bernstein, E. Solid tumours hijack the histone variant

network. *Nat. Rev. Cancer* **21**, 257–275 (2021).

26. Coleman-Derr, D. & Zilberman, D. Deposition of histone variant H2A.Z within gene bodies regulates responsive genes. *PLoS Genet.* **8**, e1002988 (2012).
27. Babiarz, J. E., Halley, J. E. & Rine, J. Telomeric heterochromatin boundaries require NuA4-dependent acetylation of histone variant H2A.Z in Saccharomyces cerevisiae. *Genes Dev.* **20**, 700–710 (2006).
28. March-Díaz, R. & Reyes, J. C. The beauty of being a variant: H2A. Z and the SWR1 complex in plants. *Mol. Plant* **2**, 565–577 (2009).
29. Sarcinella, E., Zuzarte, P. C., Lau, P. N. I., Draker, R. & Cheung, P. Monoubiquitylation of H2A.Z distinguishes its association with euchromatin or facultative heterochromatin. *Mol. Cell. Biol.* **27**, 6457–6468 (2007).
30. Long, J., Carter, B., Johnson, E. T. & Ogas, J. Contribution of the histone variant H2A.Z to expression of responsive genes in plants. *Semin. Cell Dev. Biol.* **135**, 85–92 (2023).
31. Li, S., Wei, T. & Panchenko, A. R. Histone variant H2A.Z modulates nucleosome dynamics to promote DNA accessibility. *Nat. Commun.* **14**, 1–10 (2023).
32. Weber, C. M., Ramachandran, S. & Henikoff, S. Nucleosomes Are Context-Specific, H2A.Z-Modulated Barriers to RNA Polymerase. *Mol. Cell* **53**, 819–830 (2014).
33. Silver, B. D., Willett, C. G., Maher, K. A., Wang, D. & Deal, R. B. Differences in transcription initiation directionality underlie distinctions between plants and animals in chromatin modification patterns at genes and cis-regulatory elements. *G3 Genes|Genomes|Genetics* **14**, jkae016 (2024).
34. Rispal, J. *et al.* Control of intestinal stemness and cell lineage by histone variant H2A.Z isoforms. *bioRxiv* 2023.10.10.561706 (2023) doi:10.1101/2023.10.10.561706.
35. Lorković, Z. J. *et al.* Compartmentalization of DNA damage response between heterochromatin and euchromatin is mediated by distinct H2A histone variants. *Curr. Biol.* **27**, 1192–1199 (2017).

36. Pradhan, S. K. *et al.* EP400 Deposits H3.3 into Promoters and Enhancers during Gene Activation. *Mol. Cell* **61**, 27–38 (2016).
37. Valdés-Mora, F. *et al.* Acetylated histone variant H2A.Z is involved in the activation of neo-enhancers in prostate cancer. *Nat. Commun.* **8**, 1–17 (2017).
38. Halley, J. E., Kaplan, T., Wang, A. Y., Kobor, M. S. & Rine, J. Roles for H2A.Z and its acetylation in GAL1 transcription and gene induction, but not GAL1-transcriptional memory. *PLoS Biol.* **8**, e1000401 (2010).
39. Valdés-Mora, F. *et al.* Acetylation of H2A.Z is a key epigenetic modification associated with gene deregulation and epigenetic remodeling in cancer. *Genome Res.* **22**, 307–321 (2012).
40. Colino-Sanguino, Y., Clark, S. J. & Valdes-Mora, F. H2A.Z acetylation and transcription: ready, steady, go! *Epigenomics* **8**, 583–586 (2016).
41. Sevilla, A. & Binda, O. Post-translational modifications of the histone variant H2AZ. *Stem Cell Res.* **12**, 289–295 (2014).
42. Gómez-Zambrano, Á., Merini, W. & Calonje, M. The repressive role of Arabidopsis H2A.Z in transcriptional regulation depends on AtBMI1 activity. *Nat. Commun.* **10**, 1–12 (2019).
43. Subramanian, V., Fields, P. A. & Boyer, L. A. H2A.Z: a molecular rheostat for transcriptional control. *F1000Prime Rep.* **7**, 01 (2015).
44. Carter, B. *et al.* The chromatin remodelers PKL and PIE1 act in an epigenetic pathway that determines H3K27me3 homeostasis in Arabidopsis. *Plant Cell* **30**, 1337–1352 (2018).
45. Zilberman, D., Coleman-Derr, D., Ballinger, T. & Henikoff, S. Histone H2A.Z and DNA methylation are mutually antagonistic chromatin marks. *Nature* **456**, 125 (2008).
46. Conerly, M. L. *et al.* Changes in H2A.Z occupancy and DNA methylation during B-cell lymphomagenesis. *Genome Res.* **20**, 1383–1390 (2010).
47. Edwards, J. R. *et al.* Chromatin and sequence features that define the fine and gross structure of genomic methylation patterns. *Genome Res.* **20**, 972–980 (2010).
48. Giaimo, B. D., Ferrante, F., Herchenröther, A., Hake, S. B. & Borggrefe, T. The histone

variant H2A.Z in gene regulation. *Epigenetics Chromatin* **12**, 37 (2019).

49. Altaf, M. *et al.* NuA4-dependent acetylation of nucleosomal histones H4 and H2A directly stimulates incorporation of H2A.Z by the SWR1 complex. *J. Biol. Chem.* **285**, 15966–15977 (2010).
50. Gómez-Zambrano, Á. *et al.* Arabidopsis SWC4 Binds DNA and Recruits the SWR1 Complex to Modulate Histone H2A.Z Deposition at Key Regulatory Genes. *Mol. Plant* **11**, 815–832 (2018).
51. Brahma, S. *et al.* INO80 exchanges H2A.Z for H2A by translocating on DNA proximal to histone dimers. *Nat. Commun.* **8**, 15616 (2017).
52. Willhoft, O. & Wigley, D. B. INO80 and SWR1 complexes: the non-identical twins of chromatin remodelling. *Curr. Opin. Struct. Biol.* **61**, 50–58 (2020).
53. Willige, B. C. *et al.* PHYTOCHROME-INTERACTING FACTORs trigger environmentally responsive chromatin dynamics in plants. *Nat. Genet.* **53**, 955–961 (2021).
54. Zander, M. *et al.* Epigenetic silencing of a multifunctional plant stress regulator. *Elife* **8**, (2019).
55. Zhao, F. *et al.* Coordinated histone variant H2A.Z eviction and H3.3 deposition control plant thermomorphogenesis. *New Phytol.* **238**, 750–764 (2023).
56. Xue, M. *et al.* The INO80 chromatin remodeling complex promotes thermomorphogenesis by connecting H2A.Z eviction and active transcription in Arabidopsis. *Mol. Plant* **14**, 1799–1813 (2021).
57. Sijacic, P., Holder, D. H., Bajic, M. & Deal, R. B. Methyl-CpG-binding domain 9 (MBD9) is required for H2A.Z incorporation into chromatin at a subset of H2A.Z-enriched regions in the Arabidopsis genome. *PLoS Genet.* **15**, e1008326 (2019).
58. Potok, M. E. *et al.* Arabidopsis SWR1-associated protein methyl-CpG-binding domain 9 is required for histone H2A.Z deposition. *Nat. Commun.* **10**, 1–14 (2019).
59. Luo, Y.-X. *et al.* A plant-specific SWR1 chromatin-remodeling complex couples histone

H2A.Z deposition with nucleosome sliding. *EMBO J.* **39**, e102008 (2020).

60. Nie, W.-F. *et al.* Histone acetylation recruits the SWR1 complex to regulate active DNA demethylation in Arabidopsis. *Proc. Natl. Acad. Sci. U. S. A.* **116**, 16641–16650 (2019).

Chapter 2

SWR1 is recruited to activated ABA response genes to maintain gene body H2A.Z in *Arabidopsis thaliana*

Under consideration at *Nature Communications* and available on *bioRxiv*:

https://doi.org/10.1101/2024.07.14.603444

Chapter 2: SWR1 is recruited to activated ABA response genes to maintain gene body H2A.Z in *Arabidopsis thaliana*

Ellen G. Krall[1,2] and Roger B. Deal[1]

[1]Department of Biology

[2]Graduate Program in Genetics and Molecular Biology

Emory University, Atlanta, GA 30322 USA

Abstract

The histone variant H2A.Z is important for transcriptional regulation across eukaryotes, where it can alternately promote or repress transcription. In plants, actively transcribed genes show H2A.Z enrichment in nucleosomes immediately downstream of the transcription start site (TSS), while silent genes show H2A.Z enrichment across the gene body. Previous work showed that silent genes responsive to temperature and far-red light lose gene body H2A.Z upon activation, but whether H2A.Z loss is generally required for transcription is not clear. We profiled H2A.Z and components of its deposition complex, SWR1, before and after treating Arabidopsis thaliana with the hormone abscisic acid (ABA). Our results show that transcribed genes with TSS-enriched H2A.Z have high SWR1 binding at steady-state, indicating continuous replacement of H2A.Z, while silent genes with gene body H2A.Z show lower SWR1 binding. Surprisingly, upon ABA treatment, thousands of previously silent genes activate, coincident with recruitment of SWR1 and retention of gene body H2A.Z enrichment. We also found that the SWR1-interacting protein MBD9 is not required for SWR1 recruitment to activated genes. These

results provide new insights into the relationship between H2A.Z and transcription and the mechanics of H2A.Z targeting to chromatin.

Introduction

In the eukaryotic nucleus, histone proteins drive DNA organization by binding and condensing DNA into chromatin. The basic unit of chromatin is the nucleosome, where ~147 base pairs of DNA are wrapped around a histone protein octamer composed of one H3/H4 histone tetramer flanked by two H2A/H2B histone dimers. Histones function to condense DNA, but their occupancy is also a physical barrier to DNA access. This occupancy prevents trans-acting factors from binding to regulatory elements depending on a cell's developmental, environmental, and temporal state.

The modulation of DNA-histone binding is therefore crucial to promote proper transcription and other DNA-templated activities at any given moment within the eukaryotic cell. Chromatin remodeling complexes directly modify DNA-histone interactions by hydrolysing ATP to slide, move, and eject nucleosomes as well as exchange canonical histones for specialized histone variants[1]. H2A.Z is a well-conserved histone variant of histone H2A deposited by the chromatin remodeler SWI2/SNF2-Related 1 (SWR1) [2–4].

The consequences of H2A.Z loss or misregulation on an organism are severe. H2A.Z misregulation contributes to the loss of cellular identity and the proliferation of cancer cells in melanoma, breast cancer, pancreatic ductal adenocarcinoma, prostate cancer, and hepatocellular carcinoma [5–10]. Its loss is also embryonic lethal in many organisms including *C. elegans, Drosophila melanogaster,* and mammals [11–15]. Plants, including the model plant *Arabidopsis thaliana* (Arabidopsis), tolerate the absence of H2A.Z but show pleiotropic phenotypes including early flowering, abnormal leaf development, reduced fertility, and an inability to respond appropriately to abiotic and biotic stressors [16–18]. This makes Arabidopsis an

ideal model organism to study the consequences of H2A.Z loss beyond embryonic development.

The effects of H2A.Z misregulation stem from its dual role in both positively and negatively regulating transcription, which are related to its deposition relative to occupied genes [4,11,19]. When H2A.Z is enriched in nucleosomes flanking the Transcription Start Site (TSS), it creates conditions favorable for transcription. The first nucleosome downstream of the TSS (+1 nucleosome) is an energetic barrier to RNA polymerase, and incorporation of H2A.Z can lower this barrier by creating more mobile, easily unwrapped nucleosomes [20,21]. When H2A.Z enrichment skews to cover whole gene bodies, it has a repressive effect [16,22]. Genes that have more gene body H2A.Z are more responsive to environmental and developmental cues in plants, human cell lines, embryonic stem cells, $CD4^+$ T lymphocyte cells, and intestinal epithelial cells [22–27]. Additionally, these responsive genes are targets of Polycomb Repressive Complexes 1 and 2 (PRC1 and 2), which further mark these genes with post-translational histone modifications (PTMs) H2AK121ub and H3K27me3, respectively, establishing a repressed but responsive chromatin environment [28,29].

Post-translational modifications of H2A.Z itself further distinguish the two observed profiles of H2A.Z. TSS-proximal H2A.Z is often acetylated at N-terminal lysines K4, K7 and K11 [30,31]. Acetylation of H2A.Z has been shown to contribute to gene activation in many contexts across eukaryotes and during tumorigenesis [32–35]. Gene body associated H2A.Z (gbH2A.Z), on the other hand, is often monoubiquitinated at its C-terminal end at multiple lysines [29–31]. This modification, as with canonical histone modification H2AK121ub, is deposited by PRC1 and contributes to gene repression [29,36]. Additionally, gbH2A.Z is generally associated with the PRC2 mark, H3K27me3, where this PTM appears to be dependent on the presence of H2A.Z [37].

It is reasonable to assume that these two distinct profiles of H2A.Z enrichment, TSS-proximal H2A.Z and gbH2A.Z, are interconnected. Upon gene activation, gbH2A.Z may be lost as genes shift to having only TSS-proximal H2A.Z. Once repression is re-established,

gbH2A.Z would also then be re-established. This notion is supported by experiments showing that H2A.Z is lost from genes responsive to far-red light, heat stress, and ethylene in plants once activated [38–40]. However, it remains unclear if the distribution of H2A.Z on a gene is a feature that drives transcriptional regulation or simply reflects the present transcriptional status of the gene.

The establishment and maintenance of these two distinct H2A.Z profiles must depend at least in part on the H2A.Z deposition complex, SWR1. However, how SWR1 is targeted specifically to certain genes to deposit H2A.Z is unclear. SWR1 is a multi-subunit chromatin remodeler first identified in *S. cerevisiae*, and many of the 13 core subunits are conserved across eukaryotes [4]. The ATP-hydrolyzing catalytic subunit is known as Domino in Drosophila, SRCAP/TIP60 in vertebrates, and PHOTOPERIOD-INDEPENDENT EARLY FLOWERING 1 (PIE1) in plants [41]. Previous work has established that SWR1 is recruited to nucleosome-depleted regions (NDR) in organisms including yeast and mouse embryonic stem cells [42–44]. Core components of SWR1 lack DNA-binding specificity, and therefore SWR1 interacts transiently with a variety of other factors that can directly affect its localization [41,45]. However, the general and specific mechanisms governing the targeting of SWR1 by various factors remain unclear.

There is evidence that Bromodomain-containing accessory subunits are specifically involved in TSS-associated H2A.Z patterning on genes. For example, the yeast BromoDomain Factor 1 (BDF1) may bind to hyperacetylated histones around the TSS of active genes to recruit SWR1 [46]. Similarly in Arabidopsis, the plant-specific METHYL-CPG-BINDING DOMAIN-CONTAINING PROTEIN 9 (MBD9) protein was proposed to bind to acetylation marks to recruit SWR1 for H2A.Z deposition [47,48]. Our group as well as others demonstrated that MBD9 interacts with SWR1 and is necessary for proper H2A.Z accumulation in Arabidopsis chromatin [48–50]. These publications demonstrated that plants lacking MBD9 had a reduction of H2A.Z

enrichment at a subset of euchromatic sites compared to WT plants. However, it is still unclear if MBD9 is directly involved in SWR1 recruitment or if its effects on H2A.Z levels are indirect.

Here, we developed antibodies against the Arabidopsis SWR1 catalytic subunit, PIE1, and interactor MBD9 to better understand their localization in the Arabidopsis genome relative to H2A.Z. We also employed exogenous application of the plant hormone Abscisic Acid (ABA) to assess how their localizations change during a widespread transcriptional activation event. We further analyzed MBD9 deficient plants and induced an MBD9 Bromodomain-disrupting point mutation to define the role of MBD9 in SWR1 recruitment and subsequent H2A.Z deposition.

Our results indicate that silent genes with gbH2A.Z enrichment have much lower levels of the SWR1 ATPase PIE1 and interacting protein MBD9 under steady-state conditions compared to active genes with TSS-proximal H2A.Z enrichment. Upon ABA treatment, we see that PIE1 and MBD9 are recruited to previously silent ABA responsive genes with gbH2A.Z, but this surprisingly results in only a subtle decrease in H2A.Z enrichment on gene bodies. Parallel experiments in *mbd9-1* plants show that PIE1 is still recruited to newly activated genes in the absence of MBD9, indicating that MBD9 is not a targeting factor for SWR1 in this context. We also provide evidence that the MBD9 Bromodomain is dispensable to the role of MBD9 in the maintenance of H2A.Z levels. Taken together, this work suggests that SWR1 plays an active role in maintaining H2A.Z both at genes with TSS-enriched H2A.Z and normally silent genes with gene body H2A.Z enrichment. SWR1, along with interacting protein MBD9, is normally localized to active genes to continuously replace H2A.Z in the unstable TSS-proximal nucleosomes. Upon transcriptional activation of gbH2A.Z-enriched ABA responsive genes, SWR1 moves to these newly activated genes to maintain gene body H2A.Z, indicating that H2A.Z removal is not a prerequisite for activation of all gbH2A.Z-silenced genes. We also provide evidence that MBD9 and specifically the MBD9 Bromodomain, are not required for SWR1 targeting at these responsive genes.

Results

Genes with TSS-associated H2A.Z have more PIE1 and MBD9 binding at steady state

To better understand the localization of SWR1 and MBD9 relative to H2A.Z, we utilized antibodies raised against unique peptide sequences of PIE1 and MBD9. These antibodies specifically recognize their respective proteins via Western blot (**Supp Fig.1**), and to better understand their localization in the genome, we performed Chromatin Immunoprecipitation followed by Sequencing (ChIP-Seq) in 7-day-old WT Arabidopsis seedlings using these antibodies in addition to an antibody against H2A.Z.

When visualized with respect to all Arabidopsis coding genes, MBD9 and PIE1 localize mainly upstream of the transcription start site (TSS) in the nucleosome-depleted region (NDR), while H2A.Z enrichment begins at the first nucleosome downstream of the TSS (+1 TSS nucleosome) (**Fig. 1a**). On average, H2A.Z enrichment begins at the +1 nucleosome, but this enrichment skews to cover whole gene bodies in facultatively repressed genes [16,23,41]. Genes therefore fall into one of two k-means clusters depending on their H2A.Z profile; gene body H2A.Z (**Fig. 1b,** 'C1') and +1 TSS H2A.Z (**Fig. 1b,** 'C2'). Interestingly, we see that C1 genes, which have the most H2A.Z relative to C2, have the least SWR1 associated proteins MBD9 and PIE1 (**Fig. 1b**). When investigating other histone PTMs associated with these two clusters, we see that C2 associates with PTMs implicated in active transcription, such as H3K14ac and H3K9ac while C1 is associated with with H3K27me3, a PTM deposited by PRC2 that often marks facultative heterochromatin (**Fig. 1c**). Gene ontology (GO) analysis shows that C1 has more significantly enriched terms associated with environmental responsiveness compared to C2 (**Fig. 1d**).

The lack of a strong correlation between H2A.Z abundance and PIE1/MBD9 levels is surprising considering PIE1 is directly involved in H2A.Z deposition and absence of MBD9 affects H2A.Z deposition in *mbd9-1* mutants (**Fig. 1e**). It is unclear if the distinction between C1 genes and C2 genes in reference to their patterning of H2A.Z, PIE1, and MBD9 are based on

transcription status or are an inherent aspect of these genes. To better understand how the enrichment of these proteins changes during widespread transcriptional change, we identified a subset of genes in C1 that could be inducibly activated. Although many groups of response genes are enriched in C1, genes implicated in the response to the plant hormone Abscisic Acid (ABA) were one of the significantly enriched GO pathways (**Fig. 1d**). These genes therefore represented a group whose transcription status could be altered with the exogenous application of ABA, providing us with a tool to study subsequent changes in H2A.Z, MBD9 and PIE1 localization. To this end, we treated 7-day-old WT whole seedlings with either 10 μM ABA or a Mock treatment for 4 hours and performed RNA-Seq and ChIP-Seq against H2A.Z, MBD9 and PIE1.

Fig. 1

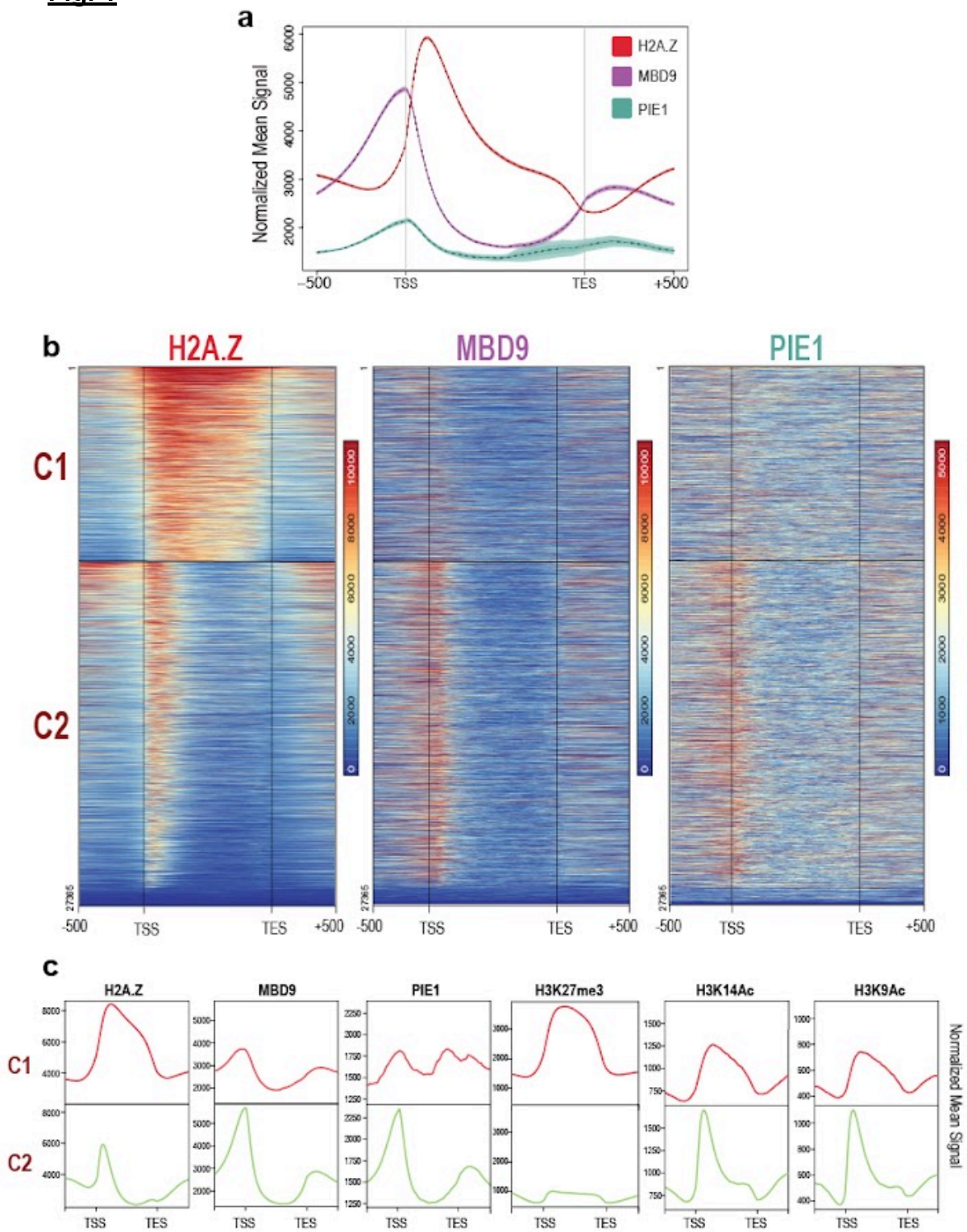
a
Normalized Mean Signal
H2A.Z
MBD9
PIE1
-500
TSS
TES
+500
b
H2A.Z
MBD9
PIE1
C1
C2
c
H3K27me3
H3K14Ac
H3K9Ac
Normalized Mean Signal

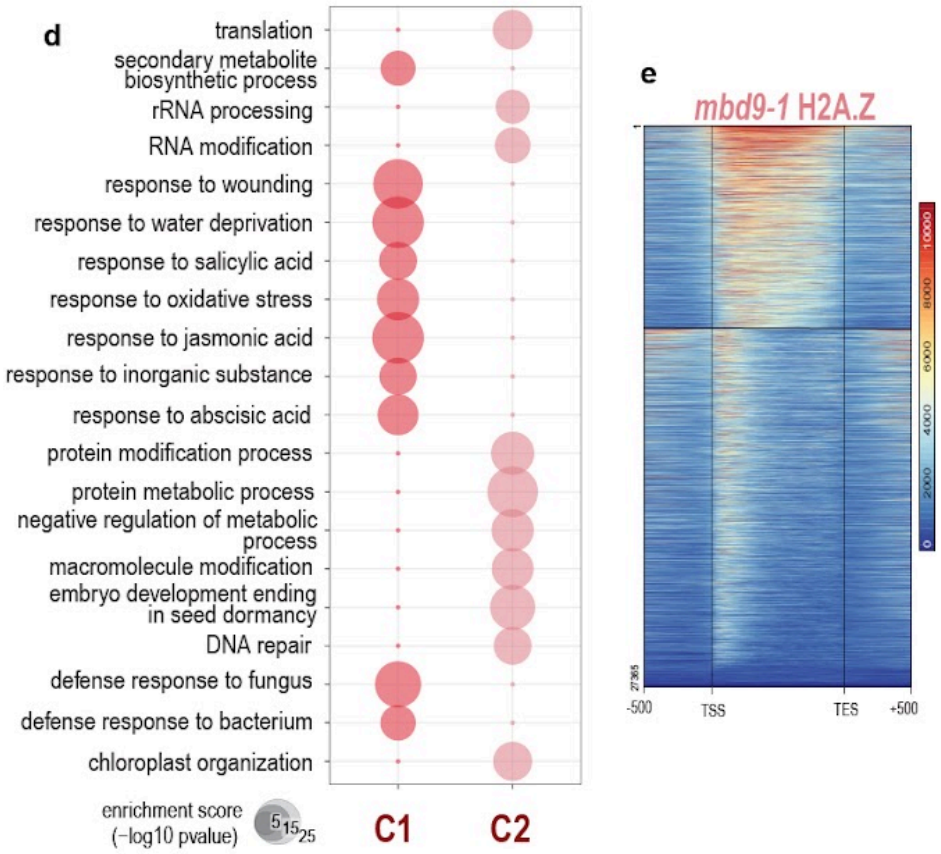

Fig. 1 H2A.Z, MBD9 and SWR1(PIE1) localization at steady state, and H2A.Z cluster definition **(a)** Average profile plot showing enrichment of H2A.Z (red), MBD9 (purple) and PIE1 (teal) in WT plants on all Arabidopsis genes plotted from their Transcription Start Site (TSS) to their Transcription End Site (TES) and 500 base pairs up and downstream. The y axis indicates the enrichment of these proteins normalized to Reads Per Kilobase Million (RPKM). MBD9 and PIE1 enrichment are centered on the TSS while H2A.Z enrichment is highest at the nucleosome just downstream of the TSS (+1 nucleosome). **(b)** Representative heatmaps showing the enrichment of H2A.Z, MBD9 and PIE1 on all Arabidopsis genes broken into two k-means clusters (C1 and C2) based on WT H2A.Z. Locations are analogous across all heatmaps. Color saturation indicates the strength of H2A.Z, MBD9 or PIE1 at given genes plotted from TSS to TES. C1 has a higher enrichment of H2A.Z but less MBD9 and PIE1 compared to C2. Regions

with high background are omitted. Data are RPKM normalized. **(c)** Average profile plots showing the enrichment of H2A.Z, MBD9, PIE1, H3K27me3, H3K14Ac, and H3K9Ac on genes in WT plants at genes in C1(top row) or C2 (bottom row). C1 has more H2A.Z and H3K27me3 while C2 has more MBD9, PIE1, H3K14Ac and H3K9Ac comparatively. Patterns indicate genes in C1 are facultatively repressed while C2 encompasses actively transcribed genes. Data are RPKM normalized. PTM plots derived from publicly available data from analogous tissue (see Methods). **(d)** Bubble plot showing the top ten most enriched Gene Ontology (GO) categories (Fisher's Exact Test, p-value <0.01) of C1 (red) and C2 (pink). Here, the size of each circle indicates the Enrichment Score (-log10 of p-value); the larger the circle, the more enriched the term. Only the top ten most enriched categories were shown here but there was no overlap in any significant terms across the two clusters. **(e)** Heatmap showing the enrichment of H2A.Z across C1 and C2 in *mbd9-1* plants. H2A.Z appears reduced in both C1 and C2 compared to WT.

Transcriptional induction by Abscisic Acid (ABA) Causes Subtle Loss of H2A.Z and Gains of PIE1 and MBD9

To verify induction, we first performed qRT-PCR against two established ABA response genes, COR15A and ANAC72, and found that our treatment was sufficient to induce significant transcript changes in these genes in WT plants (**Supp Fig. 2**). This significant change in transcript abundance was recapitulated in the RNA-seq, where we measured 3417 Differentially Expressed Genes (DEGs) (1.5 fold change over Mock, padj<0.05) (**Fig. 2a**). Genes directly involved in ABA response were overrepresented among these DEGs (**Fig. 2b**). Although the DEGs encompassed genes in both C1 and C2, the mean change in transcript abundance of C1 genes was significantly higher than changes in C2, indicating that C1 genes are more responsive to ABA (Welch Two Sample t-test, p=1.72E-19) (**Fig. 2c**).

Fig. 2

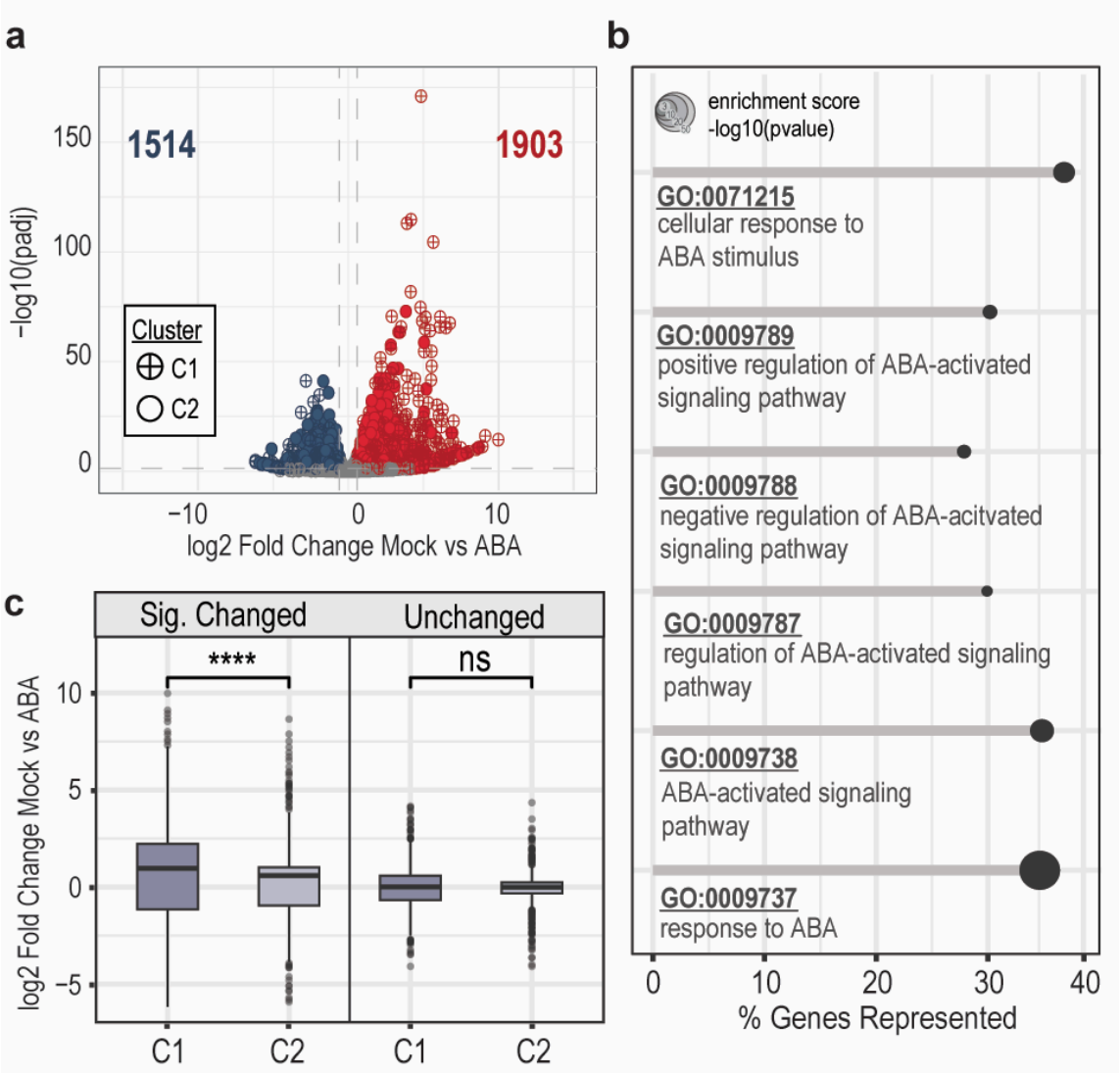

Fig. 2 RNA Response to ABA in WT seedlings **(a)** Volcano plot showing all 3417 Differentially Expressed Genes (DEGs) in WT Mock vs ABA treated plants as measured by DESeq2. 1903 genes were Upregulated with a log2 Fold Change (log2FC) greater than 0.6 and an adjusted p-value less than 0.05 (red), while 1514 genes were Downregulated with a log2FC less than -0.6 and an adjusted p-value less than 0.05 (blue). Genes in Cluster 1 (C1) visually make up a greater proportion of the most significantly upregulated genes (crossed points). Dashed lines

indicate p-value and log2FC significance thresholds. **(b)** Lollipop plot from GO Analysis of all DEGs shown in (a) displaying that several terms associated with ABA response are significantly enriched. GO names and brief descriptions are shown per category, and the length of the segment indicates the percentage of genes within that GO category represented in the 3417 DEGs. The size of the point indicates the enrichment score, calculated by taking the -log10 of the GO term p-value measured by Fisher's Exact Test. **(c)** Boxplots depicting the log2FC of significantly changed DEGs or a random selection of Unchanged genes stratified by Cluster. The means of the Unchanged genes are not statistically different (Welch Two Sample t-test, t= 0.432, df = 1494, p=0.666) while the significantly changed DEGs are significantly different between clusters (Welch Two Sample t-test, t= 9.123, df = 2006, p=1.72E-19), reinforcing that C1 genes have more pronounced transcriptional changes in response to ABA compared to C2 in WT plants.

ChIP-sequencing data also revealed changes in signal at the 1342 C1 DEGs after ABA treatment. These changes are most evident at the 813 C1 Upregulated genes (**Fig. 3a-3c**, middle panel), where there is a loss of H2A.Z enrichment and a simultaneous gain in MBD9 and PIE1 enrichment. The inverse is true at the 529 C1 Downregulated genes, where there is a slight gain in H2A.Z and a subtle loss of MBD9 and PIE1 in ABA-treated plants (**Fig. 3a-3c**, top panel). Importantly, these subtle changes were not observed in an equivalently-sized set of genes whose expression was not changed after ABA treatment (**Fig. 3a-3c**, bottom panel). These changes can also be observed on average plots of these three proteins across the different groups (**Fig. 3d**). Here we focus on C1 genes, but similar patterns are observed at C2 genes. See **Supp Fig. 3** for equivalent heatmaps showing the dynamics at C2 DEGs.

Surprisingly, there were only 24 genes genome wide that had a statistically significant change in H2A.Z after ABA treatment as measured by DESeq2, and 16 of these fell in C1

(adjusted p-value<0.05 and log2FC < -0.6 or >0.6) (**Fig. 3e**). More of the genes that lost H2A.Z belonged to C1 (14/19), and almost all of the genes that gained H2A.Z belonged to C2 (3/5). When layering our RNA-Seq and ChIP-Seq data, we found correlations between H2A.Z change, transcript abundance, and MBD9/PIE1 change upon ABA treatment (**Fig. 3f and 3g**). Of genes with differential H2A.Z enrichment after ABA treatment, the genes with gains in transcript correlated with loss of H2A.Z, and the genes with loss of transcript correlated with gain of H2A.Z. When MBD9 and PIE1 are considered, we also see that they are recruited most strongly to the genes that gain transcript and lose H2A.Z (**Fig. 3f and 3g**). This pattern is also observed on a gene-by-gene basis upon examination of two genes with significantly changed H2A.Z (**Fig. 3h**). These correlations suggest that the level of H2A.Z is a reflection of the balance between nucleosome disruption by transcription machinery and subsequent re-incorporation of H2A.Z by SWR1 at these inducible genes, with MBD9 potentially playing a role in this process. It is also notable that the original gene body enrichment of H2A.Z on C1 genes is maintained after transcriptional change. The abundance of H2A.Z increases or decreases, but it is still localized across the gene body and does not convert to TSS-proximal H2A.Z enrichment (**Fig. 3h**).

Fig. 3

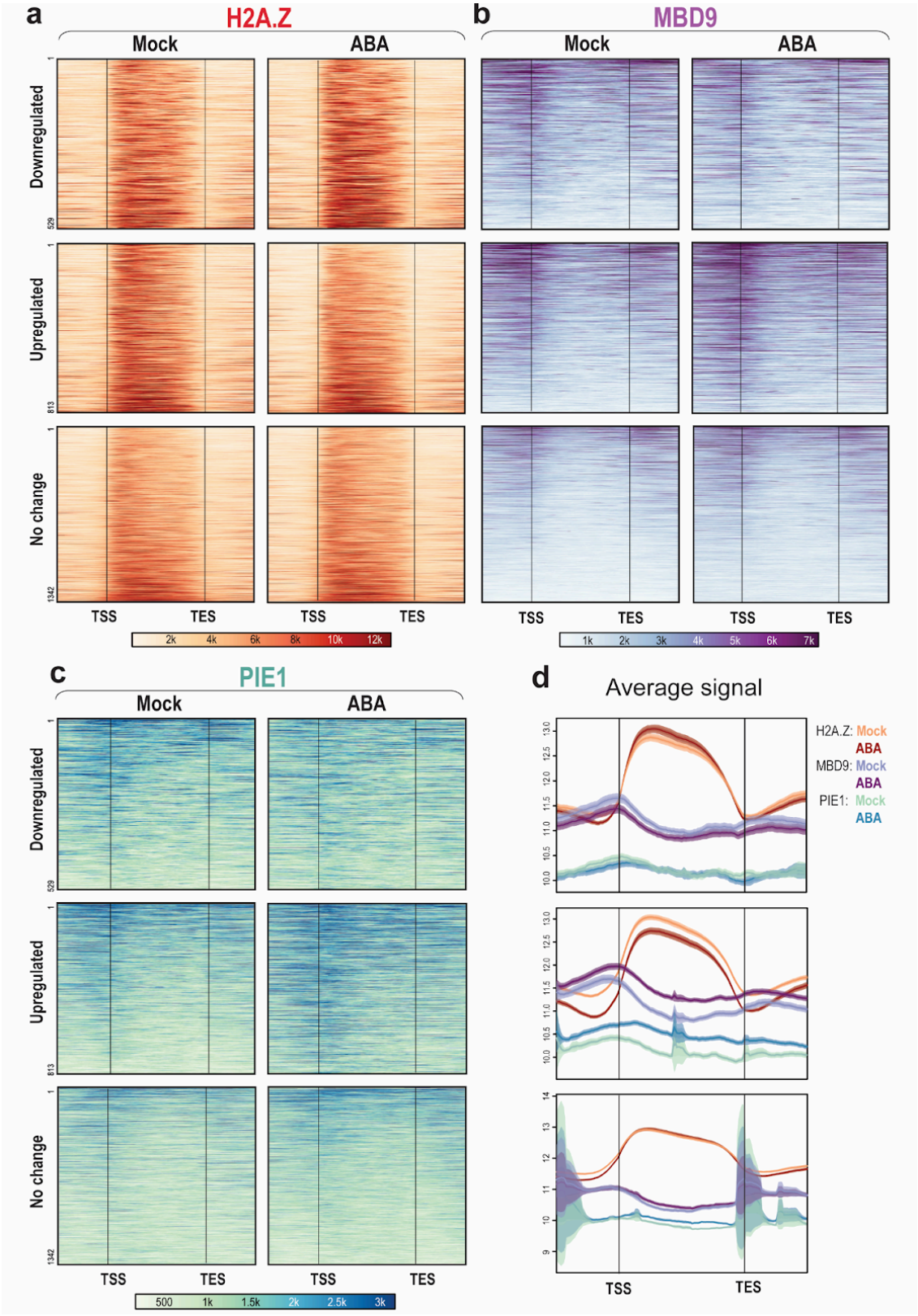
a
H2A.Z
Mock
ABA
Downregulated
Upregulated
No change
1
529
813
1342
TSS
TES
2k
4k
6k
8k
10k
12k
b
MBD9
1k
2k
3k
4k
5k
6k
7k
c
PIE1
500
1k
1.5k
2k
2.5k
3k
d
Average signal
H2A.Z: Mock
ABA
MBD9: Mock
ABA
PIE1: Mock
ABA

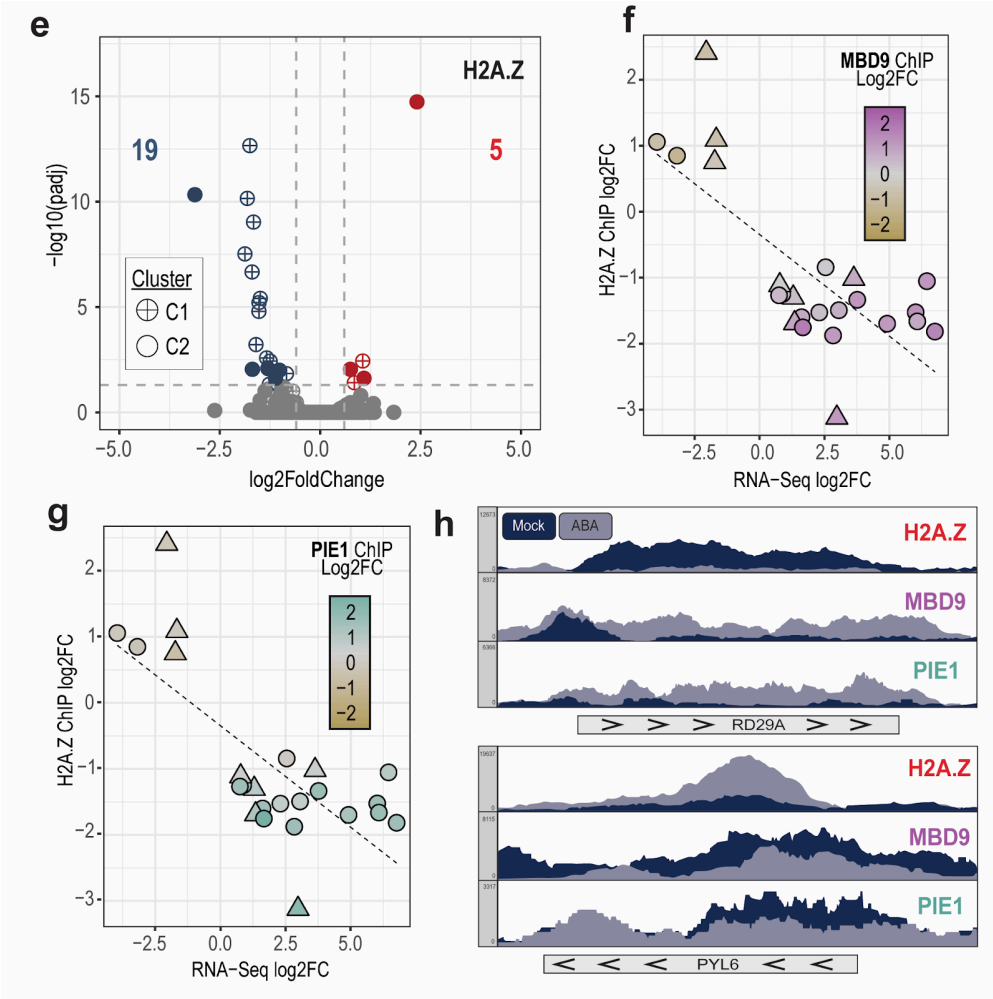

Fig. 3 Chromatin dynamics in ABA-treated WT seedlings **(a)** Representative heatmaps showing H2A.Z enrichment on 529 Downregulated DEGs (Top panel), 813 Upregulated DEGs (Middle panel) and 1342 C1 genes with no significant change in transcript abundance after ABA treatment (Bottom panel). Enrichment is plotted from the Transcription Start Site (TSS) to the Transcription End Site (TES) +/- 0.5 kb. At Upregulated genes, there is a loss of H2A.Z enrichment and a gain of MBD9 and PIE1 as shown in similar representative heatmaps in **(b)** and (**c).** All data are RPKM normalized. **(d)** Average plots showing the average signal of all genes at Downregulated (Top panel), Upregulated (Middle panel), and genes with No Change (Bottom panel). RPKM Signal from all genes is averaged and plotted on a log2 scale from their TSS to TES +/- 0.5 kb. **(e)** Volcano plot showing 24 genes differentially enriched in H2A.Z as

measured by DESeq2 in Mock vs ABA treated plants. 16 genes belong to C1 (crossed points) while 8 belong to C2 (solid points). Blue points show the 19 genes that lost H2A.Z with ABA treatment (log2FC < -0.6 and adjusted p-value<0.05) and red points show the 5 genes that gained H2A.Z with ABA treatment (log2FC>0.6 and an adjusted p-value< 0.05, red points). 14 and 2 of the H2A.Z lost and H2A.Z gained genes belonged to the C1 cluster, respectively. **(f)** 24 genes with differential H2A.Z enrichment (y-axis) correlated with RNA-seq expression (x-axis) and enrichment of MBD9 (color). There is a negative correlation between H2A.Z and transcript changes in Mock vs ABA treated plants. Genes that lose H2A.Z and increase in transcript also have the highest gain of MBD9. **(g)** shows the same trends with PIE1 changes. **(h)** Integrative Genomics Viewer (IGV) snapshots of ChIP-seq data at two genes illustrating patterns of H2A.Z, MBD9 and PIE1 changes. *RD29A (AT5G52310)* shows a loss of H2A.Z and a gain of MBD9 and PIE1 in ABA treated plants, while the *PYL6 (AT2G40330)* gene shows a gain of H2A.Z and a loss of MBD9 and PIE1 signal. Both genes belong to Cluster 1 (C1).

The MBD9 Bromodomain is Dispensable to H2A.Z Localization

Based on these observations, we hypothesized that MBD9 is recruited to newly activated ABA responsive genes through its Bromodomain, which has been shown previously to associate with acetylated histone residues characteristic of active transcription including H3K14Ac and H3K18Ac [37] . To assess the contribution of the MBD9 Bromodomain, we aimed to specifically disrupt the Bromodomain function without affecting other domains. MBD9 has several putative domains other than its acetyl lysine-binding Bromodomain including two methyl-binding Plant HomeoDomains (PHD), and a Williams-beuren Syndrome DDT (WSD) domain that may mediate interactions with Imitation SWItch (ISWI) type chromatin remodelers (**Fig. 4a**) [38,40]. MBD9 is also one of 13 family members in Arabidopsis that contain a Methyl-CpG

Binding Domain (MBD). Normally, this domain facilitates interactions with methylated DNA, but MBD9 contains several point mutations in its MBD sequence that prevent this function [42,43].

Aspartic acid 1209 of MBD9 is a well-conserved residue that spans various bromodomain-containing proteins (**Supp Fig 4**), and was previously shown to be necessary for its acetyl lysine-binding function *in vitro* [37]. We mutated this Aspartic Acid 1209 to an Alanine (D1209A) in the MBD9 sequence through site-directed mutagenesis and established stable Arabidopsis lines expressing D1209A MBD9 in the null *mbd9-1* background (D1209A plants). At the phenotypic level, we see that D1209A plants do not show an early flowering phenotype characteristic of plants lacking MBD9. D1209A plants had significantly more leaves at flowering compared to *mbd9-1* plants (Welch Two Sample t-test, p=8.84E-12) (**Fig. 4b**). Western blotting of chromatin-associated proteins from 7-day-old D1209A plants also demonstrates that D1209A MBD9 rescues the ability of H2A.Z to be incorporated into chromatin compared to *mbd9-1* plants (**Fig. 4c**). ChIP-s against MBD9, PIE1 and H2A.Z in D1209A plants at steady state and after treatment with ABA revealed that the vast majority of MBD9, PIE1 and H2A.Z sites were unchanged from WT as measured by DESeq2 both at steady-state and during an ABA response (**Fig. 4d**). D1209A plants also show no significant difference in germination rate on ABA-containing media compared to WT and *mbd9-1* plants (**Fig. 4e**). Taken together, these results demonstrate that the Bromodomain of MBD9 is likely dispensable for its effect in H2A.Z localization.

Fig. 4

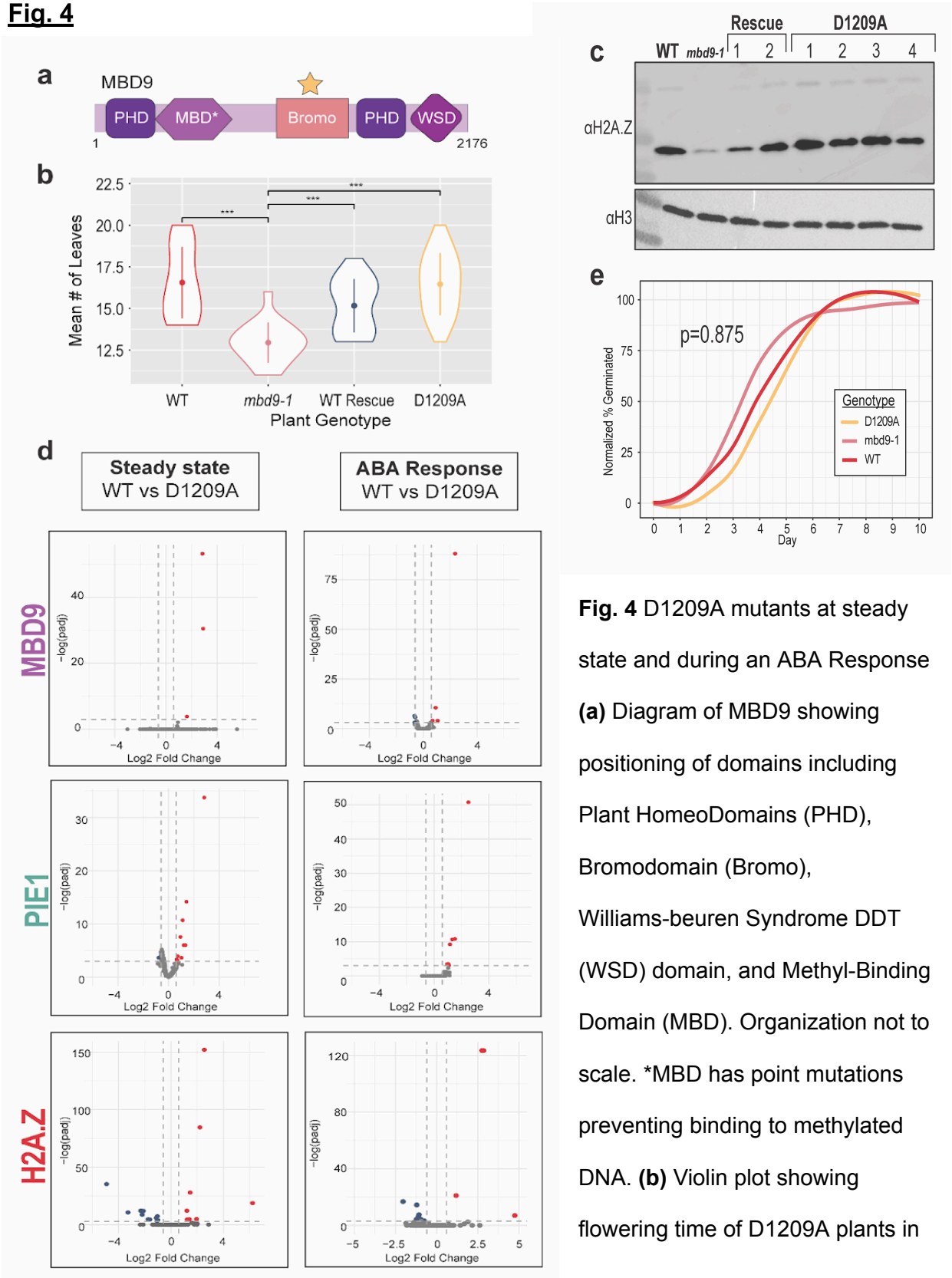

Fig. 4 D1209A mutants at steady state and during an ABA Response **(a)** Diagram of MBD9 showing positioning of domains including Plant HomeoDomains (PHD), Bromodomain (Bromo), Williams-beuren Syndrome DDT (WSD) domain, and Methyl-Binding Domain (MBD). Organization not to scale. *MBD has point mutations preventing binding to methylated DNA. **(b)** Violin plot showing flowering time of D1209A plants in

reference to WT, plants lacking MBD9 (*mbd9-1*), and plants rescued with WT MBD9 (WT Rescue). *mbd9-1* plants flower early compared to WT plants (Welch Two Sample t-test, t=-6.2125, df= 26.819,p=1.25E-06). Supplementation with WT MBD9 rescues early flowering (Welch Two Sample t-test, t=-5.1115, df= 39.994,p=8.30E-06), and D1209A plants rescue early flowering (Welch Two Sample t-test, t=9.0273, df= 46.365, p=8.84E-12). Mean values for WT Rescue and D1209A plants represent the average across two or four independent insertion lines, respectively. ***= p-value<0.001**(c)** Western blot of chromatin associated proteins for four independent D1209A lines show more H2A.Z compared to *mbd9-1*. Two independent WT Rescue lines also show more H2A.Z incorporation compared to *mbd9-1*. H3 shown as a loading control. **(d)** Volcano plots showing differences in the localization of MBD9 (top), PIE1 (middle) and H2A.Z (bottom) in WT vs D1209A plants. Blue points are genes with less H2A.Z in D1209A plants (log2 Fold Change< -0.6, adjusted p-value<0.05) and red points are genes that gain H2A.Z in D1209A plants (log2 Fold Change>0.6, adjusted p-value< 0.05). Plots on the left show differences at steady state while plots on the right are during an ABA response. There are few differentially enriched genes in any of these conditions. **(e)** Line graph depicting the germination efficiency of D1209A plants on ABA-containing media compared to WT and *mbd9-1* plants over time. The number of germinated seeds is expressed as a percentage of total seeds over the course of 10 days, normalized to the genotype germination on unsupplemented ½ MS media. Average across two independent germination experiments shown. There was no significant effect of genotype on germination efficiency (ANOVA, f=0.134, df=2, p=0.875).

Loss of MBD9 does not affect Transcriptional ABA Responsiveness

To further assess if MBD9 is required for ABA-driven changes in transcription, we also performed RNA-Seq and ChIP-seq against PIE1 and H2A.Z in Mock and ABA treated plants completely lacking MBD9 (*mbd9-1*). Comparison of Mock treated WT and *mbd9-1* plants revealed that only 184 genes are differentially expressed on a genotype basis alone (**Fig. 5a**).

mbd9-1 plants have a robust transcriptional response to ABA, with 1950 genes being Upregulated and 1716 genes being Downregulated compared to Mock Treatment (**Fig. 5b**). Overall, 75% of *mbd9-1* significantly Upregulated genes and 59% of *mbd9-1* significantly Downregulated genes are conserved between *mbd9-1* and WT in response to ABA (**Fig. 5c**). Although there are 'uniquely' Upregulated and Downregulated genes specific to each genotype, direct correlation of changes at these genes reveals that *mbd9-1* and WT responses trend similarly but do not reach statistical significance in one genotype (**Supp Fig 5**). Focusing on WT DEGs, we see that *mbd9-1* and WT changes in response to ABA are strongly correlated, but with WT changes slightly more elevated in both the negative and positive directions (**Fig. 5d**). This trend is evident at both C1 and C2 genes separately, though the mean change between clusters is not statistically significant (**Fig. 5e**).

Fig. 5 (below) *mbd9-1* vs WT RNA response to ABA treatment **(a)** Volcano plot showing differentially expressed genes (DEGs) in WT vs *mbd9-1* Mock treated plants, identifying genes that are differentially expressed on a genotype basis. Blue points show genes downregulated in *mbd9-1* (log2 Fold Change< -0.6, adjusted p-value<0.05) while red points show genes upregulated in *mbd9-1* (log2 Fold Change>0.6, adjusted p-value< 0.05, red points). There are 45 and 139 Downregulated and Upregulated genes, respectively. **(b)** Volcano plot showing differentially expressed genes (DEGs) in mbd9-1 Mock vs *mbd9-1* ABA treated plants. *mbd9-1* shows 1716 downregulated genes (log2 Fold Change< -0.6, adjusted p-value<0.05) and 1950 upregulated genes (log2 Fold Change>0.6, adjusted p-value< 0.05). **(c)** Direct comparison of DEGs in WT plants vs *mbd9-1* plants. The majority of up and downregulated genes are conserved across genotypes, but unique subsets exist in each genotype. See **Supp Fig. 5** for more info on these groups. **(d)** Scatter plot correlating RNA-Seq Log2 FoldChanges between WT and *mbd9-1* plants at WT DEGs during ABA response. The dashed red line indicates a hypothetical 1:1 relationship between WT and *mbd9-1* responses while the solid red line

indicates the linear regression of the data. The R^2 value between the groups is 0.866, indicating a strong relationship between WT and *mbd9-1* response. C1 genes are denoted by crossed points whereas C2 genes are denoted by uncrossed points. **(e)** Boxplots depicting log2FoldChanges of RNA changes in ABA vs Mock treated samples across WT and *mbd9-1* plants, stratified by Cluster. Cluster 1 (left) genes show slightly tempered changes compared to WT plants, but these changes do not reach statistical significance (Welch Two Sample t-test, t=0.21, df=2665, p=0.835). The same is observed at Cluster 2 (right) (Welch Two Sample t-test, t=-0.35, df=4111, p=0.725).

Fig. 5

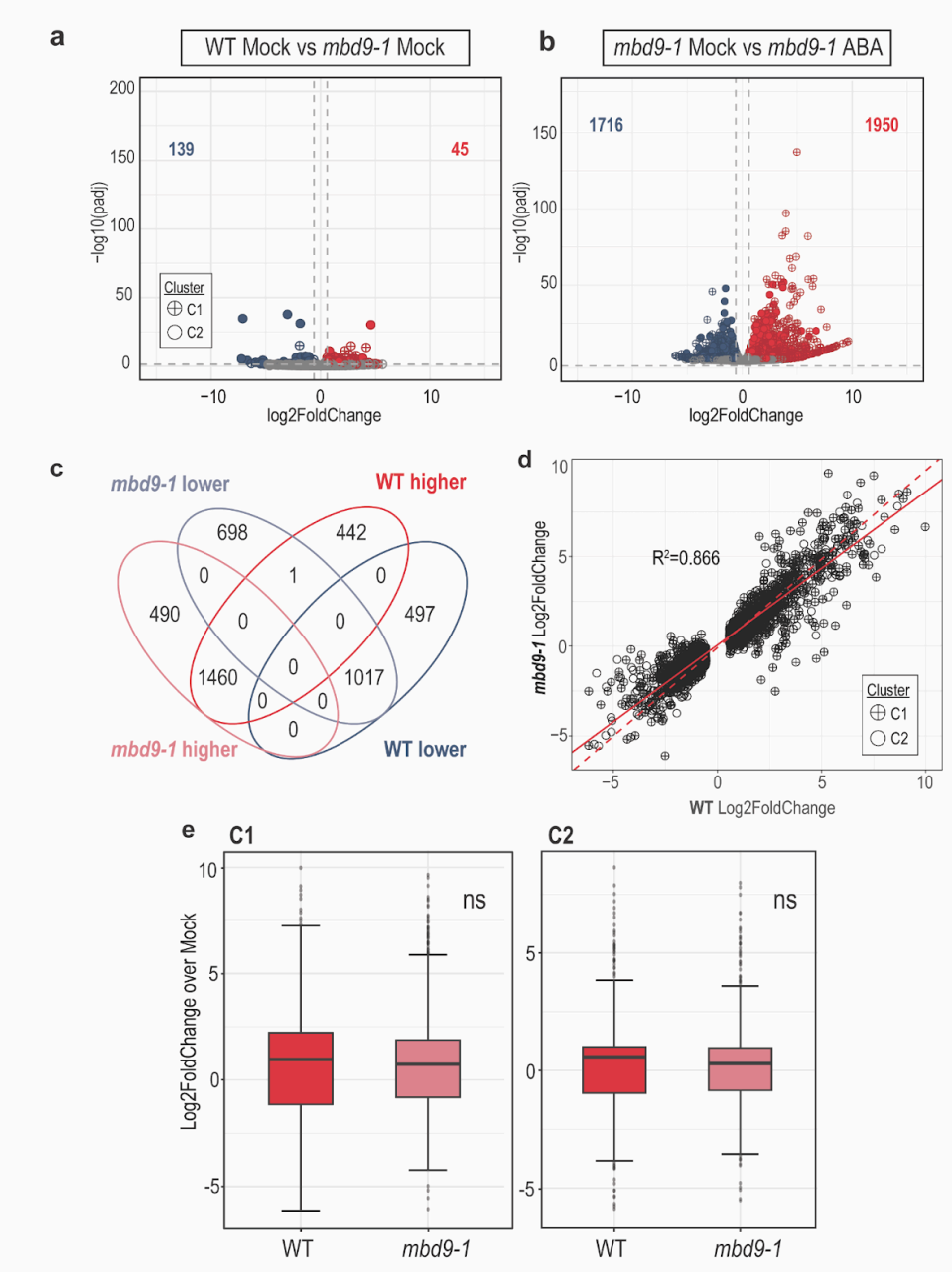

At the chromatin level, we see that mbd9-1 plants, although they start with less H2A.Z at genes than WT (compare Fig. 1b and 1e), still lose H2A.Z from ABA Upregulated genes as in WT plants (**Fig. 6a**, middle panel). Similarly, the ABA Downregulated genes gain H2A.Z in ABA-treated mbd9-1 plants (**Fig. 6a**, top panel). Also similar to WT, PIE1 levels increase specifically at ABA Upregulated genes in mbd9-1 (**Fig. 6b**, middle panel). These changes are also evident on average (**Fig. 6c**). When directly comparing average PIE1 changes at ABA upregulated genes, it is apparent that while mbd9-1 plants may start with slightly less PIE1 at upregulated genes, the gain in PIE1 during ABA treatment is equivalent to gains in WT plants (**Fig 6d**). Compared to only 24 genes in WT, mbd9-1 shows 220 genes differentially enriched in H2A.Z after ABA treatment compared to Mock treatment, with the genes losing the most H2A.Z belonging to C1 (**Fig. 6e**). When correlating the significant chromatin changes with RNA-Seq data, we see the genes that gain the most transcript lose the most H2A.Z and gain the most PIE1 in mbd9-1 plants (**Fig. 6f**), as observed in WT plants.

These data suggest that transcription rate determines the amount of H2A.Z lost, and not vice versa. To more directly rule out the possibility that the starting amount of H2A.Z affects the induction potential of genes, we isolated a set of 646 genes that have significantly less H2A.Z in mbd9-1 Mock treated plants compared to WT Mock treated plants (**Fig. 6g**). If the amount of H2A.Z affects the induction or repression of these genes, we should see that transcript levels in mbd9-1 plants, which have significantly less H2A.Z at these genes, should change less substantially after ABA treatment compared to WT. Instead, we see that the distributions of log2 Fold Changes of these genes' transcripts are not statistically different after ABA treatment, supporting the notion that the reduced amount of H2A.Z does not affect the induction potential of these genes (**Fig. 6h**).

Fig. 6

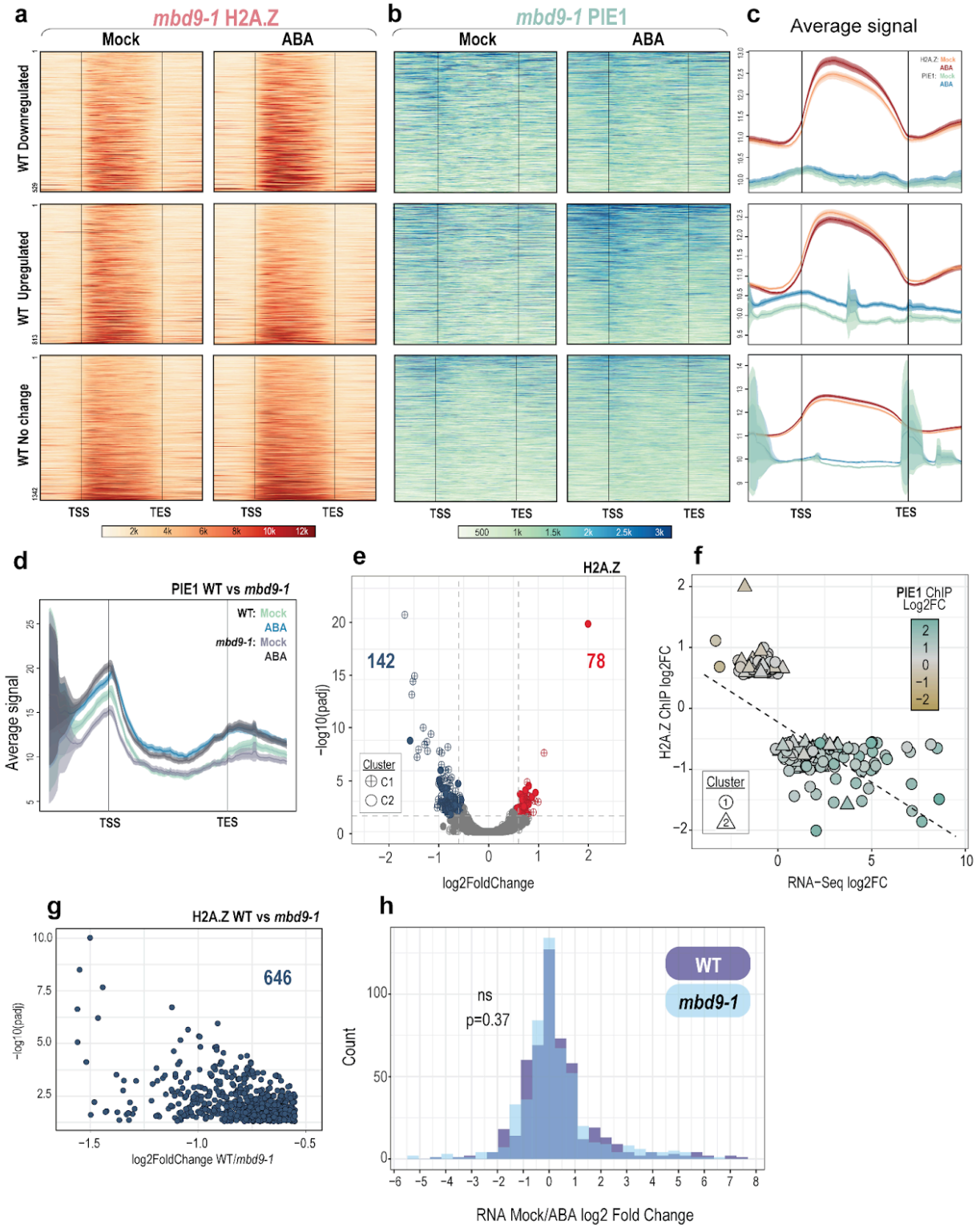
a
mbd9-1 H2A.Z
Mock
ABA
WT Downregulated
WT Upregulated
WT No change
TSS
TES
b
mbd9-1 PIE1
c
Average signal
d
PIE1 WT vs mbd9-1
WT: Mock
ABA
mbd9-1: Mock
ABA
Average signal
e
H2A.Z
142
78
−log10(padj)
log2FoldChange
Cluster
C1
C2
f
PIE1 ChIP Log2FC
H2A.Z ChIP log2FC
RNA−Seq log2FC
g
H2A.Z WT vs mbd9-1
646
log2FoldChange WT/mbd9-1
h
WT
mbd9-1
ns
p=0.37
Count
RNA Mock/ABA log2 Fold Change

Fig. 6. ABA-treated *mbd9-1* plants show similar trends in chromatin dynamics. (a) Representative heatmaps showing RPKM normalized H2A.Z enrichment on genes from Fig. 3: 529 Downregulated (Top panel), 813 Upregulated (Middle panel) and 1342 C1 genes with no significant transcript change after ABA treatment (Bottom panel). Enrichment plotted from the Transcription Start Site (TSS) to the Transcription End Site (TES). *mbd9-1* plants show a similar trend, where Upregulated genes lose H2A.Z after ABA treatment and downregulated genes gain H2A.Z.**(b)** Representative heatmaps of PIE1 enrichment over the same areas as **(a)**. PIE1 signal still increases after ABA treatment at Upregulated genes (middle panel).**(c)** Average plots depicting H2A.Z and PIE1 signal at genes that are Downregulated (Top panel), Upregulated (Middle panel), and genes with No Change (Bottom panel). RPKM Signal from all genes is averaged and plotted on a log2 scale from TSS to TES. **(d)** Average plots directly comparing average PIE1 changes at Upregulated genes in WT vs *mbd9-1* plants. *mbd9-1* PIE1 signal at upregulated genes is roughly equivalent in ABA treated conditions. RPKM Signal from all genes is averaged and plotted on a log2 scale from TSS to TES.. **(e)** Volcano plot showing 220 genes differentially enriched in H2A.Z as measured by DESeq2 in Mock vs ABA treated *mbd9-1* plants. 142 genes lose H2A.Z (log2 Fold Change< -0.6, adjusted p-value<0.05, blue) and 78 genes gain H2A.Z with ABA treatment (log2 Fold Change>0.6, adjusted p-value< 0.05, red). **(f)** 220 genes with differential H2A.Z (y-axis) correlated with RNA-Seq expression (x-axis) and abundance of PIE1 (color). The negative correlation between H2A.Z and transcription and positive correlation with PIE1 is maintained in *mbd9-1*. **(g)** Scatter plot showing 646 genes with lower H2A.Z in *mbd9-1* plants compared to WT (padj<0.05, log2FoldChange<-0.6). **(h)** Histogram showing that the 646 genes from **(g)** change similarly in transcript abundance over Mock in WT (purple) vs *mbd9-1* plants in response to ABA (Student's t-test, t=0.89904, df= 1010, p=0.3688), indicating that although these genes have less H2A.Z to start with in *mbd9-1* plants, it does not affect their responsiveness during a stress response.

Discussion

By utilizing new antibodies against SWR1 component PIE1 and associated protein MBD9, we examined the relationships between H2A.Z, MBD9, SWR1, and transcription in plants. We demonstrated that at steady state, the genes most enriched with H2A.Z (C1) have the least amount of SWR1 (PIE1) and MBD9 binding (**Fig 1a-1c**). One explanation for this phenomenon is simply that C1 genes, which encompass genes marked with H3K27me3, are not heavily transcribed under standard physiological conditions. Thus, without transcription machinery consistently disrupting these genic, stable nucleosomes, nucleosome turnover is low and there is no impetus for SWR1 to replace the H2A.Z-containing nucleosomes lost during transcription. At the more constitutively expressed C2 genes, which have TSS-proximal H2A.Z, nucleosomes are more unstable and require sustained presence of SWR1 to maintain H2A.Z enrichment. Transcript count data from Mock treated plants here and publicly available Global Run-on Sequencing (Gro-Seq) data from analogous tissue support this hypothesis [53]; C1 genes have significantly fewer counts than C2 genes in these datasets (**Supp. Fig. 6**).

To understand how PIE1 and MBD9 localizations change after activation of genes with gbH2A.Z (C1 genes), we employed ABA as a widespread transcriptional modulator to assess if changes to transcription in a subset of C1 genes led to altered recruitment of core SWR1 component PIE1 and known interacting protein MBD9. In WT plants, we saw that the genes with the highest gains in transcript abundance had the largest loss of H2A.Z and highest gains of MBD9 and PIE1 (**Fig. 3f and 3g**). This suggests that when these formerly silenced genes are activated transcriptionally, the SWR1 complex is recruited to replace the H2A.Z lost by transcription, thereby maintaining H2A.Z presence on these genes.

While the majority of H2A.Z at ABA response genes appeared unchanged after induction, it is likely that these ‘unchanged’ genes underwent constant transcription-driven loss

and SWR1-driven replacement of H2A.Z. We hypothesize that at these unchanged sites, SWR1 deposited H2A.Z at a rate closely matching the rate of H2A.Z loss caused by transcription. However, at the genes with the largest upregulation of transcription, the SWR1 complex could not keep up with the rate of H2A.Z dissociation from genes and these 19 genes significantly lost H2A.Z (**Fig. 3e**). This hypothesized high turnover of H2A.Z could then also result in exchange of repressive monoubiquitinated H2A.Z for unmodified H2A.Z by SWR1, potentially contributing to depression of these genes [29]. The phenomenon of gbH2A.Z retention during transcriptional activation of silent genes was also recently observed for phosphate-starvation induced genes in Arabidopsis root hair cells[54]. These results indicate that net H2A.Z removal from chromatin is not strictly required for transcriptional activation. This is in contrast to previous studies showing that H2A.Z removal by the chromatin remodeler INO80 is necessary for induction of environmental response genes including those responsive to temperature, far-red light, and ethylene [38–40,55]. Collectively, these results suggest the existence of both INO80-dependent and -independent pathways for activation of silent gbH2A.Z/H3K27me3 genes. While some genes may require H2A.Z removal for activation, others such as ABA responsive genes instead seem to require SWR1 recruitment to retain gbH2A.Z.

Our data also showed that MBD9, which was previously shown to interact with the SWR1 complex, was also recruited to newly activated genes. Based on this observation, we asked whether the Bromodomain of MBD9 was important for this recruitment, and perhaps that of SWR1. We used a mutation that was shown previously to hinder the ability of the MBD9 Bromodomain to bind acetylated histone peptides *in vitro* [47], but demonstrated that this mutation has little effect on plants *in vivo*. We saw that the D1209A Bromodomain mutant MBD9 can rescue the early flowering phenotype of *mbd9-1* plants (**Fig. 4b**). This recapitulated flowering time experiments performed on Bromodomain mutants previously, where Arabidopsis *mbd9-1* plants supplemented with an MBD9 harboring the D1209A mutation in combination with E1208A

showed rescue of *mbd9-1* early flowering [48]. We also found that at the molecular level, this mutation had little effect on the localization of MBD9, PIE1 or H2A.Z on genes either at steady state or when responding to ABA (**Fig. 4d**). If the Bromodomain is truly dispensable for the role of MBD9 in H2A.Z localization, it is in contradiction to a previous model that posits MBD9, binds to acetyl marks through its Bromodomain as a way to anchor the SWR1 complex for H2A.Z deposition [47]. This model, however, also suggests that another bromodomain-containing protein NPX1, which is partially conserved with yeast BDF1, acts redundantly with MBD9 in this SWR1 anchoring. NPX1 may be able to compensate for MBD9 Bromodomain loss in the context of this study. Alternatively, the MBD9 Bromodomain could mediate interactions with acetylated histones but this is not relevant to H2A.Z localization. Future work with MBD9 will uncover whether other domains are necessary for its role in proper H2A.Z localization and explore the role of the MBD9 Bromodomain in functions outside of the SWR1 complex.

To further assess the role of MBD9 during transcriptional activation, we determined how plants lacking MBD9 (*mbd9-1*) responded to ABA. Under steady state, it was previously reported that *mbd9-1* plants do not have widespread de-repression of response genes [50]. Our results support this as well; we measured only 184 genes as differentially expressed in *mbd9-1* plants compared to WT on a genotype basis alone (**Fig. 5a**). We also demonstrated that *mbd9-1* plants effectively responded to ABA, with the majority of genes induced similarly in *mbd9-1* compared to WT (**Fig. 5d**). While loss of MBD9 did not drastically affect plants' transcriptional response to ABA, trends at both C1 and C2 genes suggest that *mbd9-1* plants may not be able to induce or repress genes as effectively as in WT plants (**Fig. 5e**). These subtle changes in transcriptome response could be attributable to the reported role of MBD9 in the ISWI complex [48]. MBD9 likely serves as a bridge between remodelers, so without its presence, ISWI would not be recruited to newly activated genes to help retain newly deposited H2A.Z in chromatin. This could lead to the subtle changes in transcription dynamics of these genes with high nucleosome turnover after induction.

At the chromatin level, *mbd9-1* plants behaved similarly to WT in regard to H2A.Z and PIE1 localization. Although *mbd9-1* plants had less H2A.Z at genes on average, there was still a subtle loss of H2A.Z from upregulated genes, and a subtle gain of H2A.Z at downregulated genes (**Fig. 6a**). Interestingly, the absence of MBD9 did not inhibit SWR1 recruitment to ABA-upregulated genes (**Fig. 6b**), indicating that it is not the major targeting factor for SWR1 in this context. This is further reinforced by direct comparison of PIE1 changes in WT and *mbd9-1* plants; PIE1 was gained in ABA treated *mbd9-1* plants to the same degree as in WT (**Fig. 6d**). Instead, specific transcription factors or even the transcription machinery could directly recruit chromatin remodelers such as SWR1 to newly activated genes. A recent study demonstrated that the BAF complex is recruited by RNA Pol II upon transcriptional change in mouse embryonic stem cells [56]. It is also interesting to note that *mbd9-1* plants, which have less H2A.Z on average, did not show widespread differences in gene expression upon ABA activation compared to WT plants (**Fig. 6h**). This indicates that while H2A.Z contributes to a repressive state, the degree of H2A.Z loss in *mbd9-1* is not sufficient to derepress genes or change their responsiveness to a great extent.

We also saw that the profiles of gbH2A.Z were actively maintained in the face of transcriptional activation by ABA. It has been proposed that the two distinct profiles of H2A.Z, TSS-proximal H2A.Z (C2) and gbH2A.Z (C1) may be interconvertible. Genes with gene body H2A.Z, once activated, will shift to having TSS-proximal H2A.Z enrichment, and then revert to having gbH2A.Z after repression is re-established [27,57,58]. Here, however, changes to H2A.Z within each cluster reflected the original profile. C1 genes with lower H2A.Z after ABA treatment lost H2A.Z across the gene body, and genes with higher H2A.Z gained H2A.Z over the gene body (**Fig. 3d and Fig. 6c**). Similarly, C2 genes both gained and lost H2A.Z at TSS-proximal nucleosomes after ABA treatment on average (**Supp. Fig 3**). These results are consistent with similar studies analyzing H2A.Z distribution in Arabidopsis during drought stress [27]. Clearly the cell is utilizing energy to maintain these two distinct profiles of H2A.Z, possibly highlighting that

TSS-proximal H2A.Z and gbH2A.Z are distinct pools with separate functions that do not reflect current transcription rate as accurately as previously thought.

In summary, by tracking SWR1 component PIE1 and interactor MBD9, we gained new insights into the roles of these proteins in H2A.Z maintenance during a widespread transcriptional activation event. Surprisingly, at steady state we saw that genes with the most H2A.Z had the least amount of SWR1 component PIE1 and interactor MBD9. After treating plants with ABA, we saw that PIE1 and MBD9 move to newly induced genes, with the genes losing the most H2A.Z gaining the most PIE1 and MBD9. This indicates that SWR1 moved to activated genes to replace H2A.Z-containing nucleosomes lost by transcription. Although MBD9 was recruited to newly activated genes, its presence was largely not necessary for PIE1 recruitment or a normal transcriptional response to ABA. This indicates that MBD9 does not serve as a general SWR1 targeting factor, but instead may be necessary for full functionality of the SWR1 complex or could affect H2A.Z occupancy indirectly through ISWI-related functions.

Methods

Plant growth conditions

All *Arabidopsis thaliana* plants described are of the Columbia (Col-0) ecotype, and Col-0 was used as a wild type (WT) reference. Described mutants obtained from ABRC include *mbd9-1* (SALK_054659) and *pie1-5* (SALK_053834C). Seeds were sown on half-strength Murashige and Skoog (MS) media plates or soil and stratified at 4°C for 72 hours. After stratification, plants were moved to growth chambers at 20˚C under a 16 hour light/8 hour dark cycle under 181 µmol m^{-2} s^{-1} PPFD light intensity. Unless otherwise noted, plated plants were grown approximately 7 days and whole seedling shoot tissue (above ground tissue only) was collected at approximately 9 hours after artificial dawn for use in downstream experiments.

Antibody Development

Polyclonal antibodies against Arabidopsis proteins PIE1 (AT3G12810) and MBD9 (AT3G01460) were made using services from GenScript. The MBD9 protein fragment 'MEPSILKEVGEPHNSSYFADQMGCDPQPQEGVGDGVTRDDETSSTAYLNKNQGKSPLETDTQ PGESHVNFGESKISSPETISSPGRHELPIADTSPLVTDNLPEKDTSETLLKSVGRNHETHSPNSN AVELPTAHDASSQASQELQACQQDLSATSNEIQNLQQSIRSIESQLLKQSIRRDFLGTDASGRLY WGCCFPDENPRILVDGSISLQKPVQADLIGSKVPSPFLHTVDHGRLRLSPWTYYETETEISELVQ WLHDDDLKERDLRESILWWKRLRYGDVQKEKKQAQNLSAHHHHHH' was expressed recombinantly and the PIE1 peptide fragment 'CEEIRKAVFEERIQESKDRAAAI' was synthesized for use as antigens in polyclonal antibody production in rabbits.The antibodies were antigen affinity purified by the manufacturer and verified here through Western Blotting (**Supp. Fig. 1**). Additionally, an identical MBD9 peptide was used as an antigen for antibody production previously [47].

MBD9 BromoDomain (D1209A) Mutant Generation

The genomic sequence of MBD9 under its native promoter (2kb upstream of TSS) was cloned into pDONR221 gateway plasmid through BP recombination (Invitrogen) as previously described [39]. Aspartic acid 1209 of MBD9 was mutated to Alanine through GAT→GCT DNA sequence change using the New England Biolabs (NEB) Site Directed Mutagenesis Kit and D1209A Mutagenic primers listed in **Supplemental Table 1**. The D1209A MBD9 sequence was cloned into destination gateway plasmid pMDC99 through LR recombination (Invitrogen) and verified by Sanger Sequencing. D1209A MBD9 in pMDC99 and WT MBD9 in pMDC99 were transformed into *Agrobacterium tumefaciens* GV3101 strain via electroporation. *mbd9-1* plants were transformed with either WT MBD9 or D1029A MBD9-containing plasmids through the floral dip method. Stable transformants were identified through selection on Hygromycin B-containing

media (35 µg/mL) and selfed until homozygosity of the transgene. T4 generation plants were used for all described experiments.

Abscisic Acid (ABA) treatment and Germination Efficiency

For Chip-Seq and RNA-Seq, above-ground tissue of plate-grown seedlings was thoroughly sprayed with an ABA or Mock solution (~3 mLs solution per 150mm diameter plate). The ABA solution contained 20 µM (+/-) Abscisic Acid (ABA) (Phytotech Labs) with 0.01% Silwet® L-77 (bioWORLD PlantMedia) in water, making the active form (+) ABA 10 µM in final concentration. The Mock solution contained an equal volume of DMSO (ABA solvent) and 0.01% Silwet® L-77 in water. Sprayed seedlings were incubated at 20˚C in growth chambers and collected after 4 hours, approximately 9 hours after artificial dawn. For ABA germination experiments, half-strength Murashige and Skoog (MS) media plates were supplemented with ABA to a final concentration of 0.6 µM (+/-) Abscisic Acid (ABA) (Phytotech Labs), making the active form (+) ABA 0.3 µM. Seeds were plated at a low density (~50-80 per 150mm diameter plate) to ensure full contact with ABA-containing media and stratified and grown as described above. The emergence of root and shoot tissue was tracked on a semi daily basis. Seeds of each genotype were also germinated on standard ½ MS media simultaneously as a control for each iteration of the germination experiment.

RNA Extraction

Total RNA was isolated from three biological replicates of plate-grown seedling tissue (100 mg per replicate) using the RNeasy plant mini kit (Qiagen). Isolated RNA was treated with Ambion TURBO™ DNase (Invitrogen) using manufacturer's recommendations.

Quantitative Real-Time PCR (qRT-PCR)

First strand cDNA was synthesized from DNase-treated RNA with LunaScript® RT SuperMix Kit (NEB). Prepared cDNA was amplified in Real Time utilizing the StepOnePlus real-time PCR system (Applied Biosystems) and PowerUp SYBR Green Master Mix (Applied Biosystems) as a detection reagent. The $2^{-\Delta\Delta Ct}$ method was used to determine differential expression, with the *PP2A* gene (*AT1G13320*) used as the internal control [48]. Primers against exon junctions for genes *COR15A* (*AT2G42540*) and *ANAC72* (*AT4G27410*) were used and described in **Supplemental Table 1**. Their expression was compared across Mock and ABA treatments to ensure sufficient treatment with ABA.

RNA-Seq library generation and sequencing

500 nanograms of DNase-treated RNA from RNA Extraction was used as input for the RNA-Seq library prep. The QuantSeq FWD 3' mRNA-Seq V2 Library Prep Kit with UDI (Lexogen) was used to make sequencing libraries with manufacturer's recommendations. Resulting libraries were pooled and sequenced using paired-end 150 nt reads on an Illumina NovaSeq 6000 instrument.

RNA-seq data analysis

Read 1 from RNA-seq was trimmed with Trimmomatic using standard single end (SE) parameters [49] and then aligned to the Col-PEK genome assembly [50] using the STAR alignment software [51]. Picard MarkDuplicates function with REMOVE_DUPLICATES=T parameter was used to remove sequencing duplicates (https://broadinstitute.github.io/picard/). featureCounts was then used to convert alignment files into count matrix files for downstream analyses [52]. DESeq2 was used to identify differentially expressed genes fold change of 1.5 or greater (log2FoldChange <= -0.6 or >= 0.6) and a Benjamini-Hochberg (BH) adjusted p-value <0.05 as reported by DESeq2 [53] .

ChIP library generation and sequencing

The enhanced ChIP-Sequencing protocol was followed as previously described in [54] with the following modifications: Per replicate, 200 mg of 7-day old seedling tissue (above ground tissue only) was harvested, crosslinked in 1% formaldehyde, and flash frozen in liquid nitrogen. Tissue was ground in a mortar and pestle, homogenized into a slurry in 250 µl of Buffer S and moved directly to sonication. Post sonication, lysate was diluted 10x with Buffer F for use in pulldowns. 50 µl of diluted lysate was saved as input. αH2A.Z (2 µg/mL), αMBD9 (2 µg/mL) or αPIE1 (3 µg/mL) antibodies were added to diluted lysates and incubated overnight at 4°C on a nutator for end-over-end mixing. The H2A.Z antibody used here is described by Deal et al. in 2007 [55], and MBD9 and PIE1 antibodies described above. 20 µl of Protein G Dynabeads (Invitrogen) per replicate were washed in excess Buffer F, resuspended to their original volume and added to each pulldown. Samples were incubated with beads at 4°C on a nutator for 2 hours. ChIP DNA was extracted via the MinElute PCR Purification Kit (Qiagen) and sequencing libraries were made using the ThruPLEX DNA-Seq Kit (Takara). Two replicates of each genotype/treatment were collected for sequencing. Resulting libraries were sequenced in two batches: ABA- and Mock-treated libraries were pooled and sequenced using paired-end 150 nt reads on an Illumina NovaSeq 6000 instrument while untreated plants were pooled and sequenced using paired-end 150 nt reads on an Illumina NextSeq 500.

ChIP sequencing data analysis

Sequencing reads were aligned to the Col-PEK genome assembly [50] with Bowtie2 [56,57] using --local --very-sensitive --no-mixed --no-discordant --phred33 parameters. Samtools -view bS, -index, and -sort functions were used to process resulting alignment files [58]. Picard MarkDuplicates function with REMOVE_DUPLICATES=T parameter was used to remove sequencing duplicates (https://broadinstitute.github.io/picard/). deepTools2 bamCoverage function with parameters --normalizeUsing RPKM and --extendReads were used to create Read

Per Kilobase Million (RPKM) normalized bigwig files for visualization [59]. htseq-count with -r pos -m union -s no --nonunique all parameters were used to convert processed BAM files into count matrix files for downstream analyses [60]. The R package DESeq2 was used to identify genes with significantly changed enrichment of H2A.Z, MBD9 and PIE1 for each genotype or condition comparison mentioned in the text [53]. After running DESeq2 analysis, results were further filtered to exclude genes with low baseMean (<20 for H2A.Z, <5 for MBD9/PIE1).

Data visualization

Unless otherwise noted, heatmaps and average plots were generated using the Seqplots software using RPKM normalized bigwig files and BED files containing the genomic coordinates of all or a specified subset of Col-PEK genes [61,62]). For **Fig. 1c**, deepTools2 computeMatrix and plotHeatmap were used in lieu of Seqplots to generate average plots [59]. Integrative Genomics Viewer (IGV) was used to visualize specific loci in **Fig. 3h** [63]. All other plots including volcano plots, scatter plots, bubble plots, box plots, and germination rate plots were made in R utilizing ggplot2 [64].

Publically available data

Raw data for histone post-translational modifications (PTMs) H3K9Ac, H3K14Ac, and H3K27me3 presented in **Fig. 1c** were obtained from the NIH Sequencing Read Archive database under the following accessions, respectively; SRR5011170, SRR5011158 and SRR5278091 [65]. The two replicates of Global Run-on Sequencing (Gro-Seq) data from **Supp. Figure 6** are available under accessions SRR3647034 and SRR3647034. Raw data were processed as above into RPKM normalized bigwig files for visualization.

Gene Ontology (GO) Analysis

The Bioconductor package ViSEAGO [66] was used for Gene Ontology (GO) Analysis following the general tutorial provided by Brionne, A et al. 2024[67]. Briefly, select gene lists were mapped to their corresponding Entrez ID utilizing the select function from the AnnotationDbi package in R [68]. ViSEAGO::create_topGOdata was used with ont="BP", nodeSize=5 parameters to assign 'Biological Process' (BP) to genes. Then runTest from the R package topGO was used with algorithm ="elim", statistic = "fisher" parameters to determine statistical enrichment of GO terms using a Fisher's Exact Test (p-value threshold < 0.01) [69]. Enriched GO categories were condensed based on Semantic Similarity (SS) clustering using distance="Wang" and aggreg.method="ward.D2" parameters from the ViSEAGO::GOclusters_heatmap function.

Statistics

For ChIP-Seq and RNA-Seq data analysis, differentially enriched regions and differentially expressed genes were defined as genes with a fold change of 1.5 or greater (log2FoldChange <= -0.6 or >= 0.6) and a Benjamini-Hochberg (BH) adjusted p-value <0.05 as reported by DESeq2. Two independent biological replicates for ChIP-Seq and three for RNA-Seq were performed independently from extraction to sequencing. Unless otherwise noted, two-sided Welch Two Sample t-tests were performed for all log2 Fold Change comparisons of the resulting data. Germination efficiency values described in Fig. 4e represent the average germination of genotypes across two independent germination experiments, where the germination of an average of 68 seeds per plate were counted. A two-sided analysis of variance ANOVA was performed to determine genotype-specific germination rate differences.

Insoluble Chromatin Isolation and Western Blotting

To isolate insoluble chromatin associated proteins, we followed the isolation protocol described previously [38]. Briefly, 1 gram of 7-day-old, plate grown seedling shoots were collected,

ground in liquid nitrogen, and homogenized in 5 ml of modified Honda buffer without PMSF. Homogenates were filtered through 70 uM cell strainers and centrifuged at 1,500g at 4°C for 20 minutes. Pellets were washed three times in 2 ml modified Honda buffer and once in 2 ml 1x PBS with 1 mM EDTA, with spins at 1,500 for 5 minutes at 4°C. Resulting chromatin fractions were resuspended in equal volumes of 1X Laemmli Buffer. Western blotting was performed as previously described [39], using 1:1000 dilutions of αH2A.Z and αPIE1 antibodies and 1:500 of αMBD9 antibodies. ECL was used as a chemiluminescent detection reagent (Thermo Fisher) and scanned for signal using ChemiDoc MP imaging system (BioRad).

Data availability

ChIP-Seq are available under the GEO accession GSE269827 with the reviewer token elelcggkvziddyf, and RNA-Seq data are available under the GEO accession GSE269876 with the reviewer token orwlqmkslnojlwd

Supplemental Tables and Figures

Supp. Table 1 shows primer sequence mentioned in the text

Primer name	Primer sequence 5' to 3'
D1209A Mutagenic Forward Primer	GAAGCTGTTCTTGAGGTTGGATTT
D1209A Mutagenic Reverse Primer	AAGAAAAGCTTCAGTTGATCCG
PP2A qRT-PCR Forward Primer	TAACGTGGCCAAAATGATGC
PP2A qRT-PCR Reverse Primer	GTTCTCCACAACCGCTTGGT
COR15A qRT-PCR Forward Primer	ACAAAGAAAGCTTCAGATTTCGTGACG
COR15A qRT-PCR Reverse Primer	CACATACGCCGCAGCTTTCTC
ANAC72 qRT-PCR Forward Primer	GTAGGGGAGTATAATTGTAACTATTTAGGTAAGGC
ANAC72 qRT-PCR Reverse Primer	GTACCCGTTGCTTTCCAATAACCC

Supp. Fig. 1 PIE1 and MBD9 antibodies recognize their respective proteins by Western Blot (a) Western blot against MBD9 in WT and mbd9-1 plants. Nuclear proteins were extracted following as described in the methods for insoluble chromatin isolation nuclei isolation and Western Blotting. The band in WT is the expected size for MBD9, which is around 270 kDA, and is not detected in the *mbd9-1* extract. (b) Western blot against PIE1 in WT and *pie1-5* plants. The band in WT is the expected size for PIE1, which is around 250 kDA and is not detected in *pie1-5* extract.

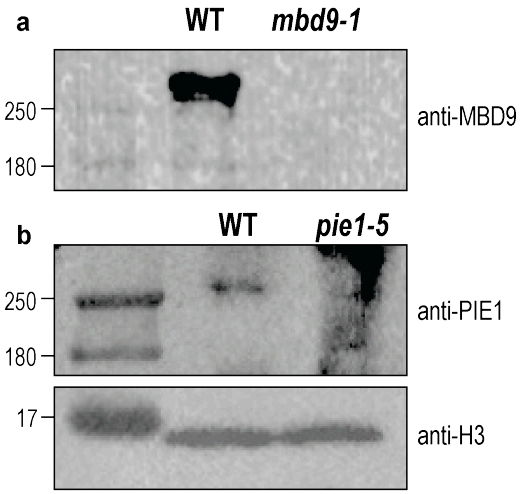

Supp. Fig. 2 Bar graph illustrating WT qRT-PCR response to 10 uM Abscisic Acid (ABA) at two genes, *COR15A* (*AT2G42540*) and *ANAC72* (*AT4G27410*) compared to Mock treatment. Normalized expression represents the change in expression of these genes compared to both an internal control (*PP2A*;*AT1G13320*) and relative to Mock treatment (no ABA). Clearly, WT plants have a strong response to ABA, with relative transcript level increasing 25x for the *ANAC72* gene and 1000x for the *COR15A* gene.

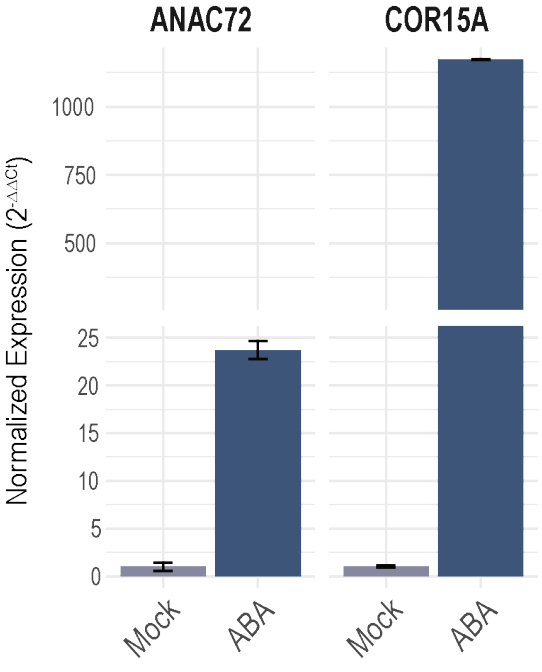

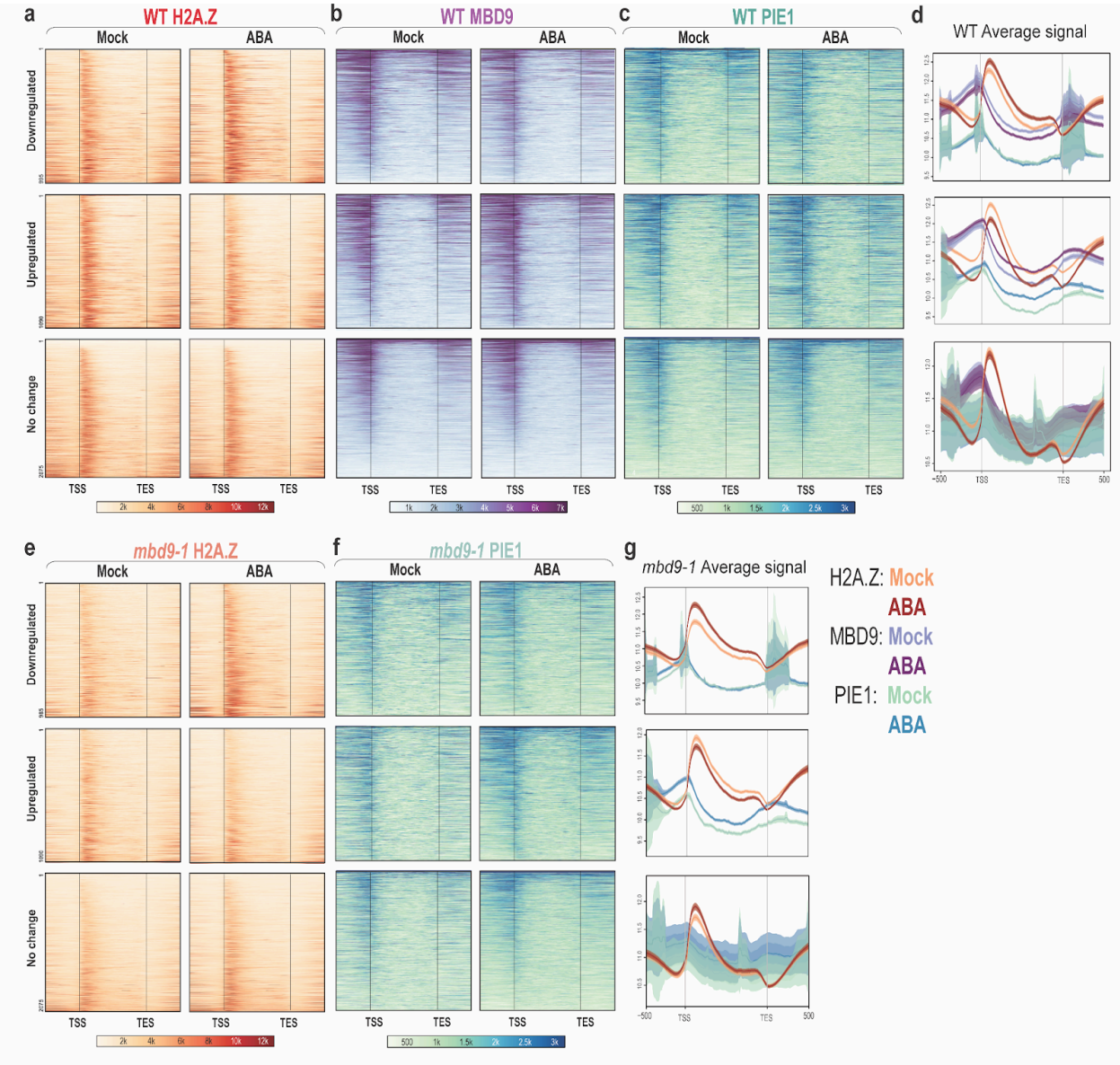

Supp. Fig 3 shows chromatin dynamics of WT and *mbd9-1* plants at C2 genes. **(a)** Heatmap showing WT H2A.Z localization at 995 C2 genes that are Downregulated (top), 1090 genes that are Upregulated (middle) and genes that have no change by RNA-Seq (bottom). H2A.Z increases slightly at downregulated genes, decreases at upregulated genes, and does not change at unchanged genes. **(b)** Heatmap with the same groups as in (a) but showing MBD9 localization on genes. There is a decrease of MBD9 at downregulated genes, a slight increase at upregulated genes, and no change at unchanged genes. **(c)** shows the same trends with

PIE1 data. All data are RPKM normalized. **(d)** Average plots illustrating the average change in signal at these genes. Profiles are plotted on a log2 scale for easy visualization. **(e)** Heatmaps illustrating H2A.Z changes in *mbd9-1* plants. Note that heatmaps are on the same scale as WT plots in (a-c). mbd9-1 plants still show gains in H2A.Z at the same C2 genes as in (a), and loss of H2A.Z in upregulated genes from (a). **(f)** Heatmaps illustrating PIE1 change in *mbd9-1* plants. The most notable change is at Upregulated genes, where more PIE1 is localized after ABA treatment. **(g)** Average plots illustrating average change in H2A.Z and PIE1 in these three groups of genes in *mbd9-1* plants. Profiles are plotted on a log2 scale for easy visualization.

Supp Fig. 4 shows ClustalOmega (1.2.4) multiple sequence alignment of the Bromodomains from Arabidopsis *MBD9 (AT3G01460)*, Arabidopsis *GTE6* (*AT3G52280*), Human GCN5 (ENST00000688188.1), Human p300/CBP-associated factor (CAF) (ENSG00000114166), *Saccharomyces cerevisiae* (Yeast) GCN5 (YGR252W), and Yeast BDF1 (YLR399C). " * "indicates identically conserved residues, , " : " indicates strongly similar residues, " . " indicates residues with weakly similar properties, and no symbol indicates residues that are not conserved. The highlighted Aspartic Acid (D) correlates to D1209A in the total *MBD9* sequence. This residue is identically conserved across all compared Bromodomains here.

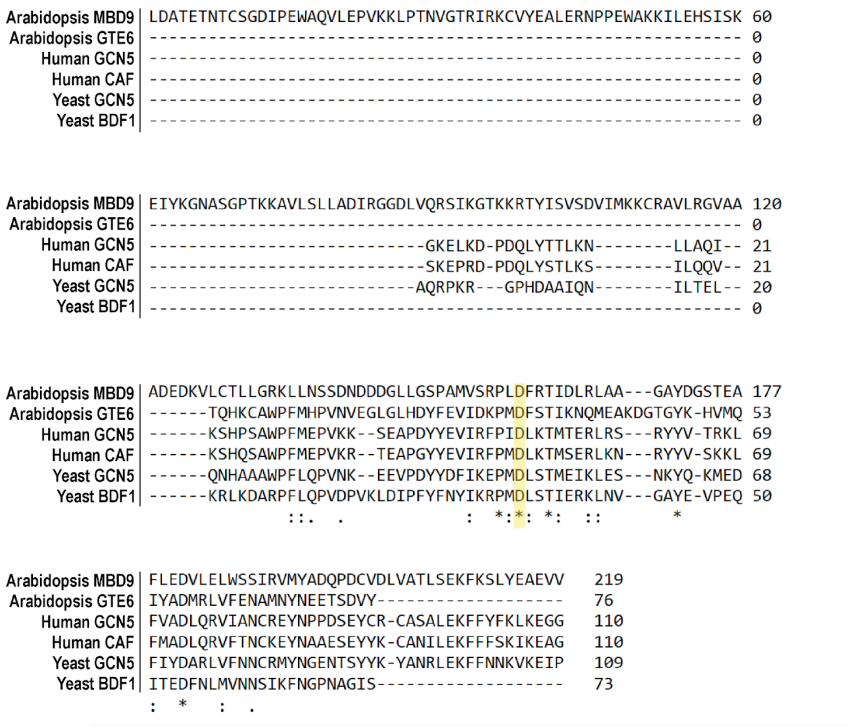

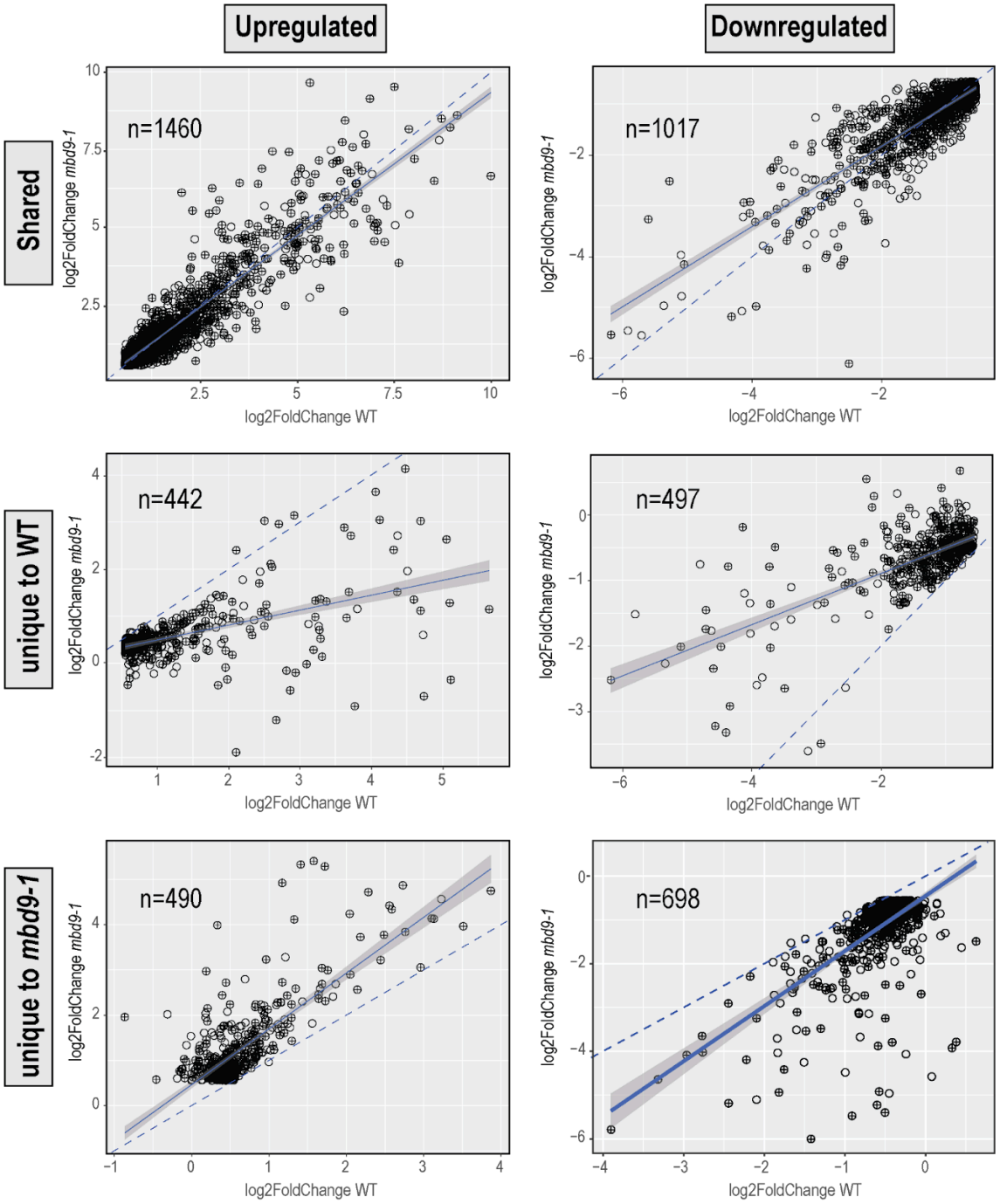

Supp. Fig 5 shows scatter plots illustrating correlation of WT and *mbd9-1* RNA-Seq reponses at gene groups from **Fig. 5c**. Here, dashed lines indicate hypothetical 1:1 relationship between WT and *mbd9-1* responses whereas solid blue lines indicate the trend of the data itself, with gray

shadows indicating the standard error of the data. Although there are upregulated and downregulated genes 'unique' in both WT and *mbd9-1* plants, many of these points still trend in the same direction but may not be called as statistically significant through DeSeq2 analysis. The group with the most notable deviation from the expected 1:1 ratio is the Upregulated Unique to WT Category (middle left panel) which has some genes that have opposing or little change in *mbd9-1* plants but a significant change in WT plants.

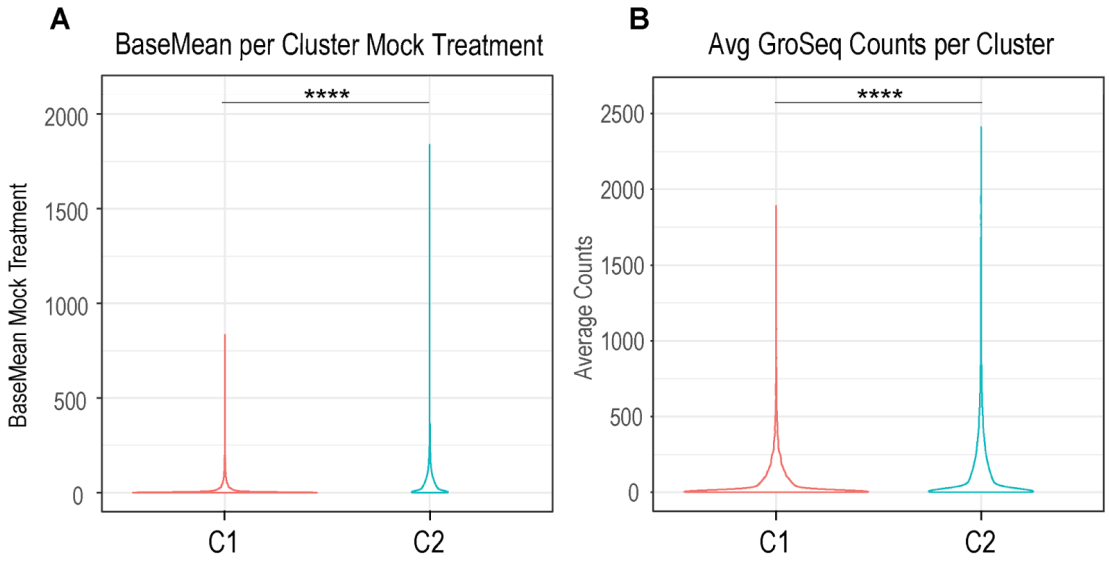

Supp. Fig 6 shows quantification of count data from RNA-Seq and publicly available nascent RNA data Global Run-on Sequencing (GRO-Seq) from analogous tissue. **(a)** Violin plot showing differences in RNA-Seq BaseMean (normalized count data outputted from DeSeq2) between Clusters in plants under Mock treatment. C2 has significantly more counts compared to C1, indicating that under Mock treatment (no ABA), C2 genes are more transcribed than C2 genes (unpaired, two-sided Wilcoxon rank-sum test,****= p-value<0.001). **(b)** Violin plot showing average differences in Gro-Seq counts from FeatureCounts across two replicates between Clusters in untreated, 6-day-old WT Arabidopsis seedlings. Again, C2 has significantly more counts compared to C1, indicating that under normal conditions, C2 genes are more transcribed

than C2 genes (unpaired, two-sided Wilcoxon rank-sum test,****= p-value<0.001).

References

1. Clapier, C. R. & Cairns, B. R. The biology of chromatin remodeling complexes. *Annu. Rev. Biochem.* **78**, 273–304 (2009).
2. Mizuguchi, G. *et al.* ATP-driven exchange of histone H2AZ variant catalyzed by SWR1 chromatin remodeling complex. *Science* **303**, 343–348 (2004).
3. Kobor, M. S. *et al.* A protein complex containing the conserved Swi2/Snf2-related ATPase Swr1p deposits histone variant H2A.Z into euchromatin. *PLoS Biol.* **2**, E131 (2004).
4. March-Díaz, R. & Reyes, J. C. The beauty of being a variant: H2A. Z and the SWR1 complex in plants. *Mol. Plant* **2**, 565–577 (2009).
5. Vardabasso, C. *et al.* Histone Variant H2A.Z.2 Mediates Proliferation and Drug Sensitivity of Malignant Melanoma. *Mol. Cell* **59**, 75–88 (2015).
6. Svotelis, A., Gévry, N., Grondin, G. & Gaudreau, L. H2A.Z overexpression promotes cellular proliferation of breast cancer cells. *Cell Cycle* **9**, 364–370 (2010).
7. Ávila-López, P. A. *et al.* H2A.Z overexpression suppresses senescence and chemosensitivity in pancreatic ductal adenocarcinoma. *Oncogene* **40**, 2065–2080 (2021).
8. Dryhurst, D., McMullen, B., Fazli, L., Rennie, P. S. & Ausió, J. Histone H2A.Z prepares the prostate specific antigen (PSA) gene for androgen receptor-mediated transcription and is upregulated in a model of prostate cancer progression. *Cancer Lett.* **315**, 38–47 (2012).
9. Tang, S. *et al.* Vital and Distinct Roles of H2A.Z Isoforms in Hepatocellular Carcinoma. *Onco. Targets. Ther.* **13**, 4319–4337 (2020).
10. Colino-Sanguino, Y., Clark, S. J. & Valdes-Mora, F. The H2A.Z-nuclesome code in mammals: emerging functions. *Trends Genet.* **38**, 273–289 (2022).
11. Zlatanova, J. & Thakar, A. H2A.Z: view from the top. *Structure* **16**, 166–179 (2008).
12. Whittle, C. M. *et al.* The genomic distribution and function of histone variant HTZ-1 during

C. elegans embryogenesis. *PLoS Genet.* **4**, e1000187 (2008).

13. van Daal, A. & Elgin, S. C. A histone variant, H2AvD, is essential in Drosophila melanogaster. *Mol. Biol. Cell* **3**, 593–602 (1992).
14. Faast, R. *et al.* Histone variant H2A.Z is required for early mammalian development. *Curr. Biol.* **11**, 1183–1187 (2001).
15. Liu, X. *et al.* Hierarchical Accumulation of Histone Variant H2A.Z Regulates Transcriptional States and Histone Modifications in Early Mammalian Embryos. *Adv. Sci.* **9**, e2200057 (2022).
16. Coleman-Derr, D. & Zilberman, D. Deposition of histone variant H2A.Z within gene bodies regulates responsive genes. *PLoS Genet.* **8**, e1002988 (2012).
17. Choi, K. *et al.* Arabidopsis homologs of components of the SWR1 complex regulate flowering and plant development. *Development* **134**, 1931–1941 (2007).
18. March-Díaz, R. *et al.* Histone H2A.Z and homologues of components of the SWR1 complex are required to control immunity in Arabidopsis. *Plant J.* **53**, 475–487 (2008).
19. Babiarz, J. E., Halley, J. E. & Rine, J. Telomeric heterochromatin boundaries require NuA4-dependent acetylation of histone variant H2A.Z in Saccharomyces cerevisiae. *Genes Dev.* **20**, 700–710 (2006).
20. Li, S., Wei, T. & Panchenko, A. R. Histone variant H2A.Z modulates nucleosome dynamics to promote DNA accessibility. *Nat. Commun.* **14**, 1–10 (2023).
21. Weber, C. M., Ramachandran, S. & Henikoff, S. Nucleosomes Are Context-Specific, H2A.Z-Modulated Barriers to RNA Polymerase. *Mol. Cell* **53**, 819–830 (2014).
22. Long, J., Carter, B., Johnson, E. T. & Ogas, J. Contribution of the histone variant H2A.Z to expression of responsive genes in plants. *Semin. Cell Dev. Biol.* **135**, 85–92 (2023).
23. Foroozani, M., Holder, D. H. & Deal, R. B. Histone Variants in the Specialization of Plant Chromatin. *Annu. Rev. Plant Biol.* **73**, 149–172 (2022).
24. Rispal, J. *et al.* Control of intestinal stemness and cell lineage by histone variant H2A.Z

isoforms. *bioRxiv* 2023.10.10.561706 (2023) doi:10.1101/2023.10.10.561706.

25. Lorković, Z. J. *et al.* Compartmentalization of DNA damage response between heterochromatin and euchromatin is mediated by distinct H2A histone variants. *Curr. Biol.* **27**, 1192–1199 (2017).
26. Subramanian, V., Fields, P. A. & Boyer, L. A. H2A.Z: a molecular rheostat for transcriptional control. *F1000Prime Rep.* **7**, 01 (2015).
27. Sura, W. *et al.* Dual Role of the Histone Variant H2A.Z in Transcriptional Regulation of Stress-Response Genes. *Plant Cell* **29**, 791–807 (2017).
28. Yin, X. *et al.* H2AK121ub in Arabidopsis associates with a less accessible chromatin state at transcriptional regulation hotspots. *Nat. Commun.* **12**, 1–12 (2021).
29. Gómez-Zambrano, Á., Merini, W. & Calonje, M. The repressive role of Arabidopsis H2A.Z in transcriptional regulation depends on AtBMI1 activity. *Nat. Commun.* **10**, 1–12 (2019).
30. Colino-Sanguino, Y., Clark, S. J. & Valdes-Mora, F. H2A.Z acetylation and transcription: ready, steady, go! *Epigenomics* **8**, 583–586 (2016).
31. Sevilla, A. & Binda, O. Post-translational modifications of the histone variant H2AZ. *Stem Cell Res.* **12**, 289–295 (2014).
32. Pradhan, S. K. *et al.* EP400 Deposits H3.3 into Promoters and Enhancers during Gene Activation. *Mol. Cell* **61**, 27–38 (2016).
33. Valdés-Mora, F. *et al.* Acetylated histone variant H2A.Z is involved in the activation of neo-enhancers in prostate cancer. *Nat. Commun.* **8**, 1–17 (2017).
34. Halley, J. E., Kaplan, T., Wang, A. Y., Kobor, M. S. & Rine, J. Roles for H2A.Z and its acetylation in GAL1 transcription and gene induction, but not GAL1-transcriptional memory. *PLoS Biol.* **8**, e1000401 (2010).
35. Valdés-Mora, F. *et al.* Acetylation of H2A.Z is a key epigenetic modification associated with gene deregulation and epigenetic remodeling in cancer. *Genome Res.* **22**, 307–321 (2012).
36. Sarcinella, E., Zuzarte, P. C., Lau, P. N. I., Draker, R. & Cheung, P. Monoubiquitylation of

H2A.Z distinguishes its association with euchromatin or facultative heterochromatin. *Mol. Cell. Biol.* **27**, 6457–6468 (2007).

37. Carter, B. *et al.* The chromatin remodelers PKL and PIE1 act in an epigenetic pathway that determines H3K27me3 homeostasis in Arabidopsis. *Plant Cell* **30**, 1337–1352 (2018).
38. Willige, B. C. *et al.* PHYTOCHROME-INTERACTING FACTORs trigger environmentally responsive chromatin dynamics in plants. *Nat. Genet.* **53**, 955–961 (2021).
39. Zhao, F. *et al.* Coordinated histone variant H2A.Z eviction and H3.3 deposition control plant thermomorphogenesis. *New Phytol.* **238**, 750–764 (2023).
40. Zander, M. *et al.* Epigenetic silencing of a multifunctional plant stress regulator. *Elife* **8**, (2019).
41. Giaimo, B. D., Ferrante, F., Herchenröther, A., Hake, S. B. & Borggrefe, T. The histone variant H2A.Z in gene regulation. *Epigenetics Chromatin* **12**, 37 (2019).
42. Ranjan, A. *et al.* Nucleosome-free region dominates histone acetylation in targeting SWR1 to promoters for H2A.Z replacement. *Cell* **154**, 1232–1245 (2013).
43. Yen, K., Vinayachandran, V. & Pugh, B. F. SWR-C and INO80 chromatin remodelers recognize nucleosome-free regions near +1 nucleosomes. *Cell* **154**, 1246–1256 (2013).
44. Li, Z. *et al.* Foxa2 and H2A.Z mediate nucleosome depletion during embryonic stem cell differentiation. *Cell* **151**, 1608–1616 (2012).
45. Aslam, M., Fakher, B., Jakada, B. H., Cao, S. & Qin, Y. SWR1 Chromatin Remodeling Complex: A Key Transcriptional Regulator in Plants. *Cells* **8**, (2019).
46. Altaf, M. *et al.* NuA4-dependent acetylation of nucleosomal histones H4 and H2A directly stimulates incorporation of H2A.Z by the SWR1 complex. *J. Biol. Chem.* **285**, 15966–15977 (2010).
47. Nie, W.-F. *et al.* Histone acetylation recruits the SWR1 complex to regulate active DNA demethylation in Arabidopsis. *Proc. Natl. Acad. Sci. U. S. A.* **116**, 16641–16650 (2019).
48. Luo, Y.-X. *et al.* A plant-specific SWR1 chromatin-remodeling complex couples histone

H2A.Z deposition with nucleosome sliding. *EMBO J.* **39**, e102008 (2020).

49. Sijacic, P., Holder, D. H., Bajic, M. & Deal, R. B. Methyl-CpG-binding domain 9 (MBD9) is required for H2A.Z incorporation into chromatin at a subset of H2A.Z-enriched regions in the Arabidopsis genome. *PLoS Genet.* **15**, e1008326 (2019).
50. Potok, M. E. *et al.* Arabidopsis SWR1-associated protein methyl-CpG-binding domain 9 is required for histone H2A.Z deposition. *Nat. Commun.* **10**, 1–14 (2019).
51. Berg, A. *et al.* Ten members of the Arabidopsis gene family encoding methyl-CpG-binding domain proteins are transcriptionally active and at least one, AtMBD11, is crucial for normal development. *Nucleic Acids Res.* **31**, 5291–5304 (2003).
52. Wu, Z. *et al.* Family-wide Characterization of Methylated DNA Binding Ability of Arabidopsis MBDs. *J. Mol. Biol.* **434**, 167404 (2022).
53. Hetzel, J., Duttke, S. H., Benner, C. & Chory, J. Nascent RNA sequencing reveals distinct features in plant transcription. *Proceedings of the National Academy of Sciences* **113**, 12316–12321 (2016).
54. Holder, D. H. & Deal, R. B. Temporal profiling of the phosphate starvation response in Arabidopsis root hair cells reveals that induction of polycomb target genes does not depend on removal of H3K27me3 or H2A.Z. *bioRxiv* 2024.07.14.603443 (2024) doi:10.1101/2024.07.14.603443.
55. Xue, M. *et al.* The INO80 chromatin remodeling complex promotes thermomorphogenesis by connecting H2A.Z eviction and active transcription in Arabidopsis. *Mol. Plant* **14**, 1799–1813 (2021).
56. Brahma, S. & Henikoff, S. The BAF chromatin remodeler synergizes with RNA polymerase II and transcription factors to evict nucleosomes. *Nat. Genet.* **56**, 100–111 (2023).
57. Lashgari, A., Millau, J.-F., Jacques, P.-É. & Gaudreau, L. Global inhibition of transcription causes an increase in histone H2A.Z incorporation within gene bodies. *Nucleic Acids Res.* **45**, 12715–12722 (2017).

58. Conerly, M. L. *et al.* Changes in H2A.Z occupancy and DNA methylation during B-cell lymphomagenesis. *Genome Res.* **20**, 1383–1390 (2010).

59. Yaish, M. W. F., Peng, M. & Rothstein, S. J. AtMBD9 modulates Arabidopsis development through the dual epigenetic pathways of DNA methylation and histone acetylation. *Plant J.* **59**, 123–135 (2009).

60. Livak, K. J. & Schmittgen, T. D. Analysis of Relative Gene Expression Data Using Real-Time Quantitative PCR and the 2−ΔΔCT Method. *Methods* **25**, 402–408 (2001).

61. Bolger, A. M., Lohse, M. & Usadel, B. Trimmomatic: a flexible trimmer for Illumina sequence data. *Bioinformatics* **30**, 2114–2120 (2014).

62. Hou, X., Wang, D., Cheng, Z., Wang, Y. & Jiao, Y. A near-complete assembly of an Arabidopsis thaliana genome. *Mol. Plant* **15**, 1247–1250 (2022).

63. Dobin, A. *et al.* STAR: ultrafast universal RNA-seq aligner. *Bioinformatics* **29**, 15–21 (2013).

64. Liao, Y., Smyth, G. K. & Shi, W. featureCounts: an efficient general purpose program for assigning sequence reads to genomic features. *Bioinformatics* **30**, 923–930 (2013).

65. Love, M., Anders, S. & Huber, W. Differential analysis of count data – the DESeq2 package. *Genome Biol.* (2013).

66. Zhao, L. *et al.* Integrative analysis of reference epigenomes in 20 rice varieties. *Nat. Commun.* **11**, 1–16 (2020).

67. Deal, R. B., Topp, C. N., McKinney, E. C. & Meagher, R. B. Repression of flowering in Arabidopsis requires activation of FLOWERING LOCUS C expression by the histone variant H2A.Z. *Plant Cell* **19**, 74–83 (2007).

68. Langmead, B., Wilks, C., Antonescu, V. & Charles, R. Scaling read aligners to hundreds of threads on general-purpose processors. *Bioinformatics* **35**, 421–432 (2018).

69. Langmead, B. & Salzberg, S. L. Fast gapped-read alignment with Bowtie 2. *Nat. Methods* **9**, 357–359 (2012).

70. Danecek, P. *et al.* Twelve years of SAMtools and BCFtools. *Gigascience* **10**, (2021).
71. Ramírez, F. *et al.* deepTools2: a next generation web server for deep-sequencing data analysis. *Nucleic Acids Res.* **44**, W160–W165 (2016).
72. Anders, S., Pyl, P. T. & Huber, W. HTSeq—a Python framework to work with high-throughput sequencing data. *Bioinformatics* **31**, 166–169 (2014).
73. Stempor, P. & Ahringer, J. SeqPlots - Interactive software for exploratory data analyses, pattern discovery and visualization in genomics. *Wellcome Open Res* **1**, 14 (2016).
74. Stempor, P. *Seqplots: :chart_with_upwards_trend:SeqPlots - An Interactive Tool for Visualizing NGS Signals and Sequence Motif Densities along Genomic Features Using Average Plots and Heatmaps*. (Github).
75. Robinson, J. T. *et al.* Integrative genomics viewer. *Nat. Biotechnol.* **29**, 24–26 (2011).
76. Wickham, H. *ggplot2*. (Springer International Publishing).
77. Leinonen, R., Sugawara, H., Shumway, M. & International Nucleotide Sequence Database Collaboration. The sequence read archive. *Nucleic Acids Res.* **39**, D19–21 (2011).
78. Brionne, A., Juanchich, A. & Hennequet-Antier, C. ViSEAGO: a Bioconductor package for clustering biological functions using Gene Ontology and semantic similarity. *BioData Min.* **12**, 16 (2019).
79. Brionne, A., Juanchich, A. & Hennequet-Antier, C. An overview of ViSEAGO: Visualisation, Semantic similarity, Enrichment Analysis of Gene Ontology. *Bioconductor* https://bioconductor.org/packages/release/bioc/vignettes/ViSEAGO/inst/doc/ViSEAGO.html (May1 2024).
80. Pagès, H., Carlson, M., Falcon, S. & Li, N. Manipulation of SQLite-based annotations in Bioconductor. *Bioconductor* https://bioconductor.org/packages/release/bioc/html/AnnotationDbi.html (2024).
81. Alexa, A. & Rahnenfuhrer, J. Enrichment Analysis for Gene Ontology. *Bioconductor* https://bioconductor.org/packages/release/bioc/html/topGO.html (2024).

Chapter 3

SWR1 remodeler activity limits ectopic H2A.Z accumulation at constitutive heterochromatin in Arabidopsis

Chapter 3: SWR1 remodeler activity limits ectopic H2A.Z accumulation at constitutive heterochromatin in Arabidopsis

Ellen G. Krall[1,2] ,

Maryam Foroozani[1], Siyan Feng[1], and Roger B. Deal[1]

[1]Department of Biology

[2]Graduate Program in Genetics and Molecular Biology

Emory University, Atlanta, GA 30322 USA

Abstract

In nuclei, DNA is packaged by histone proteins into chromatin, which can be further subdivided into functional domains including euchromatin, facultative heterochromatin, and constitutive heterochromatin. These chromatin environments are further defined by presence of DNA modifications, and histone post translational modifications, and the presence of histone variants. The histone variant H2A.Z, which is deposited by the chromatin remodeler SWR1, is important in defining both euchromatin and facultative heterochromatin, but is not typically found in constitutive heterochromatin due to its reported anticorrelation with DNA methylation. However, by utilizing a new, nearly-complete Arabidopsis genome assembly, we observed an unexpected H2A.Z enrichment in constitutive heterochromatin of mutants lacking core SWR1 components or the associated protein MBD9. This observation led us to hypothesize that SWR1 facilitates H2A.Z removal from constitutive heterochromatin. Engineering a mutant MBD9 that binds to methylated DNA allowed us to target SWR1 to these regions, revealing that SWR1 reduces ectopic H2A.Z accumulation. These results suggest a novel role for SWR1 in maintaining the H2A.Z-DNA methylation anticorrelation.

Introduction

In nuclei, DNA is packaged by histone proteins into chromatin. Chromatin is further subdivided into functional domains based on the combination of histone post-translational modifications (PTMs), DNA modifications, histone variants, non-coding RNAs, and presence of chromatin modifying enzymes on discrete portions of the genome [1]. Chromatin that is readily accessible and amenable to transcription is known as euchromatin, while chromatin that is more densely packed and averse to transcription is heterochromatin. Heterochromatin can be further broken down into quiescent chromatin that is permanently repressed (constitutive heterochromatin) and chromatin that is repressed temporarily, but needs to be activated when the appropriate developmental or environmental stimulus arises (facultative heterochromatin). The maintenance of and conversion between these different chromatin states is essential for proper organism development across eukaryotes, environmental responsiveness in plants, and tumor suppression in mammals [2–4].

Certain histone modifications, DNA modifications, and histone variants are unique to each chromatin state. For example, euchromatin is enriched in acetylation of histone tails, such as H3K14Ac and H3K27Ac and the presence of the histone variant H3.3 [5]. Constitutive heterochromatin often has methylation of DNA cytosines, along with histone PTM H3K9me2/3 and specific histone variants depending on proximity to the centromere [6]. Facultative heterochromatin, on the other hand, is primarily defined by the presence of the histone PTM H3K27me3, which is deposited by Polycomb Repressive Complex II [7]. While most histone PTMs and variants are unique to one of these categories, a variant that defies this convention is the histone variant H2A.Z, which resides both in euchromatin and facultative heterochromatin across eukaryotes, including in plants[5]. H2A.Z is deposited at these locations by the chromatin remodeler SWI2/SNF2-Related 1 Chromatin Remodeling Complex (SWR1)[8–10]. The catalytic subunit is known as PHOTOPERIOD-INDEPENDENT EARLY FLOWERING 1 (PIE1) in plants

[11]. The plant-specific SWR1-interacting protein METHYL-CPG-BINDING DOMAIN-CONTINING PROTEIN 9 (MBD9) has also been proposed to bind to acetylation marks and mediate interactions between PIE1 for and other chromatin remodelers [12,13].

In euchromatin, H2A.Z is found at nucleosomes proximal to the Transcription Start Site (TSS) of genes, while in facultative heterochromatin H2A.Z covers gene bodies [11,14,15]. H2A.Z is thought to have opposing effects on genes in these two states, where it promotes gene expression in euchromatin but contributes to a repressed state in facultative heterochromatin [16,17]. While it is still not fully understood how H2A.Z can have such opposing effects in these domains, it is commonly accepted that H2A.Z is not found at constitutive heterochromatin across eukaryotes. Previous work has shown there is an anticorrelation of H2A.Z and DNA methylation, preventing H2A.Z from localizing to constitutive heterochromatin [18–20]. For example, in Arabidopsis, when components of the DNA methyltransferase *MET1* are mutated, reductions in DNA methylation correlate with gains in H2A.Z in demethylated regions, suggesting these marks are anticorrelated and perhaps antagonistic to one another [18].

However, our ability to sequence the highly repetitive DNA often contained within constitutive heterochromatin has been limited. In 2022, release of a new Arabidopsis genome assembly, Col-PEK, changed this limitation by combining Oxford Nanopore Technologies (ONT), high-fidelity long-read PacBio, and shortread Illumina technologies to provide a high-fidelity assembly of the Arabidopsis genome including repetitive regions like centromeres, telomeres, and transposable elements [21]. After utilizing the Col-PEK assembly for alignment of ChIP-Seq data from Arabidopsis, we noticed that several mutants of the SWR1 complex had an unexpected enrichment of H2A.Z at pericentromeric heterochromatin regions. This observation led us to hypothesize that SWR1 may play a role in removal of H2A.Z at constitutive heterochromatin. To test this hypothesis, we cloned a mutant version of the putative SWR1-targeting factor MBD9, which only binds to methylated DNA. We cloned this mutant MBD9 by swapping the endogenous, disrupted Methyl-Binding Domain (MBD) from MBD9 for

the functional MBD of a similar family member, MBD7, which binds strongly to methylated DNA. We found that this mutant MBD9 is able to re-localize away from protein coding genes to constitutive heterochromatin, and that SWR1 follows it to these sites as well. Furthermore, re-localization of SWR1 to heterochromatin results in a decrease of ectopic H2A.Z accumulation, supporting the hypothesis that SWR1 normally contributes to H2A.Z removal from these sites.

Results

Plants deficient for SWR1 core components or interacting protein MBD9 show H2A.Z enrichment at constitutive heterochromatin

Several previous studies established that Arabidopsis mutants lacking the putative SWR1- targeting factor MBD9 (*mbd9-1*) have a reduction of H2A.Z across protein coding genes on average [13,22,23]. However, little work has focused on the effect of MBD9 on H2A.Z outside of euchromatin. Additionally, the release of the new Col-PEK genome assembly, which includes long-read sequencing over repetitive DNA, allows for exploration into previously difficult-to-sequence constitutively repressed regions including centromeric and pericentromeric regions [21]. Considering these observations and developments, we performed ChIP-seq against H2A.Z in 7-day-old WT and *mbd9-1* Arabidopsis seedlings and mapped the resulting data to the Col-PEK assembly. We found that two independent replicates of WT and *mbd9-1* ChIP experiments show expected enrichment of H2A.Z for each genotype on protein coding genes, with *mbd9-1* plants having an overall reduction of H2A.Z on average (**Fig. 1a**). In contrast, we see the opposite pattern at transposable element genes, which are mainly found in pericentromeric regions and are normally constitutively repressed by DNA methylation, H3K9me2, and the histone variant H2A.W. There, *mbd9-1* mutants have more H2A.Z on average than WT (**Fig. 1b**). To further explore this surprising finding, we also analyzed publicly

available ChIP-Seq data against H2A.Z in mutants of the SWR1 complex. Interestingly, we saw that the amount of accumulation of H2A.Z at pericentromeric and centromeric heterochromatin increases with the severity of the SWR1 mutation, with *mbd9-1* plants having the least accumulation and *pie1-5* plants having the most accumulation (**Fig. 1c**). This is surprising considering that SWR1 is thought to strictly deposit H2A.Z, but the most parsimonious explanation of these gains in H2A.Z at centromeric regions is that normally SWR1 contributes to removal or maintenance of H2A.Z at these regions.

Fig 1

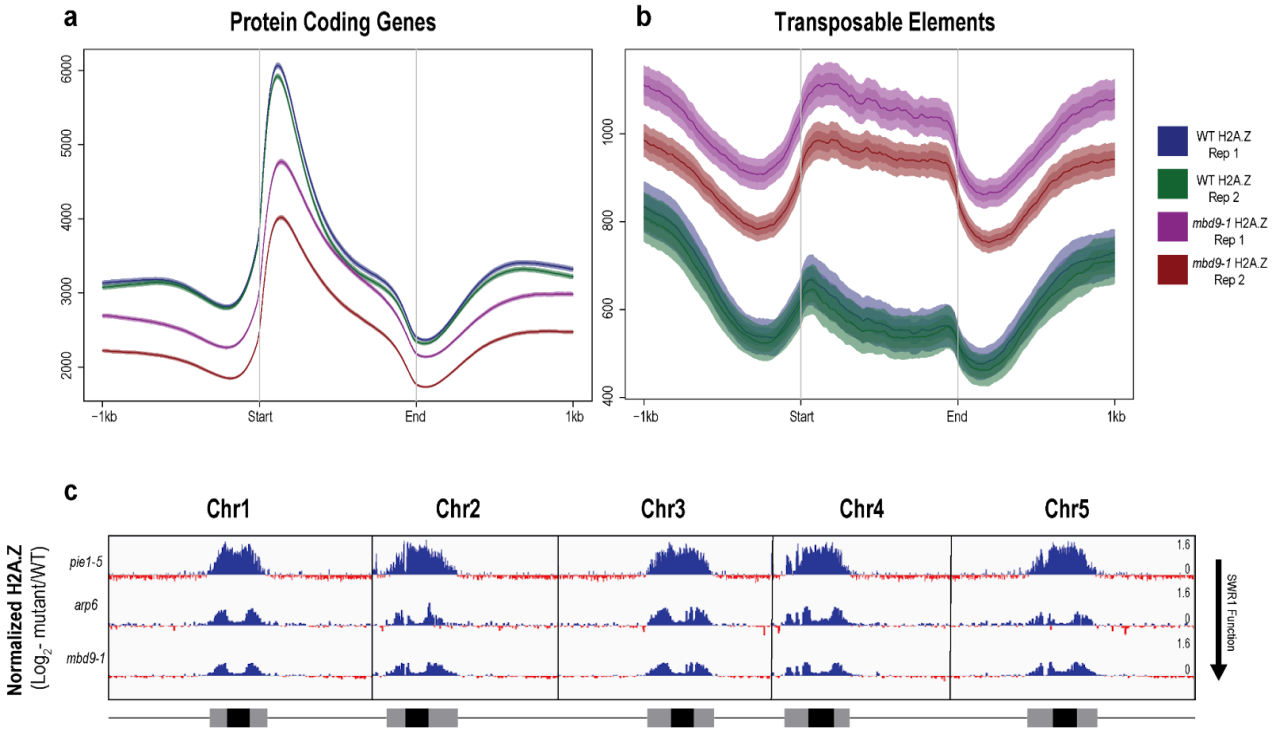

Fig. 1 shows unexpected accumulation of H2A.Z at heterochromatin in *mbd9-1* and SWR1

mutants. **(a)** shows average plots of two replicates of H2A.Z ChIP-seq data from WT (blue and green) and *mbd9-1* (red and pink) plants at all protein coding genes. WT has more H2A.Z at protein coding genes compared to *mbd9-1*. **(b)** shows an average plot with the same H2A.Z data plotted on transposable element genes. These genes have the opposite trend of protein coding genes; *mbd9-1* has more H2A.Z compared to WT at these areas. **(c)** shows the log2 H2A.Z enrichment of SWR1 core and associated mutants in reference to their matched WT. Blue regions indicate areas that have more H2A.Z in mutants, red shows areas that have less H2A.Z in mutants. Across all mutants, there is more H2A.Z enrichment at centromeric and pericentromeric regions (defined by black and grey boxes, respectively). The amount of H2A.Z gain at the centromere/pericentromere scales with the severity of the mutation, with *pie1-5* mutants, which affect the catalytic domain of SWR1, having the most H2A.Z gain and mbd9-1 mutants, which only associate with SWR1, having the most modest gain.

MBD9^{ds} localizes to constitutive heterochromatin with PIE1

In an effort to investigate whether SWR1 could play a role in H2A.Z removal from heterochromatin, we aimed to target SWR1 to areas with high DNA methylation such as transposable elements. To do this, we manipulated the MBD9 protein, a putative targeting factor of SWR1, to bind to areas with DNA methylation to target SWR1 to these regions as well. Although MBD9 is a family member of the Methyl-CpG-Binding Domain (MBD)-containing protein family in Arabidopsis, the MBD of MBD9 contains several point mutations that prevent this methyl-cytosine binding function [24]. Therefore, we cloned a mutant version of MBD9 that has this domain swapped for the MBD of the MBD7 protein that binds strongly to methylated DNA (**Fig. 2a**). The MBD of MBD7 contains three tandem methyl-binding domains and binds to methylated DNA [25,26]. We transformed this domain swap version of MBD9 (MBD9^{ds}) under its native promoter into *mbd9-1* plants. We saw that phenotypically MBD9^{ds} rescued the early flowering phenotype characteristic of *mbd9-1* plants (**Fig. 2b and 2c**). Additionally, while

transposable element genes overlap with pericentromeric regions, we saw that H3K9me2 peaks encompassed both pericentromeric and core centromeric regions, so further analysis described here focused on dynamics at H3K9me2 peaks (**Fig 2d**).

Fig. 2

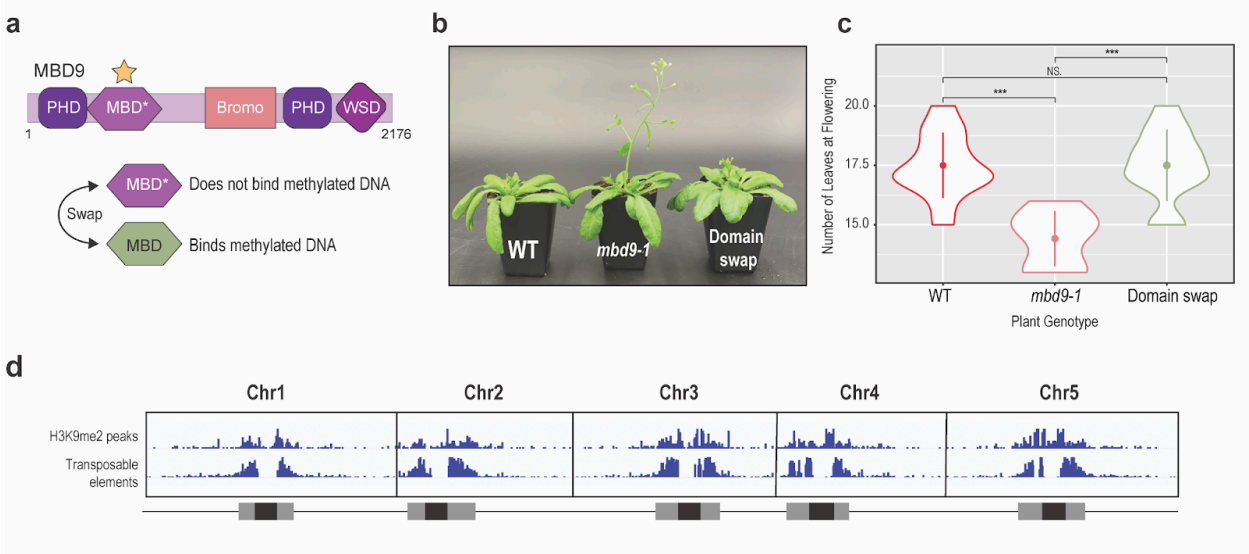

Fig. 2 shows details about the domain swap mutant generation and phenotype. **(a)** depiction of the MBD9^{ds} cloning strategy, where we swapped the endogenous methyl-binding domain (MBD) from MBD9, which does not bind methylated DNA, for the MBD of a family member, MBD7, which has a MBD that binds to methylated DNA. **(b)** supplementation of *mbd9-1* plants with MBD9^{ds} rescues their early flowering, as seen in the photo, where at this time point *mbd9-1* is the only one with a full inflorescence. **(c)** flowering time is quantified as the number of leaves at flowering and presented as violin plots here. While *mbd9-1* plants have significantly fewer leaves at flowering compared to WT, the Domain swap line (*mbd9-1* + MBD9^{ds}) has significantly more than mbd9-1 and no difference compared to WT (Welch two-sample t-test, ***= p<0.001, NS= not significant, n=6 per genotype). **(d)** demonstrates that H3K9me2 peaks encompass both pericentromeric and centromeric regions, while transposable elements are primarily localized to the pericentromere. Therefore we will use H3k9me2 as a proxy for constitutive heterochromatin

in future figures rather than transposable elements.

To analyze the effect of MBD9^{ds} on SWR1 and H2A.Z localization, we performed ChIP-seq in WT and *mbd9-1*+MBD9^{ds}plants against H2A.Z, MBD9 and PIE1. We also performed ChIP-seq in *mbd9-1* against H2A.Z and PIE1 to better understand if MBD9^{ds} can target SWR1 to heterochromatic regions and if this has any effect on H2A.Z accumulation at centromeres. First, we verified that MBD9^{ds} is localized to expected heterochromatic regions. Compared to WT plants, domain swap plants had more MBD9 signal at previously identified H3K9me2 peaks, a histone PTM known to overlap with areas of DNA methylation (**Fig. 3a**). Furthermore, if we examine the signal across an entire chromosome, we can see that MBD9 signal in the domain swap mutant accumulates at the centromere and pericentromere compared to WT MBD9 (**Fig. 3b**). These data suggest that MBD9^{ds} is able to re-localize to constitutively repressed regions. Interestingly, we found that SWR1(PIE1) is also specifically recruited to the same constitutively repressed regions in the domain swap mutant. Compared to WT and *mbd9-1* plants, there is substantially more PIE1 localizing to H3K9me2 peaks in the domain swap mutant (**Fig. 3c**). This pattern is also observed across an entire chromosome, where there is an accumulation of PIE1 at the centromere and pericentromere of chromosome 1 in the domain swap mutant exclusively (**Fig. 3d**). These data suggest that MBD9^{ds} is sufficient for targeting SWR1 (PIE1) to areas where SWR1 is not normally found, including constitutively repressed regions like the centromere.

Fig. 3

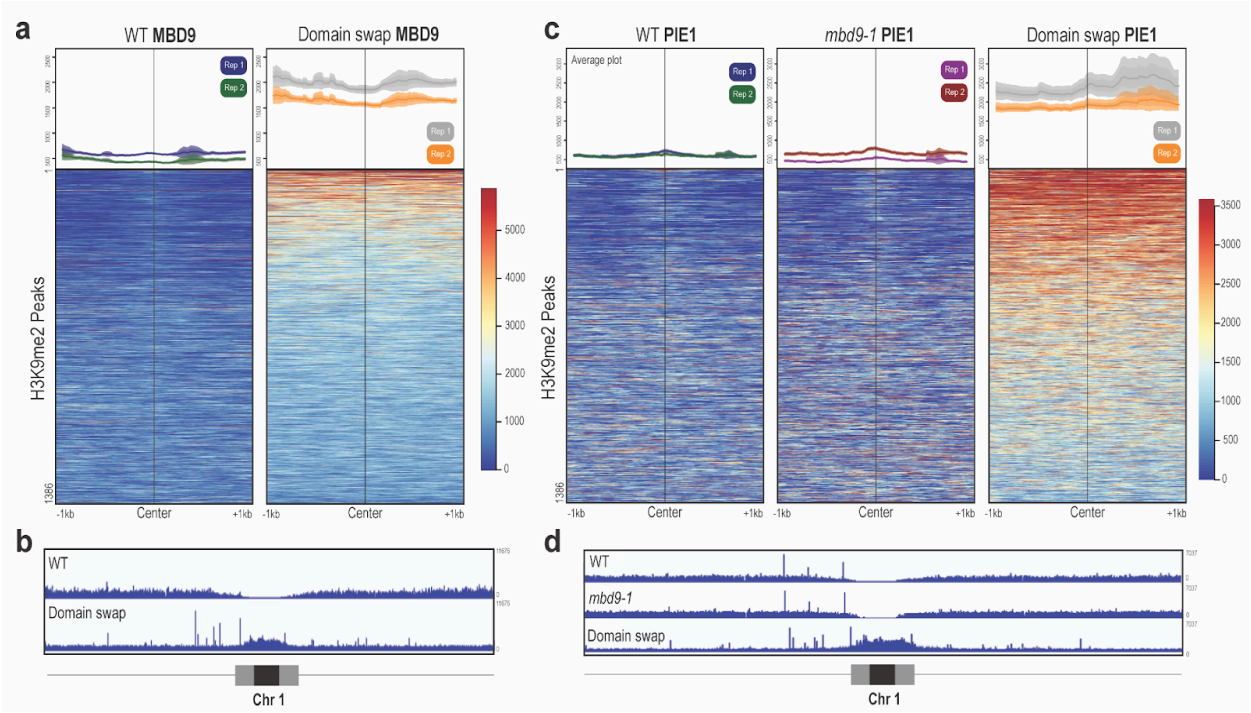

Fig 3 shows the dynamics of MBD9 and PIE1 at centromeres in WT and *mbd9-1*+ MBD9^{ds} (Domain swap) plants. **(a)** shows MBD9 localization in WT and domain swap plants on average (top) and as a heatmap. There is clearly more MBD9^{ds} localizing to H3K9me2 peaks compared to WT MBD9. **(b)** shows accumulation of MBD9 signal across Chromosome 1 (Chr1). There is more MBD9 signal in the domain swap centromeres. **(c)** shows PIE1 signal in WT, mbd9-1 and domain swap plants. There is clearly more PIE1 signal at H3K9me2 peaks in the domain swap plants specifically. **(d)** shows PIE1 signal at Chr1, there is more PIE1 signal at the centromere in domain swap plants. All data are RPKM normalized.

Ectopic enrichment of H2A.Z at centromeres is reduced in *mbd9-1* + MBD9^{ds} compared to *mbd9-1*, while H2A.Z is mostly restored at protein coding genes

We next assessed the effect on ectopic H2A.Z levels in the *mbd9* null mutant background in which SWR1 localizes to constitutively repressed regions. We see that supplementation of *mbd9-1* with MBD9^{ds} causes a reduction in the ectopic accumulation of H2A.Z at constitutively repressed regions. This can be visualized by examining H2A.Z signal at all H3K9me2 peaks, where *mbd9-1* plants have more H2A.Z than WT, but this signal is closer to WT levels in the domain swap mutant (**Fig. 4a**). This pattern is more easily observed looking on average, where MBD9^{ds} partially rescues the ectopic accumulation of H2A.Z observed in *mbd9-1* plants closer to WT levels (**Fig. 4b**). This suggests that when SWR1 is targeted to constitutively repressed regions, it is removing H2A.Z from these areas.

Fig. 4

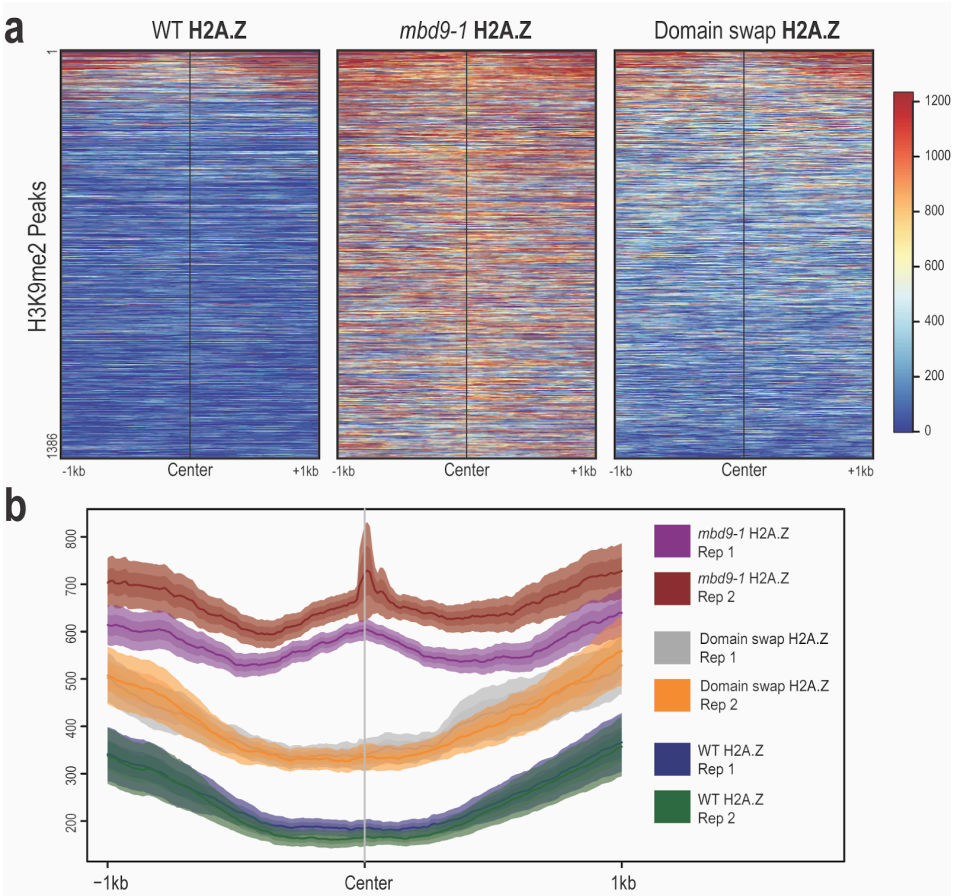

Fig. 4 shows H2A.Z enrichment at H3K9me2 peaks in WT, *mbd9-1* and domain swap (*mbd9-1*+ MBD9^{ds}) plants. **(a)** shows representative, RPKM normalized heatmaps of H2A.Z enrichment in WT, mbd9-1 and *mbd9-1*+ MBD9^{ds}plants. Ectopic H2A.Z in *mbd9-1* mutants is much reduced in the *mbd9-1*+ MBD9^{ds}. **(b)** shows the same data as an average plot across two replicates, where there is the most H2A.Z in the two *mbd9-1* replicates (red and pink) , the least in WT (blue and green), and an intermediate amount of H2A.Z in domain swap plants (gray and orange) at these sites.

Although there are clear differences in the presence of MBD9, PIE1 and H2A.Z at constitutively repressed regions in the domain swap mutants, there are also some unexpected changes at protein coding genes as well. In WT plants, both MBD9 and PIE1 localize to the promoters of active genes while H2A.Z enrichment begins at the nucleosome just downstream of the transcription start site (TSS). In the domain swap mutant, we see that H2A.Z returns to near-WT levels across protein coding genes (**Fig 5a and 5b**). This would not be particularly surprising if not for the clear redistribution of MBD9 and PIE1 away from promoters onto the gene bodies of these protein coding genes (**Fig 5d and Fig 5f**). It is also worth noting that there seems to be an overall reduction of MBD9 and PIE1 signal at protein coding genes as well (**Fig. 5c and 5e**), likely because much of the amount of MBD9 and PIE1 being targeted to the gene poor regions at the centromere and pericentromere.

Fig. 5

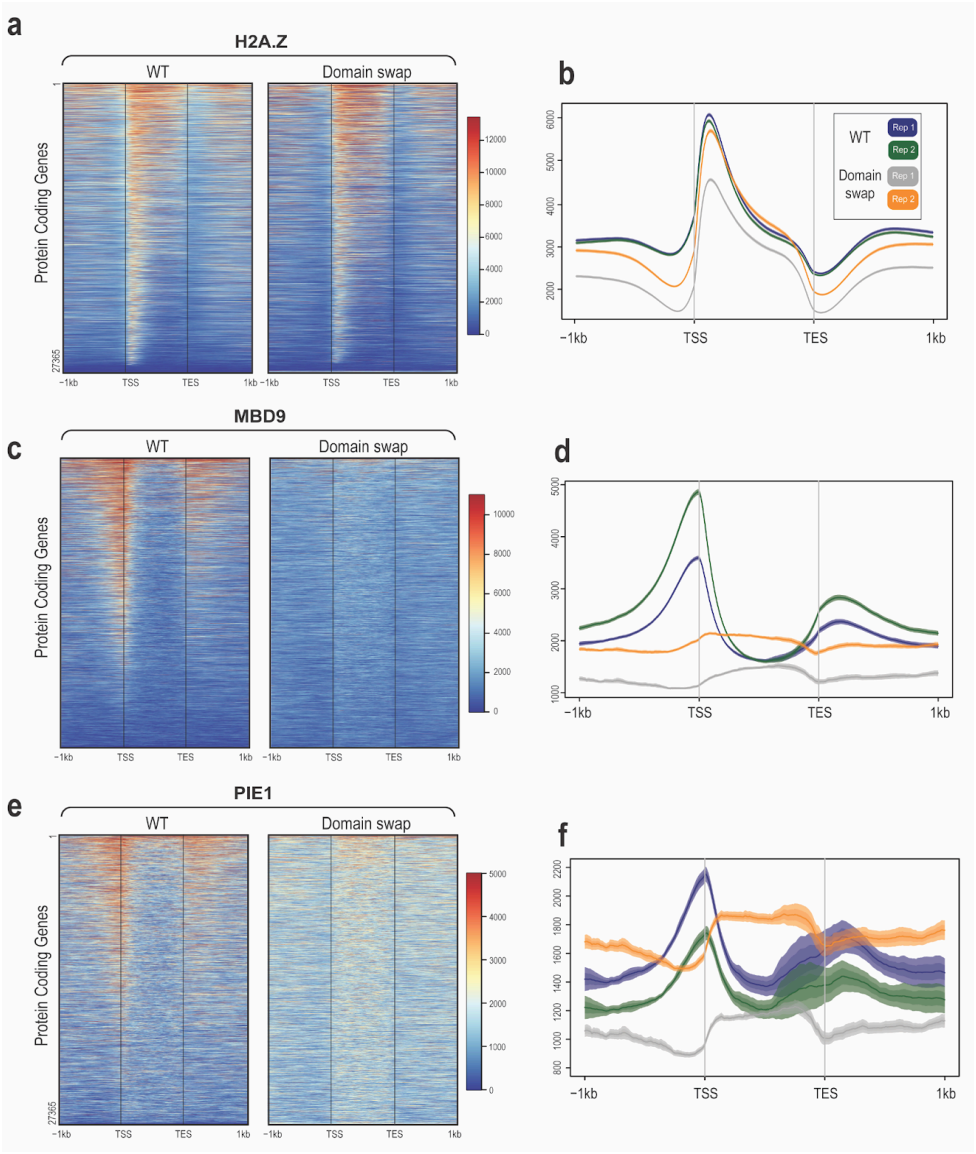

Fig. 5 shows dynamics of H2A.Z, MBD9 and PIE1 in WT and domain swap (mbd9-1+ MBD9^{ds}) at 27365 protein coding genes in Arabidopsis (transposable elements not included). **(a)** shows representative heatmaps of H2A.Z enrichment at protein coding genes. There is no obvious difference in enrichment here between the genotypes. **(b)** shows H2A.Z on average in two replicates of each genotype. WT replicates are shown in blue and green, while domain swap plants are shown in gray and orange. This color scheme is used throughout the figure. **(c)** shows MBD9 enrichment at the same genes. There is a clear difference between the heatmaps

in WT vs domain swap plants, where there is much less MBD9 at coding genes in the domain swap plants. **(d)** shows average plots of MBD9 enrichment in two replicates of each genotype. Interestingly, the profile of MBD9 is now localized along the gene body rather than centered on the Transcription Start Site (TSS). **(e)** shows a representative heatmap at the same genes but showing PIE1 enrichment. Again there is clearly less PIE1 associating with genes in the domain swap mutant. **(f)** shows average plots of PIE1 enrichment at genes in both replicates from each genotype. Similarly to (d), PIE1 is now localized across the gene body rather than centered at the TSS.

Discussion

Here, we describe experiments investigating an unexpected observation that histone variant H2A.Z is enriched at constitutively repressed regions in SWR1 mutants. Historically, there is an anticorrelation between H2A.Z and DNA methylation, but it is unclear how much of this reported anticorrelation is due to limitations with aligning high-throughput sequencing data to highly repetitive regions. Here, with the added ability to align to repetitive regions with the Col-PEK genome assembly, we show that there may be some instances where H2A.Z and DNA-methylation broadly overlap in constitutive heterochromatin.

We first noticed an inverse relationship of H2A.Z enrichment on protein coding genes and heterochromatin in mutants null for MBD9 (*mbd9-1*). MBD9 was shown by several independent groups to interact with SWR1 through co-immunoprecipitation and mass spectrometry [13,22,23]. These groups also demonstrated that *mbd9-1* plants have a reduction of H2A.Z on protein coding genes compared to WT. Through ChIP-seq against H2A.Z in WT and *mbd9-1* mutant Arabidopsis seedlings, we see a similar pattern at protein coding genes (**Fig. 1a**). However, we noticed the inverse relationship at pericentromeric transposable element genes, which are normally constitutively repressed. At these genes, *mbd9-1* mutants have more

H2A.Z on average (**Fig. 1b**). We went on to further verify that this pattern was common among other major SWR1 component mutants including mutants of the catalytic subunit PIE1 (*pie1-5*) and core subunit ARP6 (*arp6*) (**Fig. 1c**). Based on previously established phenotypes and the effect of these mutations on H2A.Z deposition, *pie1-5* is the most severe, followed by arp6, with *mbd9-1* being the most mild. Interestingly, the severity of the mutation also scales with the amount of ectopic H2A.Z accumulation. Given these patterns, we predicted that SWR1 may be directly involved in maintaining the observed anticorrelation between DNA methylation and H2A.Z by actively removing H2A.Z from centromeric regions.

To test this hypothesis, we targeted SWR1 to constitutive heterochromatin in *mbd9-1* to ask whether the ectopic centromeric accumulation of H2A.Z would be reduced. To do this, we cloned a mutant version of MBD9 that binds strongly to methylated DNA and stably integrated this domain swap MBD9 (MBD9^{ds}) in a *mbd9-1* background under the native MBD9 promoter (**Fig. 2a**). MBD9^{ds} was able to effectively rescue the early flowering phenotype of *mbd9-1* mutants (**Fig. 2b and 2c**).

ChIP-seq against MBD9, PIE1 and H2A.Z in domain swap mutant seedlings also revealed that MBD9^{ds} is sufficient to target SWR1(PIE1) to constitutively repressed regions. It is important to note that the MBD9 antibody used here is a polyclonal antibody raised against an MBD9 peptide fragment outside of the MBD domain, so the antibody should equally recognize WT MBD9 and MBD9^{ds}. Using H3K9me2 ChIP-seq peaks as a proxy for constitutive heterochromatin, we observed more MBD9^{ds} localizing to constitutive heterochromatin compared to WT MBD9 (**Fig. 3a**). This enrichment of MBD9^{ds} at constitutive heterochromatin is also noticeable at the centromere and pericentromere if we visualize the signal across the entirety of chromosome 1 (**Fig. 3b**). Although here we show only chromosome 1, a similar pattern is observed across the centromeric regions of all chromosomes. The recruitment of SWR1(PIE1) was also observed at the same regions (**Fig. 3c and 3d**). Previous work has suggested that MBD9 is a potential targeting factor for SWR1 [13,22,23], and this work directly

demonstrates that in this context, changing the localization of MBD9 is sufficient to change the localization of the catalytic SWR1 subunit, PIE1, to the same areas. However, as we demonstrated in Chapter 2, MBD9 is not necessary for SWR1 recruitment to newly activated response genes. It is also important to note that the behavior of MBD9^{ds} may not necessarily reflect the behavior of WT MBD9. Future work should focus on understanding if the full SWR1 complex is recruited in domain swap mutants.

When MBD9^{ds} and SWR1 are re-localized to centromeres, there is a decrease in the ectopic accumulation of H2A.Z. WT plants have little H2A.Z at H3K9me2 peaks, and *mbd9-1* plants have more H2A.Z at these same regions. This is evident visualized on a heatmap (**Fig. 4a**), but the pattern is more evident looking at average plots (**Fig. 4b**). Considering that domain swap mutants are in the *mbd9-1* background, this represents a partial rescue of the WT H2A.Z level at these sites. These results are consistent with the model that SWR1 has the ability to remove H2A.Z from methylated DNA regions in constitutive heterochromatin. However, these results also do not rule out other models. For example, MBD9 likely mediates interactions between SWR1 and other chromatin remodelers including Imitation SWItch (ISWI) type chromatin remodelers, which are involved with sliding and positioning nucleosomes [13]. It is possible that recruitment of MBD9 to constitutive heterochromatin also recruits ISWI, which in turn slides these H2A.Z-containing nucleosomes, increasing their likelihood of dissociation from DNA. This could also result in an apparent loss of H2A.Z from these constitutive heterochromatin regions.

Another interesting observation is that while H2A.Z is changed at constitutive heterochromatin, supplementation of *mbd9-1* with MBD9^{ds} is sufficient to rescue the deposition of H2A.Z at protein coding genes. This is evident looking at H2A.Z on heatmaps (**Fig. 5a**), and on average plots (**Fig. 5b**). It is important to note that on average plots, one replicate of the domain swap mutant does not show a full rescue of H2A.Z to the same level as in WT plants. However, considering that the domain swap plants are not showing early flowering (**Fig. 2b and**

Fig. 2c), it is more likely that the amount of H2A.Z is rescued at genes as flowering is tightly regulated by the amount of H2A.Z at flowering control genes [27]. This rescue is surprising considering that there is less SWR1(PIE1) being recruited to protein coding genes in the domain swap mutant (**Fig. 5e**). This is likely because much of the MBD9 and PIE1 are being recruited to constitutive heterochromatin. The localization of MBD9 and PIE1 is also changed to cover gene bodies instead of being localized to the promoter region of genes (**Fig. 5d and 5f**). This is consistent with the presence of gene body methylation across protein coding genes in Arabidopsis [6], which is not associated with gene repression. However, if the purpose of SWR1(PIE1) at genes is to maintain H2A.Z-containing nucleosomes at promoters, it is surprising that a reduction of SWR1 does not result in a decrease in H2A.Z at these locations. It is possible that the small amount of SWR1 being recruited is sufficient to maintain H2A.Z, and its specific location in reference to a gene does not affect its function. So whether SWR1 is recruited to the TSS or the gene body, as long as it is near the gene it can maintain H2A.Z there.

Taken together, these experiments further define the role of SWR1 in H2A.Z patterning in *Arabidopsis thaliana*. We show that MBD9^{ds} is sufficient to recruit SWR1 to constitutive heterochromatin, where it helps ameliorate the ectopic accumulation of H2A.Z observed in *mbd9-1* mutants. We also show that MBD9^{ds} can restore H2A.Z levels at protein coding genes despite associating with these genes less than in WT plants. Overall, these results support that SWR1 may be directly involved in maintaining the observed anticorrelation between H2A.Z and DNA methylation in Arabidopsis constitutive heterochromatin.

Methods

Plant growth conditions

All *Arabidopsis thaliana* plants described are of the Columbia (Col-0) ecotype, and Col-0 was used as a wild type (WT) reference. We obtained *mbd9-1* mutants from ABRC

(SALK_054659). Seeds were sown on half-strength Murashige and Skoog (MS) media plates or soil and stratified at 4°C for 72 hours. After stratification, plants were moved to growth chambers at 20˚C under a 16 hour light/8 hour dark cycle under 181 µmol m^{-2} s^{-1} PPFD light intensity. Plated plants were grown approximately 7 days and whole seedling shoot tissue (above ground tissue only) was collected at approximately 9 hours after artificial dawn for use in downstream experiments. For flowering time calculations, plants were grown on soil until bolting, where the number of rosette leaves were counted.

Publicly available data and mutants

Publicly available data utilized to investigate ectopic H2A.Z accumulation in SWR1 mutants include H2A.Z ChIP-Seq data from *pie1-5* (SALK_096434), *mbd9-1* (SALK_054659), *arp6* (SAIL_236_C07) and matched WT controls. These data are available under the NCBI Gene Expression Omnibus (GEO) accession number GSM4141897 [13]. Additionally, H3K9me2 peaks were derived from data available under the GEO accession GSE150434. See 'ChIP sequencing data analysis' subheading for data processing details.

MBD9^{ds} cloning and domain swap mutant generation

The three tandem MBD7 domains were amplified from genomic Arabidopsis DNA along with appropriate overhangs using the following primers: 5' agttgtttctgcaaaatctcATCGCGGATCCCACCTC and 5' tgagtaccagatttaacggcAGGAAGCCGCTCCGAATG. Linear fragments of the MBD9 coding sequence in pDONR221 with its native promoter but without its native MBD domain were amplified using the following primers: 5'GAGATTTTGCAGAAACAAC and 5' GCCGTTAAATCTGGTACTC. The products were assembled via Gibson Assembly (New England Biolabs) to create the MBD9^{ds} coding sequence, which was verified by Sanger Sequencing. The MBD9^{ds} sequence was cloned into destination gateway plasmid pMDC99

through LR recombination (Invitrogen). MBD9^{ds} in pMDC99 were transformed into *Agrobacterium tumefaciens* GV3101 strain via electroporation. *mbd9-1* plants were transformed with MBD9^{ds} in pMDC99 through the floral dip method. Stable transformants were identified through selection on Hygromycin B-containing media (35 µg/mL) and selfed until homozygosity of the transgene. T4 generation plants were used for all described experiments.

ChIP library generation and sequencing

The enhanced ChIP-Sequencing protocol was followed as previously described in Zhao, L. *et al.* 2020 with the following modifications: Per replicate, 200 mg of 7-day old seedling tissue (above ground tissue only) was harvested, crosslinked in 1% formaldehyde, and flash frozen in liquid nitrogen. Tissue was ground in a mortar and pestle, homogenized into a slurry in 250 µl of Buffer S and moved directly to sonication. Post sonication, lysate was diluted 10x with Buffer F for use in pulldowns. 50 µl of diluted lysate was saved as input. αH2A.Z (2 µg/mL), αMBD9 (2 µg/mL) or αPIE1 (3 µg/mL) antibodies were added to diluted lysates and incubated overnight at 4°C on a nutator for end-over-end mixing. The H2A.Z antibody used here is described by Deal et al. in 2007 [25], and MBD9 and PIE1 antibodies described in Methods of Chapter 1. 20 µl of Protein G Dynabeads (Invitrogen) per replicate were washed in excess Buffer F, resuspended to their original volume and added to each pulldown. Samples were incubated with beads at 4°C on a nutator for 2 hours. ChIP DNA was extracted via the MinElute PCR Purification Kit (Qiagen) and sequencing libraries were made using the ThruPLEX DNA-Seq Kit (Takara). Two replicates of each genotype/treatment were collected for sequencing. Resulting libraries were pooled and sequenced using paired-end 150 nt reads on an Illumina NovaSeq 6000 instrument.

ChIP sequencing data analysis

Sequencing reads were aligned to the Col-PEK genome assembly[21] with Bowtie2 [28,29] using --local --very-sensitive --no-mixed --no-discordant --phred33 parameters. Samtools -view bS, -index, and -sort functions were used to process resulting alignment files[30]. Picard MarkDuplicates function with REMOVE_DUPLICATES=T parameter was used to remove sequencing duplicates (https://broadinstitute.github.io/picard/). deepTools2 bamCoverage function with parameters --normalizeUsing RPKM and --extendReads were used to create Read Per Kilobase Million (RPKM) normalized bigwig files for visualization[31]. For H3K9me2 data, peaks were called on two individual replicates using the HOMER findPeaks command with processed alignment files[32]. Replicate peaks were combined using the bedtools merge function to create a single H3K9me2 peak file for generating heatmaps and average plots presented here[33]. For **Fig. 1c**, the log2 ratio of mutant H2A.Z enrichment relative to WT were calculated using the deeptools bigwigCompare function[31].

Data visualization

Heatmaps and average plots were generated using the Seqplots software using RPKM normalized bigwig files and BED files containing the genomic coordinates of a specified subset of Col-PEK genes, or previously called ChIP-Seq peaks [34,35]). Integrative Genomics Viewer (IGV) was used to visualize log2 ratio across chromosomes[36]. Violin plots from **Fig. 2c** were made in R utilizing ggplot2[37].

References

1. Morrison, O. & Thakur, J. Molecular complexes at euchromatin, heterochromatin and centromeric chromatin. *Int. J. Mol. Sci.* **22**, 6922 (2021).
2. Gopi, L. K. & Kidder, B. L. Integrative pan cancer analysis reveals epigenomic variation in cancer type and cell specific chromatin domains. *Nat. Commun.* **12**, 1–20 (2021).

3. Srivastava, S., Mishra, R. K. & Dhawan, J. Regulation of cellular chromatin state: insights from quiescence and differentiation. *Organogenesis* **6**, 37–47 (2010).
4. Chang, Y.-N. *et al.* Epigenetic regulation in plant abiotic stress responses. *J. Integr. Plant Biol.* **62**, 563–580 (2020).
5. Foroozani, M., Holder, D. H. & Deal, R. B. Histone Variants in the Specialization of Plant Chromatin. *Annu. Rev. Plant Biol.* **73**, 149–172 (2022).
6. Schmitz, R. J., Lewis, Z. A. & Goll, M. G. DNA Methylation: Shared and Divergent Features across Eukaryotes. *Trends Genet.* **35**, 818–827 (2019).
7. Margueron, R. & Reinberg, D. The Polycomb complex PRC2 and its mark in life. *Nature* **469**, 343–349 (2011).
8. Aslam, M., Fakher, B., Jakada, B. H., Cao, S. & Qin, Y. SWR1 Chromatin Remodeling Complex: A Key Transcriptional Regulator in Plants. *Cells* **8**, (2019).
9. Kobor, M. S. *et al.* A protein complex containing the conserved Swi2/Snf2-related ATPase Swr1p deposits histone variant H2A.Z into euchromatin. *PLoS Biol.* **2**, E131 (2004).
10. Mizuguchi, G. *et al.* ATP-driven exchange of histone H2AZ variant catalyzed by SWR1 chromatin remodeling complex. *Science* **303**, 343–348 (2004).
11. March-Díaz, R. & Reyes, J. C. The beauty of being a variant: H2A. Z and the SWR1 complex in plants. *Mol. Plant* **2**, 565–577 (2009).
12. Nie, W.-F. *et al.* Histone acetylation recruits the SWR1 complex to regulate active DNA demethylation in Arabidopsis. *Proc. Natl. Acad. Sci. U. S. A.* **116**, 16641–16650 (2019).
13. Luo, Y.-X. *et al.* A plant-specific SWR1 chromatin-remodeling complex couples histone H2A.Z deposition with nucleosome sliding. *EMBO J.* **39**, e102008 (2020).
14. Coleman-Derr, D. & Zilberman, D. Deposition of histone variant H2A.Z within gene bodies regulates responsive genes. *PLoS Genet.* **8**, e1002988 (2012).
15. Zlatanova, J. & Thakar, A. H2A.Z: view from the top. *Structure* **16**, 166–179 (2008).
16. Long, J., Carter, B., Johnson, E. T. & Ogas, J. Contribution of the histone variant H2A.Z to

expression of responsive genes in plants. *Semin. Cell Dev. Biol.* **135**, 85–92 (2023).

17. Weber, C. M., Ramachandran, S. & Henikoff, S. Nucleosomes Are Context-Specific, H2A.Z-Modulated Barriers to RNA Polymerase. *Mol. Cell* **53**, 819–830 (2014).
18. Zilberman, D., Coleman-Derr, D., Ballinger, T. & Henikoff, S. Histone H2A.Z and DNA methylation are mutually antagonistic chromatin marks. *Nature* **456**, 125 (2008).
19. Conerly, M. L. *et al.* Changes in H2A.Z occupancy and DNA methylation during B-cell lymphomagenesis. *Genome Res.* **20**, 1383–1390 (2010).
20. Edwards, J. R. *et al.* Chromatin and sequence features that define the fine and gross structure of genomic methylation patterns. *Genome Res.* **20**, 972–980 (2010).
21. Hou, X., Wang, D., Cheng, Z., Wang, Y. & Jiao, Y. A near-complete assembly of an Arabidopsis thaliana genome. *Mol. Plant* **15**, 1247–1250 (2022).
22. Sijacic, P., Holder, D. H., Bajic, M. & Deal, R. B. Methyl-CpG-binding domain 9 (MBD9) is required for H2A.Z incorporation into chromatin at a subset of H2A.Z-enriched regions in the Arabidopsis genome. *PLoS Genet.* **15**, e1008326 (2019).
23. Potok, M. E. *et al.* Arabidopsis SWR1-associated protein methyl-CpG-binding domain 9 is required for histone H2A.Z deposition. *Nat. Commun.* **10**, 1–14 (2019).
24. Berg, A. *et al.* Ten members of the Arabidopsis gene family encoding methyl-CpG-binding domain proteins are transcriptionally active and at least one, AtMBD11, is crucial for normal development. *Nucleic Acids Res.* **31**, 5291–5304 (2003).
25. Wang, C. *et al.* Methyl-CpG-binding domain protein MBD7 is required for active DNA demethylation in Arabidopsis. *Plant Physiol.* **167**, 905–914 (2015).
26. Scebba, F. *et al.* Arabidopsis MBD proteins show different binding specificities and nuclear localization. *Plant Mol. Biol.* **53**, 715–731 (2003).
27. Deal, R. B., Topp, C. N., McKinney, E. C. & Meagher, R. B. Repression of flowering in Arabidopsis requires activation of FLOWERING LOCUS C expression by the histone variant H2A.Z. *Plant Cell* **19**, 74–83 (2007).

28. Langmead, B., Wilks, C., Antonescu, V. & Charles, R. Scaling read aligners to hundreds of threads on general-purpose processors. *Bioinformatics* **35**, 421–432 (2018).
29. Langmead, B. & Salzberg, S. L. Fast gapped-read alignment with Bowtie 2. *Nat. Methods* **9**, 357–359 (2012).
30. Danecek, P. *et al.* Twelve years of SAMtools and BCFtools. *Gigascience* **10**, (2021).
31. Ramírez, F. *et al.* deepTools2: a next generation web server for deep-sequencing data analysis. *Nucleic Acids Res.* **44**, W160–W165 (2016).
32. Heinz, S. *et al.* Simple combinations of lineage-determining transcription factors prime cis-regulatory elements required for macrophage and B cell identities. *Mol. Cell* **38**, 576–589 (2010).
33. Quinlan, A. R. & Hall, I. M. BEDTools: a flexible suite of utilities for comparing genomic features. *Bioinformatics* **26**, 841–842 (2010).
34. Stempor, P. & Ahringer, J. SeqPlots - Interactive software for exploratory data analyses, pattern discovery and visualization in genomics. *Wellcome Open Res* **1**, 14 (2016).
35. Stempor, P. *Seqplots: :chart_with_upwards_trend:SeqPlots - An Interactive Tool for Visualizing NGS Signals and Sequence Motif Densities along Genomic Features Using Average Plots and Heatmaps*. (Github).
36. Robinson, J. T. *et al.* Integrative genomics viewer. *Nat. Biotechnol.* **29**, 24–26 (2011).
37. Wickham, H. *ggplot2*. (Springer International Publishing).

Chapter 4

Discussion

Chapter 4: Discussion

H2A.Z plays a variety of vital roles in developmental and environmental responsiveness across eukaryotes. Without H2A.Z, metazoan embryos do not develop properly, and perturbations to H2A.Z expression levels are a hallmark of several cancers [1,2]. Furthermore, in plants, H2A.Z dynamics ensure proper environmental responsiveness [3]. H2A.Z plays such a variety of roles due to its complex relationship with transcriptional regulation, where it can alternately promote or repress transcription depending on its surrounding chromatin context [4–6]. But H2A.Z deposition into these different contexts is dependent on its deposition machinery SWR1 [6]. Therefore, there must be tight regulation of when, how, and where SWR1 is targeted to ensure H2A.Z is engaging in its appropriate function at the appropriate loci. To contribute to expanding knowledge in this area, we performed experiments that further define the role of SWR1 and known interactor MBD9 in maintaining distinct H2A.Z profiles at protein coding genes and constitutive heterochromatin in *Arabidopsis thaliana*.

Generation of a SWR1(PIE1)-specific antibody greatly advanced our understanding of the relationship between SWR1 and H2A.Z. In Chapter 2, we found that at steady state, genes with the most H2A.Z had the least SWR1. Based on this initial observation, we hypothesized that SWR1 occupancy on genes is related to their transcriptional status, where genes that have constitutive expression need a more sustained SWR1 presence to replace the unstable H2A.Z-containing nucleosomes disrupted by transcription machinery. This hypothesis was supported when we treated Arabidopsis plants with Abscisic Acid (ABA) to activate facultatively repressed genes. After treatment, we saw that SWR1 moved to newly activated genes at a level proportional to their induction, supporting the idea that higher nucleosome disruption by transcription necessitates more SWR1 presence for H2A.Z replacement.

The fact that we see the most SWR1 localized to genes with the highest transcriptional activation also supports a model where H2A.Z loss is more reflective of transcription rather than a prerequisite. Previous studies, with only the lens of H2A.Z distribution and transcription,

concluded that direct H2A.Z loss *resulted* in transcriptional change [7,8]. Here, with the added ability to track SWR1 changes, we argue that while H2A.Z loss may contribute to the de-repression of genes, it is more accurate that this 'loss' is a reflection of the tug-of-war between nucleosome disruption by transcription and H2A.Z replacement by SWR1 **(Fig. 1)**. Additionally, we demonstrate that *mbd9-1* mutants, which have less H2A.Z on average compared to WT plants, do not show widespread transcriptional derepression of facultatively silenced genes. This finding further supports the notion that H2A.Z loss itself is not sufficient to activate genes or change their responsiveness. However, it is possible that other groups of environmental response genes could be more dependent on direct H2A.Z removal by INO80, and changes in H2A.Z enrichment on those genes is a reflection of direct H2A.Z loss in addition to H2A.Z loss by transcription. It is also possible that the timing of our ABA response does not capture the full range of chromatin dynamics; perhaps larger changes in H2A.Z would be measurable at earlier time points when transcriptional induction is first initiated.

In Chapter 2, we also demonstrated that during transcriptional induction, the original profile of H2A.Z distribution across genes was maintained. We initially hypothesized that the profiles of H2A.Z, TSS-associated H2A.Z in active genes and gene body enriched H2A.Z in facultatively repressed genes, are interconnected. In this scenario, transcriptional activation of facultatively repressed genes would result in conversion of the gene body H2A.Z enrichment into TSS-associated H2A.Z enrichment. Interestingly, our results show that ABA responsive genes, which have gene body H2A.Z enrichment, lose H2A.Z only moderately across the entire gene body, and do not convert into strictly TSS-associated H2A.Z. Clearly the cell makes great efforts to maintain the original profile of H2A.Z- implying that the distribution of H2A.Z could have specific effects on the chromatin and transcriptional landscapes. However, this study does not address if sustained transcriptional activation could fully 'convert' gene body H2A.Z to TSS-associated H2A.Z. For example, if we chronically exposed plants to ABA over multiple

days or weeks, the H2A.Z profile may eventually better reflect the TSS-associated H2A.Z patterning as response genes become constitutively active.

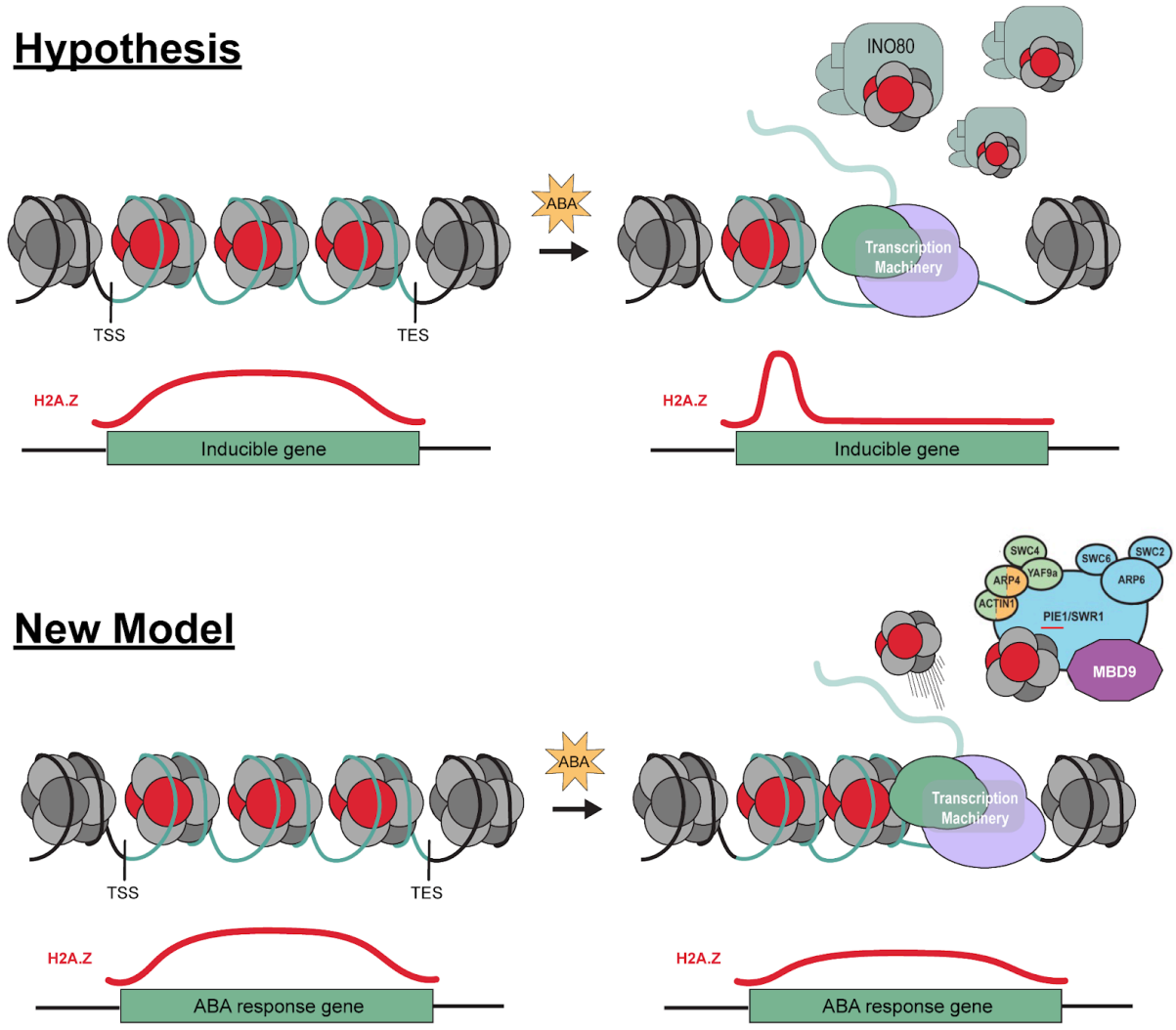

Fig.1 illustrates the hypothesis and new model resulting from experiments described in Chapter 2. Our hypothesis was that direct removal of H2A.Z (likely through INO80) would result in a conversion of gene body H2A.Z to TSS-proximal H2A.Z (top). Instead our results support a new model where H2A.Z loss by transcription is remediated by recruitment of SWR1 to ABA response genes to replace the H2A.Z lost by transcription, resulting in a slight loss of H2A.Z across the gene body but no conversion to TSS-proximal H2A.Z (bottom).

We also saw that MBD9 is recruited to newly activated ABA genes, but it likely does not play a role in SWR1 recruitment to these genes. Previous work has suggested that MBD9 is a targeting factor for SWR1 [9–11]. Although our ABA-treatment experiments in WT plants are in line with MBD9-mediated SWR1 recruitment, analogous experiments in ABA-treated *mbd9-1* plants clarify that MBD9 is not required for SWR1 recruitment to newly activated genes or for a proper transcriptional response to ABA. Based on this clarification, it is reasonable to conclude that the effect of MBD9 on H2A.Z levels relates to functions outside of the SWR1 complex.

Generation of the SWR1-specific and MBD9-specific antibodies also enabled us to investigate the interesting observation that mutants in core SWR1 components and interactors have an ectopic accumulation of H2A.Z at constitutive heterochromatin, In Chapter 3, we utilized a mutant version of MBD9 that binds to methylated DNA (MBD9^{ds}) to recruit SWR1 to these constitutively repressed regions with ectopic H2A.Z. Re-localization of SWR1 to these regions resulted in a partial rescue of H2A.Z back to WT levels. This result suggests that SWR1 directly removes H2A.Z from constitutively repressed regions, such as transposable elements and pericentromeric chromatin, to prevent H2A.Z accumulation at these sites. Alternatively, ectopic H2A.Z accumulation could be a result of altered source-sink dynamics, where a decreased amount of functional H2A.Z deposition machinery results in passive accumulation of H2A.Z at constitutive heterochromatin that is alleviated by recruitment of MBD9 [12]. Previous work indicates that MBD9 interacts with other complexes such as Imitation SWItch (ISWI)-type chromatin remodelers [10,11] and DNA demethylation complexes [13]. Recruitment of ISWI through MBD9^{ds} could also result in the repositioning and sliding of nucleosomes, increasing their likelihood of dissociation from DNA. Similar recruitment of DNA demethylases could remove DNA methylation, thereby altering 3D chromatin compaction and increasing dissociation of labile H2A.Z-containing nucleosomes. Future work should focus on decoupling SWR1 recruitment from MBD9 recruitment to further understand these observations. For example, expression of the MBD9^{ds} in *arp6/mbd9-1* double mutants would result in the recruitment of a

less functional SWR1 to regions with ectopic H2A.Z. If SWR1 is truly responsible for removing H2A.Z from these regions, we would expect to see little rescue of ectopic H2A.Z accumulation. Alternative SWR1 targeting through dCas9 or other methods would also remove the confounding effect of MBD9 potentially recruiting other factors in addition to SWR1.

The recruitment of SWR1 through MBD9^{ds} in Chapter 3 suggests that MBD9 is sufficient for SWR1 recruitment to heterochromatic regions in the context of MBD9^{ds} , but MBD9 presence is not necessary for SWR1 recruitment to ABA-induced genes as shown in Chapter 2. These two seemingly conflicting results would suggest that MBD9 is sufficient but not necessary for SWR1 recruitment. This could simply mean that MBD9, although it can have a strong effect on SWR1 localization, is redundant in its recruitment functions. The pre-initiation complex itself may recruit SWR1 to activated ABA-response genes; a recent publication suggests this is the case with recruitment of the BAF complex to induced genes in mouse embryonic stem cells [14]. However this assertion will require direct testing in Arabidopsis before we can confidently conclude that this is the case.

Broadly, this work challenges several assumptions in the field of epigenetics and H2A.Z biology. We found that H2A.Z eviction is not strictly necessary for gene activation, as we saw that many induced genes in Chapter 2 did not have measurable changes to H2A.Z. This challenges the notion that direct H2A.Z removal by INO80 precedes gene activation. Instead the changes we observed in H2A.Z were strongly correlated with transcription, and future work should be careful to determine whether H2A.Z loss reflects direct removal by INO80, indirect removal through transcription, or a combination of the two. We also challenged the idea that MBD9 acts as a targeting factor for SWR1; we demonstrated that MBD9 is not necessary for SWR1 recruitment to newly activated ABA response genes. MBD9 is still recruited to these newly activated genes, and could instead be acting to keep newly-deposited H2A.Z in nucleosomes through its functions in the ISWI complex. Finally, in Chapter 3, we also provided evidence for a mechanism that could drive the anticorrelation between DNA methylation and

H2A.Z observed across Eukaryotes. Direct removal of H2A.Z by SWR1, rather than simple antagonism, could explain why this patterning was observed previously.

In summary, the experiments described here better define the role of SWR1 in maintaining H2A.Z across the epigenomic landscape of Arabidopsis. Although SWR1 recruitment is a complex and context dependent process, we further clarified this process by tracking SWR1 during the activation of facultatively repressed ABA-response genes and by artificially localizing SWR1 to constitutive heterochromatin. We learned that SWR1 localizes to actively transcribed genes to replace the H2A.Z lost by transcription, and while MBD9 is also recruited, it is not required for SWR1 recruitment or gene activation. We also provided evidence that SWR1 may play an alternate role at constitutive heterochromatin, removing H2A.Z from these regions to prevent its accumulation. We also demonstrated that MBD9 is sufficient to target SWR1 to constitutive heterochromatin. These insights will contribute to future work focused on the manipulation of H2A.Z and its broader regulatory network as it relates to cancer therapeutics and improving plant resilience to environmental stresses.

References

1. Dijkwel, Y. & Tremethick, D. J. The Role of the Histone Variant H2A.Z in Metazoan Development. *J Dev Biol* **10**, (2022).
2. Giaimo, B. D., Ferrante, F., Herchenröther, A., Hake, S. B. & Borggrefe, T. The histone variant H2A.Z in gene regulation. *Epigenetics Chromatin* **12**, 37 (2019).
3. Long, J., Carter, B., Johnson, E. T. & Ogas, J. Contribution of the histone variant H2A.Z to expression of responsive genes in plants. *Semin. Cell Dev. Biol.* **135**, 85–92 (2023).
4. Babiarz, J. E., Halley, J. E. & Rine, J. Telomeric heterochromatin boundaries require NuA4-dependent acetylation of histone variant H2A.Z in Saccharomyces cerevisiae. *Genes Dev.* **20**, 700–710 (2006).

5. Zlatanova, J. & Thakar, A. H2A.Z: view from the top. *Structure* **16**, 166–179 (2008).
6. March-Díaz, R. & Reyes, J. C. The beauty of being a variant: H2A. Z and the SWR1 complex in plants. *Mol. Plant* **2**, 565–577 (2009).
7. Zhao, F. *et al.* Coordinated histone variant H2A.Z eviction and H3.3 deposition control plant thermomorphogenesis. *New Phytol.* **238**, 750–764 (2023).
8. Willige, B. C. *et al.* PHYTOCHROME-INTERACTING FACTORs trigger environmentally responsive chromatin dynamics in plants. *Nat. Genet.* **53**, 955–961 (2021).
9. Sijacic, P., Holder, D. H., Bajic, M. & Deal, R. B. Methyl-CpG-binding domain 9 (MBD9) is required for H2A.Z incorporation into chromatin at a subset of H2A.Z-enriched regions in the Arabidopsis genome. *PLoS Genet.* **15**, e1008326 (2019).
10. Luo, Y.-X. *et al.* A plant-specific SWR1 chromatin-remodeling complex couples histone H2A.Z deposition with nucleosome sliding. *EMBO J.* **39**, e102008 (2020).
11. Potok, M. E. *et al.* Arabidopsis SWR1-associated protein methyl-CpG-binding domain 9 is required for histone H2A.Z deposition. *Nat. Commun.* **10**, 1–14 (2019).
12. Murphy, P. J. & Berger, F. The chromatin source-sink hypothesis: a shared mode of chromatin-mediated regulations. *Development* **150**, (2023).
13. Nie, W.-F. *et al.* Histone acetylation recruits the SWR1 complex to regulate active DNA demethylation in Arabidopsis. *Proc. Natl. Acad. Sci. U. S. A.* **116**, 16641–16650 (2019).
14. Brahma, S. & Henikoff, S. The BAF chromatin remodeler synergizes with RNA polymerase II and transcription factors to evict nucleosomes. *Nat. Genet.* **56**, 100–111 (2023).